DEVELOPMENT OF A SMART MULTI-CHANNEL TWO-DIMENSIONAL MICRO-GAS CHROMATOGRAPHY

by

Jing Liu

A dissertation submitted in partial fulfillment
of the requirements for the degree of
Doctor of Philosophy
(Biomedical Engineering)
in The University of Michigan
2012

Doctoral Committee:

Associate Professor Xudong Fan, Chair
Professor Yogesh B. Gianchandani
Professor Katsuo Kurabayashi
Associate Professor Xiaoyu Deng

To my family,

My parents Rengang Liu and Hanrong Chen

My husband Dong Sun

Acknowledgements

There have been so many people that have helped me reach the point I am at today, and for that I am grateful forever.

I would first like to thank my family, my parents Rengang Liu and Hanrong Chen and my husband Dong Sun, who always love me, believe in me, and support me. Without their love, trust and support, I could not accomplish this.

I also want to give my specially thank to my advisor Prof. Xudong Fan for his inspiring instruction during the past four years. He made all of this work possible.

I would like to thank all my committee members Prof. Yogesh Gianchandani, Prof. Katsuo Kurabayashi, and Prof. Cheri Deng for giving me many helpful advices and supports to my research.

I want to thank all the past and remaining members in Prof. Xudong Fan's research group for providing me an unforgettable graduate school experience. I especially like to thank Dr. Maung Kyaw Khaing Oo, Dr. Yunbo Guo, Dr. Hongying Zhu, Dr. John Suter, Dr. Yuze Sun, Dr. Chung-jie Wu, John Goring, Karthik Reddy, Wonsuk Lee, Di Chen, Qiushu Chen, Prof. Xiang Wu, Prof. Yunhan Luo, Prof. Yubo Li, Prof. Xiangwei Zhao, Prof. Xiaoyun Pu, Dr. Hao Li, and Xingwang Zhang. I also offer my sincerest thank to Naveen Gupta and Junghwan Seo for their help on my experiment.

I also want to thank all my friends who helped me get through the tough times in my life. My special thanks gives to Ying Wan, Jin Zhang, Xiaole Shao, Norma McCormack, Nick Carter, Xuan Wang, Li Liu, and An Mao.

I would like to thank all the staff of Biomedical Engineering Department at University of Michigan and of Biological Engineering Department at University of Missouri for providing invaluable assistance.

Finally, I want to thank National Science Foundation and Engineering Center for Wireless Integrated Microsystems for providing financial support and state-of-the-art micro-fabrication facilities.

Table of Contents

List of Figures

Figure

List of Appendices

Appendices

Abstract

DEVELOPMENT OF A SMART MULTI-CHANNEL TWO-DIMENSIONAL MICRO-GAS CHROMATOGRAPHY

By
Jing Liu

Chair: Xudong Fan

Micro-gas chromatography (μGC), which is capable of conducting fast on-site gas analysis, has broad applications in various fields, such as environmental monitoring, homeland security, anti-terrorism, and disease screening. This dissertation presents the development and applications of a smart multi-channel two-dimensional (2-D) μGC, which not only greatly improves the separation capability but also resolves many disadvantages associated with traditional 2-D μGCs.

The proposed μGC consists of a preconcentrator to sample gas analytes, microfabricated separation columns to conduct rapid sample mixture separation, on-column optical detectors to detect separated analytes, and pumps to provide carrier gas flow. The working principle, fabrication method, and calibration of each component are discussed in detail. One-dimensional μGC sub-system is also tested to have improved

separation capability and shortened analysis time.

Finally, a smart multi-channel 2-D μGC system is demonstrated. In this system, a non-destructive on-column gas detector and a flow routing system are installed between the first dimensional separation column and multiple second dimensional separation columns. The eluent from the first dimensional column is monitored in real-time and decision is then made to route the eluent to one of the second dimensional columns for further separation. As compared to conventional 2-D μGC systems, the greatest benefit of the smart adaptive 2-D μGC architecture is the enhanced separation capability of the second dimensional column and hence the overall 2-D GC performance. All the second dimensional columns are independent of each other, whose coating, length, flow rate and temperature can be customized for best separation result. In particular, there is no limit on the second dimensional column length and separation time in our architecture. Such flexibility is critical when long second dimensional separation is needed for optimal gas analysis. In addition, the smart μGC is advantageous in terms of elimination of the power intensive thermal modulator, higher peak amplitude enhancement, simplified 2-D chromatogram re-construction and potential scalability to higher dimensional separation.

Several important applications are explored based on this system. First, it analyzes a mixture of plant emitted volatile organic compounds (VOCs) that can provide highly specific information for use in agriculture and defense. Then, it is employed for the separation of 31 workplace hazardous VOCs, and rapid detection and identification of target gas analytes from interference background.

Chapter I

Introduction

1.1 Gas chromatography

Gas chromatography (GC) is a standard and powerful analytic technique used in analytical chemistry for separating and analyzing volatile or semi-volatile organic compounds that can be vaporized without decomposition. The schematic of a standard GC system is shown in Fig. 1.1. It has been widely used in various application areas that range from environmental monitoring to oil exploration and homeland security.

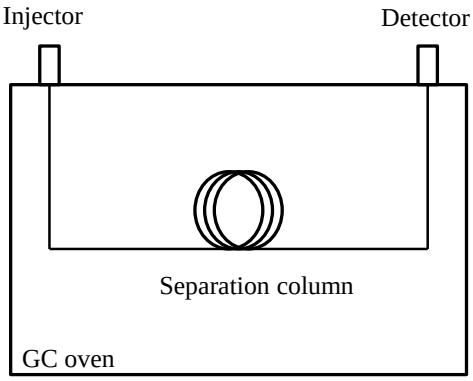

Figure 1.1. Schematic of a standard GC system.

The GC analysis follows a standard procedure. The sample mixture is vaporized under a high temperature at the injection port of the GC system, which is then delivered in gaseous phase by an inertia carrier gas, such as helium or nitrogen, onto a downstream separation

column. The separation column has a polymer layer, known as the stationary phase, coated on its inner surface to interact with the each gas analyte in the sample mixture, slowing down its travelling speed in the column. The interaction strength between the gas analyte and the stationary phase differs according to the physical or chemical properties of the analyte, and thus analytes in the sample mixture elute out of the column sequentially and are individually detected by a gas detector placed at the end of the column. The analysis result is presented in a chromatogram, from which each analyte in the sample mixture is identified by its unique elution time, also called retention time. Figure 1.2 presents an example of the chromatogram obtained from Varian GC 3800 and Varian mass spectrometer (MS) Saturn 2000.

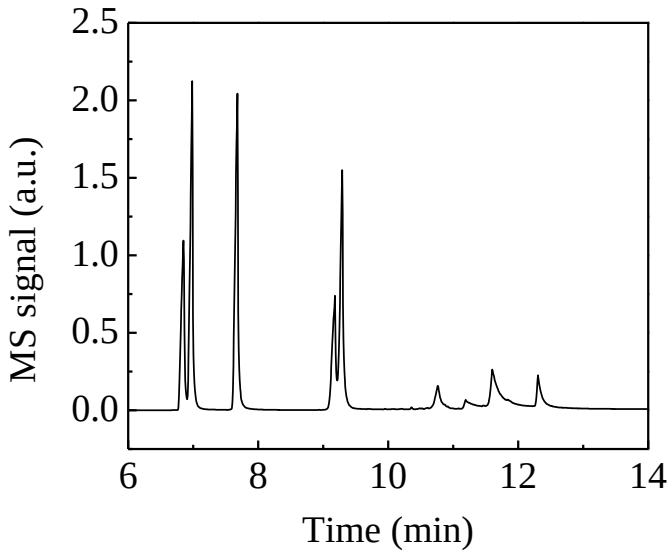

Figure 1.2. Separation chromatogram obtained from Varian GC 3800 and mass spectrometer Saturn 2000.

Although they have powerful separation and analysis capabilities, conventional GCs are bulky and time/power consuming as shown in Fig. 1.3, which can barely satisfy the large demands for compact, rapid, and robust gas analysis systems that are able to detect/identify *in situ* trace level of volatile organic compounds (VOCs) in real-time. In contrast,

miniaturized or micro-gas chromatography (μGC) is particularly suited for rapid analyzing VOC mixtures *in situ*.

Figure 1.3. Varian GC 3800 and mass spectrometer Saturn 2000.

1.2 Micro-gas chromatography

Typically, a μGC system, as shown in Fig. 1.4, is consistent with the conventional GC system, which consists of a pre-concentrator for analyte sampling, a short capillary column or micro-fabricated column for rapid VOC separation, one detector or more for analytes detection, and one gas pump or more for providing carrier gas flow for sample delivery. During several decades of research and development, μGC has undergone significant breakthroughs, especially with respect to miniaturization and rapid detection [1-11]. In the following section, several μGCs will be reviewed as examples.

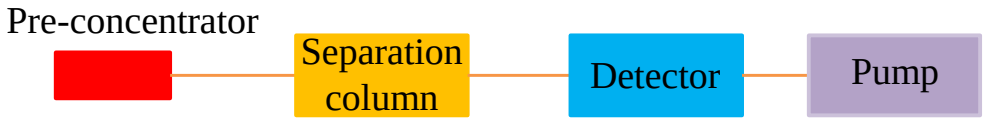

Figure 1.4. Schematic of a standard μGC system.

1.2.1 Review of micro-gas chromatography systems

The first μGC was reported in 1979 by Terry Stephen and his coworkers at Stanford Electronic Laboratory (see Fig. 1.5) [1]. It consisted of a sample injection system, a 1.5 m capillary column, and a thermal conductivity detector, all of which were fabricated on a single silicon wafer of 5 cm diameter using standard photolithography and wet etching techniques. The device was characterized by separating a mixture of eight hydrocarbons within ten seconds. It is the first demonstration of the possibility that GC can be implemented in a compact size and conduct rapid separation and detection.

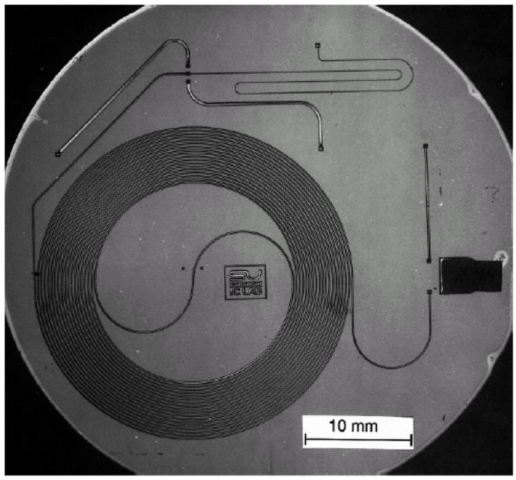

Figure 1.5. Photo of the μGC system developed by Terry and coworkers. Reprinted with permission from [1]. Copyright 1979 IEEE.

This exciting report encouraged more and more research on miniaturized GC systems. One of them is Sandia's MicroChemLab program initiated in 1996 [12]. The μGC developed in Sandia National Lab used a micro-machined pre-concentrator, a separation column, and quartz surface acoustic wave (SAW) array detector. All components were fabricated with standard silicon micro-fabrication processes. The planar pre-concentrator was packed with selective adsorbent to implement selective pre-concentrating target analytes followed by

rapid thermal desorption at 200 ^{o}C. The thermal desorption pulse width was approximately 200 ms at typical system flow rate of 5 mL/min, consuming 100 mW. In order to increase the capacity of the pre-concentrator, a three-dimensional pre-concentrator was developed based on previous planar structure with an increase of the surface area up to 20 folds while maintaining the other aspects of performance (see Fig. 1.6(A)). The micro-fabricated separation column was etched on silicon substrate to produce a rectangular cross section of 400 μm deep and 100 μm wide, allowing for high flow rate at reduced gauge pressure (see Fig. 1.6(B)). A four-element array of SAW detector was used in the system to detect the column eluent. Three elements had different active coatings for sensing, while one element had no coating as a reference. The three major components of pre-concentrator, micro-fabricated column and SAW detector were integrated into a hand-held system as shown in Fig. 1.6(C) and demonstrated the capability to conduct separation and detection of target analytes in ambient air in a short time (approximately 1 min).

Figure 1.6. Micro-GC system developed by Lewis and coworkers in Sandia National Lab. (A) Photo of the 3D pre-concentrator. (B) SEM image of the micro-fabricated column. (C) Photo of the integrated handheld system. Reprinted with permission from [12]. Copyright 2006 IEEE.

Another research group that is active in the area of μGC development is Professor Edward Zellers' group at University of Michigan. A recent work from his group reported a μGC which was capable to detect trichloroethylene (TCE) vapor at sub-parts-per-billion concentrations in complex mixtures, as shown in Fig. 1.7 [10]. In this device, a front-end pre-concentrator-focuser was used, which consisted of two adsorbent-packed metal tubes (outer diameter: 0.64 cm; inner diameter: 0.54 cm; length: 6 cm) as a pre-trap for capturing semi-volatile interferences and a high-volume sampler for capturing volatile compounds. An additional micro-focuser, fabricated by packing adsorbent in a 3.2 mm (width) × 3.45 mm (length) × 0.38 mm (height) cavity etched on silicon substrate, was used to provide additional concentration of TCE. Two 3-meter micro-fabricated separation columns (cross section dimension: 150 μm wide and 240 μm deep) were used to separate TCE from background interferences. An array of chemiresistor detectors was implemented to detect eluents. The integrated system had a dimension of 44 cm (width) × 25.5 cm (length) × 14.5 cm (height). It also demonstrated its capability to identify TCE vapor from 46 background interferences with a concentration of 20 ppb, though the background interferences were not all resolved.

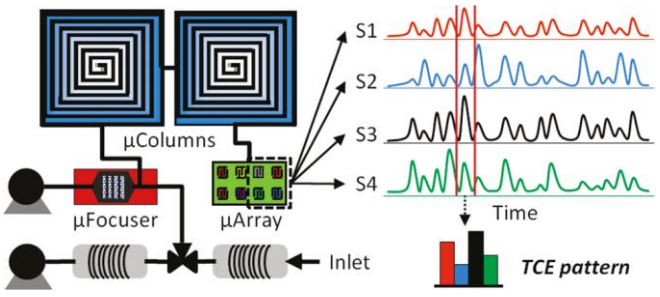

Figure 1.7. Schematic of the μGC system developed by Kim and coworkers and detected TCE pattern from chemiresistor array. Reprinted with permission from [10]. Copyright 2011 American Chemical Society.

Besides the scientific research of μGC in laboratories, several μGCs have been commercially developed. One example is a device called zNose developed by Electronic Sensor Technology Inc. (see Fig. 1.8) [5]. It uses a 3 cm stainless steel tube filled with Tenax as the pre-concentrator to trap target analytes from ambient air. The trapped analytes are then released at 150 ^{o}C and injected onto a 1-meter separation column. After separation, column eluents are detected by a SAW detector. The device is demonstrated to have a detection limit in the range of pico-gram and rapid detection of approximately several minutes. Another commercially available μGC system is Agilent 490 (see Fig. 1.9). It has two independent separation modules, with each having an injection valve, a narrow bore or packed separation column, a thermal conductivity detector, and a flow control system. The module can be replaced easily so that customers can choose different modules according to different applications, largely improving the system versatility. The whole system is integrated into a portable size of 28 (height) × 30 (length) × 15 (wide) inches and has a detection limit of approximately 1 ppm.

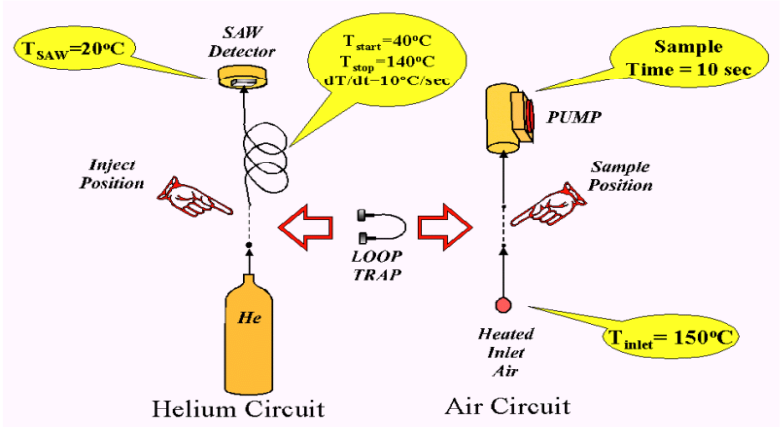

Figure 1.8. Schematic of zNose μGC system. Reprinted with permission from [5]. Copyright 2005 IEEE.

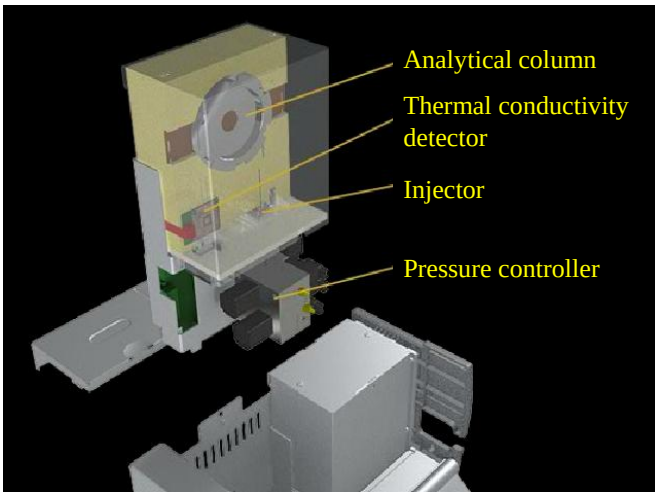

Figure 1.9. Schematic of one separation module of the Agilent 490 μGC.

1.2.2 Shortcomings of micro-gas chromatography

Although the μGC system, as mentioned above, has compact size and conducts rapid analysis, it achieves these advantages at the cost of its separation capability, one of the most important features for GC systems. The main reason caused this deficiency is that the columns used in the μGC system are usually several times shorter than those used in a conventional GC system, resulting in the co-elution and incomplete separation of analytes. Many methods have been developed to increase the resolution of μGC systems. One of them is the tandem-column configuration, which connects two GC columns coated with different polymers in series [13-20]. Typically, the first column is the primary separation column having longer length and non-polar coating, whereas the second column is shorter and coated with polar polymer. However, the tandem-column configuration may still suffer from the same co-elution problem as in a short single-column μGC, because analytes separated by the first column may still co-elute after passing through the second column [21, 22]. Since current GC detectors are placed at the end of the second column, the co-eluted analytes cannot be differentiated by this configuration. Another configuration widely used in a μGC

system to improve its separation capability is the two dimensional (2-D) GC, which has greatly improved separation capability than one-dimensional GC by providing two-dimensional separation information.

1.3 Two-dimensional gas chromatography

A typical 2-D GC configuration connects two different GC columns in series with a modulator in between, as shown in Fig. 1.10 [23-25]. The modulator collects effluent from the first column for a fraction of the time equal to peak width, dividing the peak from the first column into several cuts. Each cut is focused into a very narrow band in the modulator and then sequentially introduced onto the second column, resulting in additional separation. Since the modulator makes the separation at two columns independently, analytes can be differentiated from each other by the retention times at the first and the second column, thus providing the 2-D separation information. Currently, two-dimensional GC can be mainly divided into three categories based on its modulation method: heart cutting, valve based modulation [13, 26-29] and thermal based modulation [25, 30-33]. The following sections will briefly review these three categories.

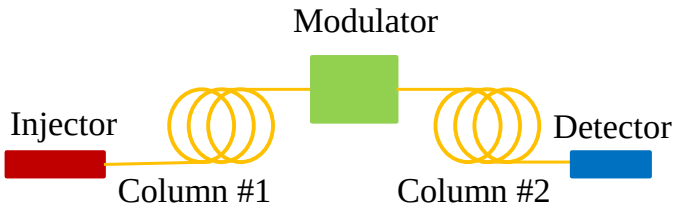

Figure 1.10. Schematic of a standard 2-D GC system.

1.3.1 Heart cutting technique

Heart cutting is a technique of isolating a pair or more unresolved solutes from the first column and sending the mixture onto second column to resolve it. In this system configuration, the gas mixture is initially separated at the first column and detected by a detector installed at the end of the first column. If two or more analytes co-elute at the first column, the peak containing the co-eluted analytes is sent onto the second column for further separation and detected by another detector at the end of the second column. The analytes that are already separated at the first column are not sent onto the second column.

A typical 2-D system using the heart cutting technique is illustrated in Fig. 1.11 [18]. In the system, a valve is connected to the junction point of the two columns on one side, and to a pressure controller, which controls its operation, on the other. A flame ionization detector (FID) is also connected to the column junction point. When the valve is closed, analytes are separated in the first column and detected by the FID. When the valve is open, unresolved co-eluting analytes pass along the second column for further separation and detected by the mass spectrometer (MS) installed at the end of the second column. Meanwhile, the pressure pulse is applied at the junction point to balance the pressure at the injection port so that the separation at the first column is suspended. Although this system provide second dimensional separation to unresolved solute pair(s) from the first dimensional column, it is difficult to determine when the valve should be turned on and off within one analysis.

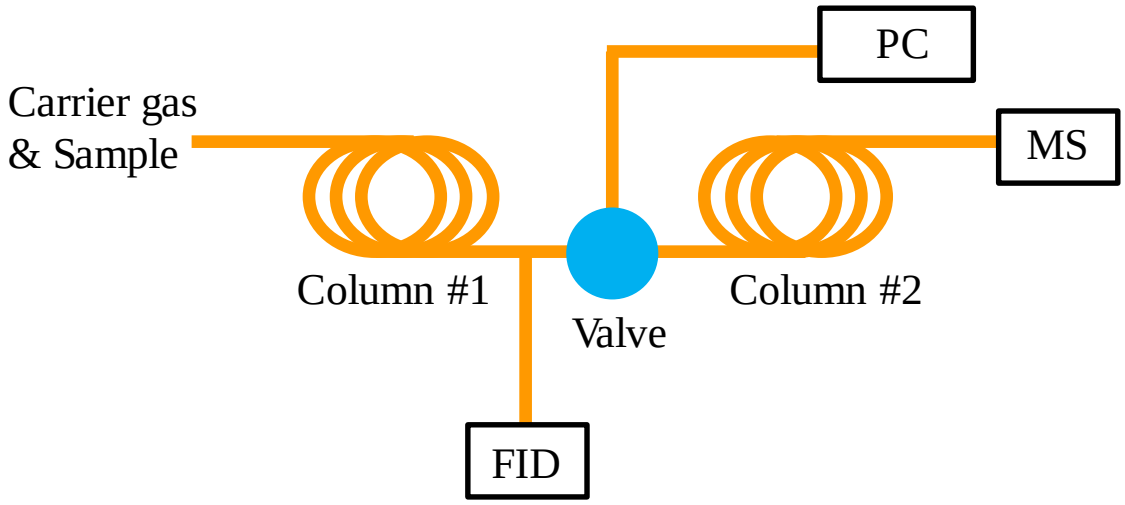

Figure 1.11. Schematic of a chromatography system using heart cutting technique. PC: pressure controller. Reprinted with permission from [18]. Copyright 2001 American Chemical Society.

1.3.2 Valve based modulation

The valve based modulation realizes the 2-D GC modulation by precise control of flow using one or more valves [18, 19, 34-45]. Compared to the 2-D GCs based on heart cutting technique, valve modulation based 2-D GCs work at a constant modulation frequency to continuously send the eluent or a fraction of the eluent from the first column within the modulation period onto the second column. Figure 1.12 shows a simple and typical valve modulation based 2-D GC [35]. A valve is used to switch the connection of the first column and the second column and a vent channel alternatively. The system modulation time is 500 milliseconds, corresponding to a valve working frequency of 2 Hz, and transfer time is 50 milliseconds. It means that the valve cuts the eluent from the first column into 500-ms-pieces and a 50-ms-fraction of each piece is transferred onto the second column while the other fraction is vented to ambient air. Since the system continuously sends the eluent from the first column onto the second column, it does not require pre-test to determine the valve turn

on/off time, and thus, greatly simplified the analysis. However, this system configuration vented 90% of the sample which may significantly degrade the system detection limit.

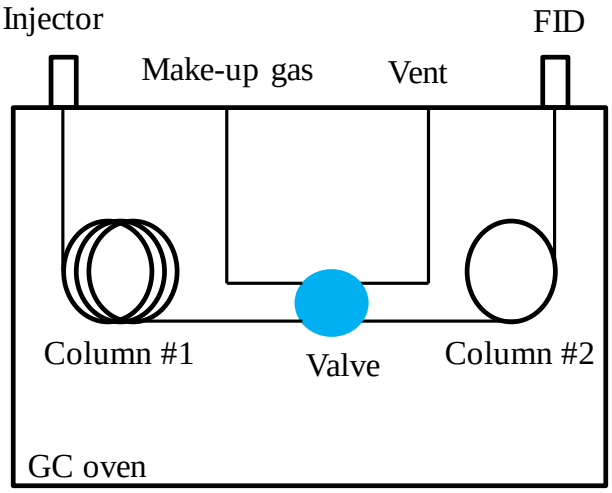

Figure 1.12. Schematic of a valve modulation based 2-D GC with sample loss. Reprinted with permission from [35]. Copyright 1998 American Chemical Society.

In order to eliminate the sample loss problem, another valve modulation based 2-D GC configuration has been developed, as shown in Fig. 1.13 [41]. A six-port valve connects the first and the second column. A sample loop is used to collect the eluent from the first column during one modulation period, and at the end of the modulation it transfers the collected eluent onto the second column. In this case, the eluent from the first column is completely sent onto the second column, eliminating any sample loss. However, the sample loop should have enough capacity to collect all the eluent and to re-inject the eluent onto the second column in a reasonably sharp peak; otherwise, it may degrade the separation resolution on the second column.

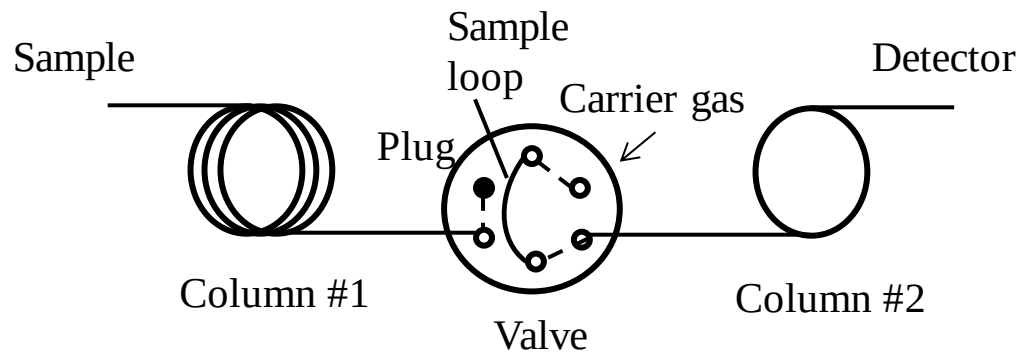

Figure 1.13. Schematic of a valve modulation based 2-D GC without sample loss. Reprinted with permission from [41]. Copyright 2006 American Chemical Society.

Previous two valve modulation based 2-D GC have the valves installed in line with the separation column. The other category of valve modulation based 2-D GC uses valves that are out line of columns, which can be illustrated by Fig. 1.14 [45]. During the bypass period, the valve directs the carrier gas flow in the arrow direction in Fig. 1.14(A), and as a result, the eluent from the first column goes to the vent channel. During the injection period, the valve switches the flow direction as shown in Fig. 1.14(B) to deliver the eluent from the first column into the second column. This system configuration suffers from the same sample loss problem as the system in Fig. 1.12.

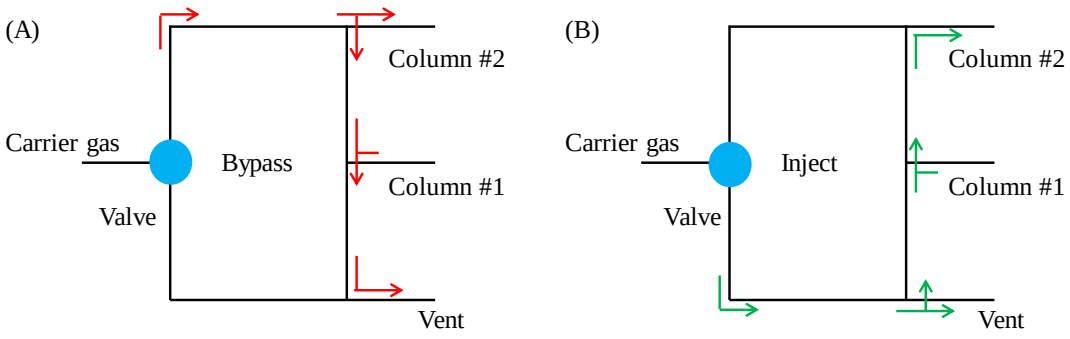

Figure 1.14. Schematic of 2-D GC with a valve out lined of columns. Reprinted with permission from [45]. Copyright 2007 American Chemical Society.

1.3.3 Thermal based modulation

Thermal based modulation implements 2-D modulation by creating a cold zone to trap eluent out from the first column and re-inject it onto the second column in a narrow band at a hot zone [33]. Compared to the 2-D GCs using heart cutting technique, thermal modulation based 2-D GCs, as well as some of the valve modulation based 2-D GCs, send all eluents from the first column onto the second column for second dimensional separation, and thus, it is called comprehensive 2-D GC.

The thermal modulators developed before 1999 mainly used mechanical movement to create cold and hot zones [46-51]. Two examples are shown in Fig. 1.15 and 1.16. In the configuration shown in Fig. 1.15, a heater is attached to a shaft which rotates in an anti-clock direction under a constant speed [48]. It works in four steps: 1) eluents from the first column accumulates at the left part of the thermal modulator (Fig. 1.15(A)), 2) the shaft rotates and locates the heater to the part where eluent accumulates to generate an elution band (Fig. 1.15(B)), 3) shaft continues rotating to move the elution band forward and compress it (Fig. 1.15(C)), 4) as the shaft rotates to the right, the heater re-injects the compressed elution band into the second column. On the left, the new eluent from the first column accumulates (Fig. 1.15(D)). Another thermal modulation, shown in Fig. 1.16, is implemented through vertical movement of a cold trap [51]. The capillary column is placed in the GC oven under a high temperature. When the cold trap moves upward, it traps the eluent from the first column. The trapped eluent then moves downward as the cold trap moves down. During the injection process, the cold trap starts to move upward, and the eluent is re-injected onto the second column under the high temperature of the GC oven. The thermal modulators based on

mechanical movement have limited modulation frequency and are easily worn out, significantly degrading the modulation performances.

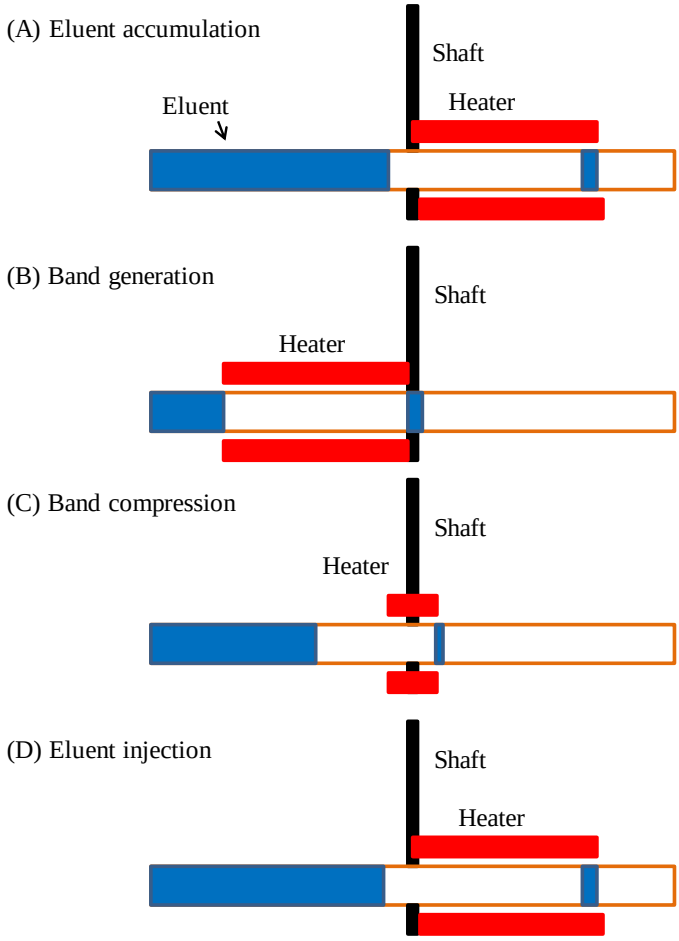

Figure 1.15. Schematic of a thermal modulator based on a rotation shaft. Reprinted with permission from [48]. Copyright 1996 John Wiley&Sons, Inc..

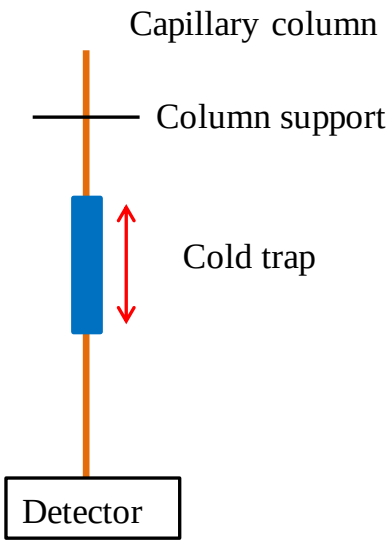

Figure 1.16. Schematic of a thermal modulator based on vertical movement. Reprinted with permission from [51]. Copyright 1998 John Wiley&Sons, Inc..

After year 1999, due to the development of electronic control, the thermal modulator started to use multiple hot and cold jets to create hot and cold zone alternatively to replace mechanical movements [52-54]. Figure 1.17 is an example of such thermal modulator. The thermal modulator has one cold jet and one hot jet installed at both left and right part. At the beginning of a modulation period, the cold jet at the left part and the hot jet at the right part are turned on to trap the new eluent from the first column and re-inject previously trapped eluent onto the second column, respectively. Then, the hot jet at the left part and the cold jet at the right part are turned on to remobilize the trapped eluent onto the right part. At the end of the modulation, it returns to step one to inject the eluent onto the second column and starts a new modulation period. This configuration eliminates mechanical movement, leading to less maintenance and a longer life-time. However, under high frequency modulation, the temperature of the thermal modulator may not be able to achieve the ideal value, resulting in

eluent breakthrough. Additionally, the high frequency thermal modulation consumes a considerable amount of power.

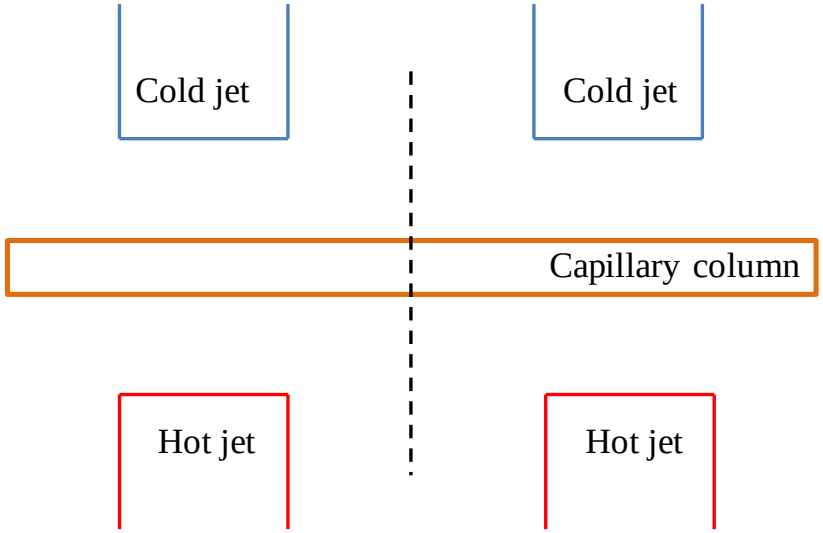

Figure 1.17. Schematic of a quad-jet thermal modulator. Reprinted with permission from [52]. Copyright 2001 Elsevier B. V..

1.3.4 Disadvantages of current two-dimensional gas chromatography

Despite the significantly improved separation capability, existing 2-D GC technology faces several challenges which prevent it from broad applications. (1) Since the modulator has to continuously cut and send the effluent from the first dimensional column to the second dimensional column at a high frequency, the separation at the second dimensional column needs to be finished within only a few seconds before the modulator injects the next effluent to the second dimensional column, which greatly limits the separation capability of the second dimensional column. (2) High frequency operation of the modulator consumes considerably large amount of power, which is not suitable for portable instruments such as those used for on-site gas analysis or in remote distributed gas surveillance/monitoring. (3) Very precise synchronization is required between the modulator and vapor detector at the terminal end of the second dimensional column. Failure in synchronization may cause a

serious problem in data reconstruction. (4) 2-D GC generates a much larger amount of data than 1-D GC, making the data analysis extremely complicated and challenging [55].

1.4 Toward two-dimensional micro-gas chromatography

To date, several 2-D μGC systems have been reported with improved separation capability compared to 1-D μGC systems [54, 56, 57]. However, they did not eliminate the aforementioned problems suffered by existing 2-D GC systems.

The aim of this dissertation is to develop a novel smart 2-D μGC system which has greatly improved separation capability, decreased power consumption, simplified data processing procedure, and highly automatic control/operation algorism..

1.5 Outline of dissertation chapters

The dissertation is divided into six chapters. Chapter One gives an overview of current status of μGCs and 2-D GCs. The following two chapters are focused on the development of individual component used in μGC. Chapter Two discusses the development of a Fabry-Pérot based on-column optical gas detector for μGC, whereas Chapter Three discusses the fabrication and calibration of pre-concentrator, micro-fabricated separation column, and gas pump. Chapter Four demonstrates the integration of a one-dimensional sub-μGC system. Chapter Five presents the work on building the smart multi-channel two-dimensional μGC. The final chapter, Chapter Six, concludes the contribution of the work and discusses the future work to optimize the system.

References

1. S. C. Terry, J. H. Jerman, and J. B. Angell, "A gas chromatographic air analyzer fabricated on a silicon wafer," IEEE Trans. Electron. Devices **26**, 1880-1886 (1979).
2. M. Philips, K. Gleeson, J. M. B. Hughes, J. Greenberg, R. N. Cataneo, L. Baker, and W. P. McVay, "Volatile organic compounds in breath as markers of lung cancer: a cross-sectional study," Lancet **353**, 1930-1933 (1999).
3. F. J. Santos, and M. T. Galceran, "The application of gas chromatography to environmental analysis," TrAC Trend. Anal. Chem. **21**, 672-685 (2002).
4. T. H. Risby, and S. F. Solga, "Current status of clinical breath analysis," Appl. Phys. B **85**, 421-426 (2006).
5. E. J. Staples, S. Viswanathan, "Ultrahigh-speed chromatography and virtual chemical sensors for detecting explosives and chemical warfare agents," IEEE Sens. J. **5**, 622-631 (2005).
6. J. L. Chia, C. Jin, and E. T. Zellers, "Chamber evaluation of a portable GC with tunable retention and microsensor-array detection for indoor air quality monitoring," J. Environ. Monitor. **8**, 270-278 (2006).
7. B. Veyrand, A. Brosseaud, L. Sarcher, V. Varlet, F. Monteau, P. Marchand, F. Andre, and B. Lebizec, "Innovative method for determination of 19 polycyclic aromatic hydrocarbons in food and oil samples using gas chromatography coupled to tandem mass spectrometry based on an isotope dilution approach," J. Chromatogr. A **1149**, 333-344 (2007).
8. Y. Sun, J. Liu, G. Frye-Mason, S.-j. Ja, A. K. Thompson, and X. Fan, "Optofluidic ring resonator sensors for rapid DNT vapor detection," Analyst **134**, 1386-1391 (2009).
9. G. W. Cook, P. T. LaPuma, G. L. Hook, and B. A. Eckenrode, "Using gas chromatography with ion mobility spectrometry to resolve explosive compounds in the presence of interferents," J. Forensic. Sci. **55**, 1582-1591 (2010).
10. S. K. Kim, H. Chang, and E. T. Zellers, "Microfabricated gas chromatograph for the selective determination of trichloroethylene vapoer at sub-parts-per-billion concentrations in complex mixtures," Anal. Chem. **83**, 7198-7206 (2011).
11. S. Popiel, and M. Sankowska, "Determination of chemical warfare agents and related compounds in environmental samples by solid-phase microextraction with gas chromatography," J. Chromatogr. A **1218**, 8457-8479 (2011).
12. P. R. Lewis, R. P. Manginell, D. R. Adkins, R. J. Kottenstette, D. R. Wheeler, S. S. Sokolowski, D. E. Trudell, J. E. Byrnes, M. Okandan, J. M. Bauer, R. G. Manley, and G. C. Frye-Mason, "Recent advancements in the gas-phase MicroChemLab," IEEE Sens. J. **6**, 784-794 (2006).
13. C.-J. Lu, J. Whiting, R. D. Sacks, and E. T. Zellers, "Portable Gas Chromatograph with Tunable Retention and Sensor Array Detection for Determination of Complex Vapor Mixtures," Anal. Chem. **75**, 1400-1409 (2003).
14. M. P. Rowe, W. H. Steinecker, and E. T. Zellers, "Chamber evaluation of a portable GC with tunable retention and microsensor-array detection for indoor air quality monitoring," J. Environ. Monit. **8**, 270-278 (2007).
15. J. R. Jones, and J. H. Purnell, "Prediction of retention times in serially linked open-tubular gas chromatographic columns and optimization of column lengths," Anal. Chem. **62**, 2300-2306 (2002).

16. D. R. Deans, and I. Scott, "Gas chromatographic columns with adjustable separation characteristics," Anal. Chem. **45**, 1137-1141 (2002).
17. J. H. Purnell, and M. H. Wattan, "Separation of aliphatic hydrocarbon mixtures by gas chromatography using serial liquid-phase and solid-phase columns," Anal. Chem. **63**, 1261-1264 (2002).
18. T. Veriotti, and R. Sacks, "A tandem column ensemble with an atmospheric pressure junction-point vent for high-speed GC with selective control of peak-pair separation," Anal. Chem. **73**, 813-819 (2001).
19. M. Libardoni, M. McGuigan, Y. J. Yoo, and R. Sacks, "Band acceleration device for enhanced selectivity with tandem-column gas chromatography," J. Chromatogr. A **1086**, 151-159 (2005).
20. R. Sacks, C. Coutant, T. Veriotti, and A. Grail, "Pressure-tunable dual-column ensembles for high-speed GC and GC/MS," J. Sep. Sci. **23**, 225-234 (2000).
21. Y. Sun, J. Liu, D. J. Howard, X. Fan, G. Frye-Mason, S.-j. Ja, and A. K. Thompson, "Rapid tandem-column micro-gas chromatography based on optofluidic ring resonators with multi-point on-column detection," Analyst **135**, 165-171 (2010).
22. J. Liu, Y. Sun, D. J. Howard, G. Frye-Mason, A. K. Thompson, S.-j. Ja, S.-K. Wang, M. Bai, H. Taub, M. Almasri, and X. Fan, "Fabry-Pe´ rot cavity sensors for multipoint on-column micro gas chromatography detection," Anal. Chem. **82**, 4370-4375 (2010).
23. J. Blomberg, P. J. Schoenmakers, J. Beens, and R. Tijssen, "Compehensive two-dimensional gas chromatography (GC×GC) and its applicability to the characterization of complex (petrochemical) mixtures," J. High. Resolut. Chromatogr. **20**, 539-544 (1997).
24. M. Adahchour, J. Beens, R. J. J. Vreuls, and U. A. T. Brinkman, "Recent developments in comprehensive two-dimensional gas chromatography (GC X GC): I. Introduction and instrumental set-up," TrAC Trend. Anal. Chem. **25**, 438-454 (2006).
25. J. Beens, H. Boelens, R. Tijssen, and J. Blomberg, "Quantitative Aspects of Comprehensive Two-Dimensional Gas Chromatography (GC×GC)," J. High. Resolut. Chromatogr. **21**, 47-54 (1998).
26. C. A. Bruckner, B. J. Prazen, and R. E. Synovec, "Comprehensive Two-Dimensional High-Speed Gas Chromatography with Chemometric Analysis," Anal. Chem. **70**, 2796-2804 (1998).
27. C. G. Fraga, B. J. Prazen, and R. E. Synovec, "Comprehensive Two-Dimensional Gas Chromatography and Chemometrics for the High-Speed Quantitative Analysis of Aromatic Isomers in a Jet Fuel Using the Standard Addition Method and an Objective Retention Time Alignment Algorithm," Analytical Chemistry **72**, 4154-4162 (2000).
28. B. J. Prazen, K. J. Johnson, A. Weber, and R. E. Synovec, "Two-Dimensional Gas Chromatography and Trilinear Partial Least Squares for the Quantitative Analysis of Aromatic and Naphthene Content in Naphtha," Anal. Chem. **73**, 5677-5682 (2001).
29. J. V. Seeley, F. J. Kramp, and K. S. Sharpe, "A dual-secondary column comprehensive two-dimensional gas chromatograph for the analysis of volatile organic compound mixtures," J. Sep. Sci. **24**, 444-450 (2001).
30. Z. Liu, S. R. Sirimanne, D. G. Patterson, L. L. Needham, and J. B. Phillips, "Comprehensive Two-Dimensional Gas Chromatography for the Fast Separation and Determination of Pesticides Extracted from Human Serum," Anal. Chem. **66**, 3086-3092 (1994).

31. J. B. Phillips, and E. B. Ledford, "Thermal modulation: A chemical instrumentation component of potential value in improving portability," Field Anal. Chem. Technol. **1**, 23-29 (1996).
32. P. J. Marriott, and R. M. Kinghorn, "Longitudinally Modulated Cryogenic System. A Generally Applicable Approach to Solute Trapping and Mobilization in Gas Chromatography," Anal. Chem. **69**, 2582-2588 (1997).
33. S.-J. Kim, S. M. Reidy, B. P. Block, K. D. Wise, E. T. Zellers, and K. Kurabayashi, "Microfabricated thermal modulator for comprehensive two-dimensional micro gas chromatography: design, thermal modeling, and preliminary testing," Lab Chip **10**, 1647-1654 (2010).
34. D. R. Deans, "A new technique for heart cutting in gas chromatography," Chromatogr. **1**, 18-22 (1968).
35. C. A. Bruckner, B. J. Prazen, and R. E. Synovec, "Comprehensive two-dimensional high-speed gas chromatography with chemometric analysis," Anal. Chem. **70**, 2796-2804 (1998).
36. J. V. Seeley, F. J. Kramp, and K. S. Sharpe, "A dual-secondary column comprehensive two-dimensional gas chromatograph for the analysis of volatile organic compound mixtures," J. Sep. Sci. **24**, 444-450 (2001).
37. J. V. Seeley, F. J. Kramp, K. S. Sharpe, and S. K. Seeley, "Characterization of gaseous mixtures of organic compounds with dual-secondary column comprehensive two-dimensional gas chromatography," J. Sep. Sci. **25**, 53-59 (2002).
38. A. E. Sinha, K. J. Johnson, B. J. Prazen, S. V. Lucas, C. G. Fraga, and R. E. Synovec, "Comprehensive two-dimensional gas chromatography of volatile and semi-volatile components using a diaphragm vavle-based instrument," J. Chromatogr. A **983**, 195-204 (2003).
39. J. Harynuk, and T. Gorecki, "Comprehensive two-dimensional gas chromatography in stop-flow mode," J. Chromatogr. Sci. **27**, 431-441 (2004).
40. H. Cai, and S. D. Stearns, "Partial modulation method via pulsed flow modulator for comprehensive two-dimensional gas chromatography," Anal. Chem. **76**, 6064-6076 (2004).
41. R. E. Mohler, B. J. Prazen, and R. E. Synovec, "Total-transfer, valve-based comprehensive two-dimensional gas chromatography," Anal. Chim. Acta **555**, 68-74 (2006).
42. N. E. Watson, W. C. Siegler, J. C. Hoggard, and R. E. Synovec, "Comprehensive three-dimensional gas chromatography with parallel factor analysis," Anal. Chem. **79**, 8270-8280 (2007).
43. F. C.-Y. Wang, "New valve switching modulator for comprehensive two-dimensional gas chromatography," J. Chromatogr. A **1188**, 274-280 (2008).
44. N. Oldridge, O. Panic, and T. Gorecki, "Stop-flow comprehensive two-dimensional gas chromatography with pneumatic switching," J. Sep. Sci. **31**, 3375-3384 (2008).
45. J. V. Seeley, N. J. Micyus, S. V. Bandurski, S. K. Seeley, and J. D. McCurry, "Microfluidic Dean switch for comprehensive two-dimensional gas chromatography," Anal. Chem. **79**, 1840-1847 (2007).
46. Z. Liu, and J. B. Phillips, "High-speed gas chromatography using an on-column thermal desorption modulator," J. Microcol. Sep. **1**, 249-256 (1989).
47. Z. Liu, and J. B. Phillips, "Comprehensive two-dimensional gas chromatography using an on-column thermal modulator," J. Chromatogr. Sci. **29**, 227-231 (1991).

48. J. B. Phillips, and E. B. Ledford, "Thermal modulation: A chemical instrumentation component of potential value in improving portability," Field Anal. Chem. Technol. **1**, 23-29 (1996).
49. J. Blomberg, P. J. Schoenmakers, J. Beens, and R. Tijssen, "Compehensive two-dimensional gas chromatography (GC×GC) and its applicability to the characterization of complex (petrochemical) mixtures," J. High. Resolut. Chromatogr. **20**, 539-544 (1997).
50. H.-J. d. Geus, J. d. Boer, J. B. Phillips, E. B. L. Jr., and U. A. T. Brinkman, "Increased signal amplitude due to mass conservation in a thermal desorption modulator," J. High Resolut. Chromatogr. **21**, 411-413 (1998).
51. R. M. Kinghorn, and P. J. Marriott, "Comprehensive two-dimensional gas chromatography using a modulating cryogenic trap," J. High Resolut. Chromatogr. **21**, 620-622 (1998).
52. J. Beens, M. Adahchour, R. J. J. Vreuls, K. v. Altena, and U. A. T. Brinkman, "Simple, non-moving modulation interface for comprehensive two-dimensional gas chromatography," J. Chromatogr. A **919**, 127-132 (2001).
53. R. B. Gaines, and G. S. Frysinger, "Temperature requirements for thermal modulation in comprehensive two-dimensional gas chromatography," J. Sep. Sci. **27**, 380-388 (2004).
54. S. J. Kim, S. M. Reidy, B. P. Block, K. D. Wise, E. T. Zeller, and K. Kurabayashi, "Microfabricated thermal modulator for comprehensive two-dimensional micro gas chromatography: design, thermal modeling, and preliminary testing," Lab Chip **10**, 1647-1654 (2010).
55. S. E. Reichenbach, M. Ni, V. Kottapalli, and A. Visvanathan, "Information technologies for comprehensive two-dimensional gas chromatography," Chemometr. Intell. Lab. **71**, 107-120 (2004).
56. J. J. Whiting, C. S. Fix, J. M. Anderson, A. W. Staton, R. P. Manginell, D. R. Wheeler, E. B. Myers, M. L. Roukes, and R. J. Simonson, "High-speed two-dimensional gas chromatography using microfabricated GC columns combined with nanoelectromechanical mass sensors," in *International Conference on Solid State Sensors and Actuators - Transducers, 2009*(Denvor, CO, 2009), pp. 1666-1669.
57. G. Serrano, D. Paul, S.-J. Kim, K. Kurabayashi, and E. T. Zellers, "Comprehensive two-dimensional gas chromatographic separations with a microfabricated thermal modulator," Anal. Chem. **84**, 6973–6980 (2012).

Chapter II

Detectors in Micro-Gas Chromatography

2.1 Introduction

Gas detectors used in μGCs can be divided by two standards. First, based on their detection methods, μGC detectors are divided into destructive and non-destructive detectors. Destructive detectors destroy the gas analyte during the detection, such as flame ionization detector (FID), mass spectrometer (MS), while non-destructive detectors do not destroy gas analytes during analysis, such surface acoustic wave (SAW) detector [1, 2], thermal conductivity detector (TCD) [3-5], chemirisistor [6]. Since they do not destroy gas analyte, non-destructive detectors can be used in combination with other detectors to conduct multipoint detection. Second, based on the detection location, gas detectors are divided into end-column and on-column detectors. End-column detectors are placed at the end of the column, while on-column detectors can be placed at any pre-determined locations along the column.

Among these detectors, on-column non-destructive detectors provide a very promising approach to address the co-elution problem discussed in Chapter One. In this scheme, detectors can detect analytes at any place along the column, rather than just at the elution end of the column, providing the highly desirable flexibility in selecting the detection location along the column [7-9]. Moreover, multiple detectors can be installed at predetermined

locations along the column to independently measure the retention times of the analyte at respective locations to provide complementary chromatograms. As a result, each analyte can be separated on at least one detection location in a single test without having to use any additional components, considerably simplifying the detection operation and system design. Additionally, on-column detectors do not retain any analytes. Therefore, they do not add any additional dead volumes, thus minimizing related peak broadening. Finally, since the gas flow is uninterrupted in the on-column detection scheme, analytes can easily be passed along to subsequent columns or instruments for further analysis. This feature offers a great potential to improve the detection selectivity and sensitivity by employing different detectors in a single μGC system.

Recently, an on-column detection scheme has been explored in the form of an opto-fluidic ring resonator (OFRR) [9-12]. The OFRR is connected to a regular GC column and acted as both separation column and on-column detector. Rapid separation and detection capability have been obtained with the OFRR-based μGC system. However, due to its thin-walled structure the OFRR is relatively fragile, making it difficult to implement in many field applications. In addition, since the OFRR column is coated with a single type of polymer for both separation and sensing purposes, it may be sensitive to only a certain class of analytes, which may limit its versatility in detecting a wide range of analytes.

2.2 Fabry-Pérot based on-column optical gas detector

In order to address the problems suffered by OFRR, an alternative, highly versatile on-column non-destructive detector for μGC systems is developed, which is based on a Fabry-Pérot (FP) cavity sensing probe (see Figure 2.1) [13]. The FP sensing probe is fabricated by depositing a thin layer of metal and a layer of polymer sequentially on the

endface of a single-mode optical fiber. Light partially reflected from the metal and from the polymer-air interface creates an interference modulation. When an analyte travels along the sensor module, the polymer-analyte interaction changes the refractive index or the thickness of the polymer coated on the FP sensor, resulting in a spectral shift of the interference modulation, which can be detected quantitatively in real time.

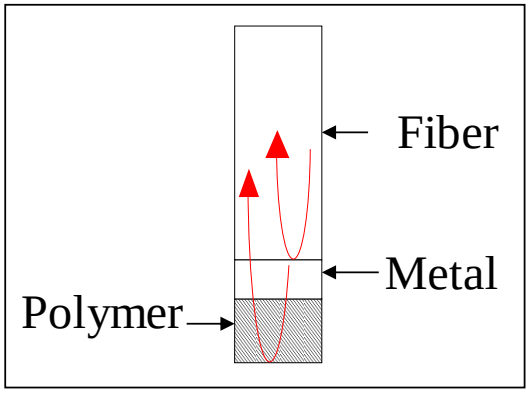

Figure 2.1. Schematic of the FP sensing probe.

The proposed FP sensor has a few distinctive advantages. First, the FP sensor is robust and easy to fabricate and handle, which makes it very attractive for mass production and field applications. Second, different sensing polymer layers can be coated on the FP sensors to accommodate the detection of a wide range of analytes. Third, since the FP sensor module can be easily connected to a GC column through a universal quick seal column connector, various types of GC columns with different lengths can be used to achieve great versatility in analyte detection.

2.1.2 Sensing probe

2.1.2.1 Fabrication process

The sensing probe is prepared by coating a thin layer of metal, such as silver and gold, on the endface of an optical fiber, followed by depositing a layer of the vapor-sensitive polymer. Electroless plating and sputtering coating methods are used to coat the metal layer. For the silver coating, we use the electroless plating method [14]. First, a single mode fiber (SMF-28) is cleaved and cleaned by deionized (DI) water. Then, it is sensitized and catalyzed by immersing it into sensitization and catalyst solution for 3 minutes, respectively. Sensitization solution is a mixture of tin chloride (10 g/L) and hydrochloric acid (40 mL/L) in DI water, whereas catalyst solution is a mixture of palladium chloride (0.5 g/L) and hydrochloric acid (40 mL/L) in DI water. After sensitization and catalyzation, the fiber is immersed in the plating bath containing silver nitrate (0.002 g), ammonia in water (20%) (50 μL), hydrazine hydrate (1 μL), ammonium carbonate (0.02 g), and 1.6 mL of DI water. After approximately 2 minutes of plating, the fiber is cleaned with DI water and air dried for the subsequent polymer coating. The silver coating prepared in this way has thickness on the order of tens of nanometers and allows 10-20% light intensity to be reflected. For gold coating, sputtering method is used to coat a 5 nm thick layer on the fiber endface. Since silver and gold have very low refractive indexs (RI) (complex RI=0.3+11j for silver and RI=0.56+9.8j for gold at 1550 nm), small thickness variations in the silver layer do not significantly change the optical path of the FP probe. In the experiment, we employ two vapor sensitive polymers, polyethylene glycol (PEG) 400 and Norland Optical Adhesive (NOA) 81. Both polymers have been used extensively for chemical detection [10, 15]. They are chosen to simulate the situation where the polymer RI is nearly the same as or dissimilar to that of the fiber, and to represent vapor-sensitive polymers with high (PEG 400) and low (NOA 81) polarity. The polymer layer is deposited by the dip coating method, where the metal-coated fiber is

immersed in polymer solution for 5 minutes. PEG 400-coated probe is dried in a vertical position at room temperature for 2 hours, and NOA 81-coated probe is cured slightly with ultraviolet light (365 nm) for 10 seconds. The resultant thickness of the polymer is usually on the order of tens of micrometers.

2.1.2.2 Sensing experimental set-up

The experimental setup is presented in Fig. 2.2. The sensing probe is placed in a capillary of 900 μm in inner diameter that serves as the gas fluidic channel. For continuous flow mode experiments, various concentrations of air/analyte mixture are flowed continuously through the capillary by a syringe pump at a flow rate of 0.5 mL/min. In pulsed mode experiments, the analyte is extracted from the headspace of the sample vials using a solid-phase microextraction (SPME) fiber and then injected through a GC injector, thus forming a vapor pulse that travels along the capillary. Helium is used as the carrier gas and purging gas. A three-port valve is used to switch between helium gas and analyte. A tunable diode laser (Optical Sensing Interrogator sm125, Micron Optics) is scanned at 2 Hz within a wavelength range of 1510-1590 nm with a spectral resolution of 1 pm. The light reflected from the sensor probe is acquired by the photo-detector on the Micron Optics laser. The corresponding interference spectrum is recorded for post-analysis.

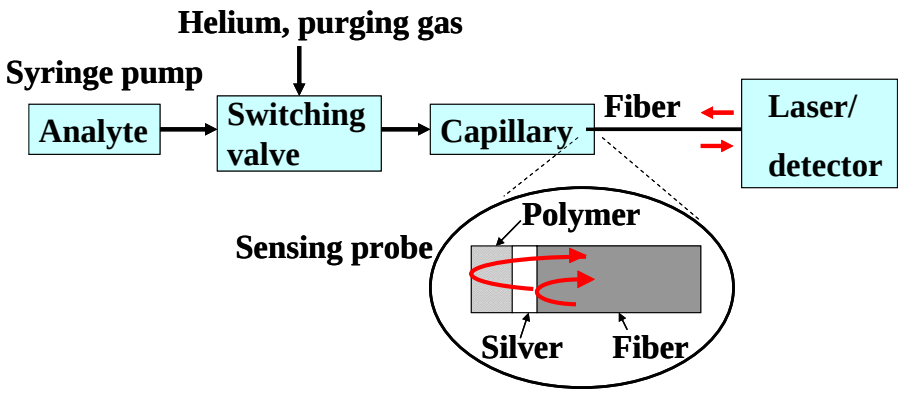

Figure 2.2. Experimental setup. Reprinted with permission from [13]. Copyright 2009 Optical Society of America.

2.1.2.3 Sensitivity and detection limit calibration

The advantages of using a metal layer are clearly demonstrated by Fig. 2.3, which shows the interference spectra of both fiber-metal-polymer structure and fiber-polymer structure. With the metal coating, both interference spectra (Fig. 2.3 (A) and (B)) from PEG 400-coated and NOA 81-coated sensing probes are clean, stable, and have large contrast. However, no distinctive interference spectrum is observed with the PEG 400 coating in the absence of the metal layer (Fig. 2.3 (C)). With the NOA 81 coating, the interference spectrum (Fig. 2.3 (D)) is noisy and contrast is low due to the low reflectivity at the fiber-polymer interface, which results in a deteriorated detection limit in the sensor. Based on the free spectral range in Fig. 2.3 (A) and (B), the coating thickness is estimated to be 30.3 μm and 29.2 μm for PEG-400 and NOA 81, respectively.

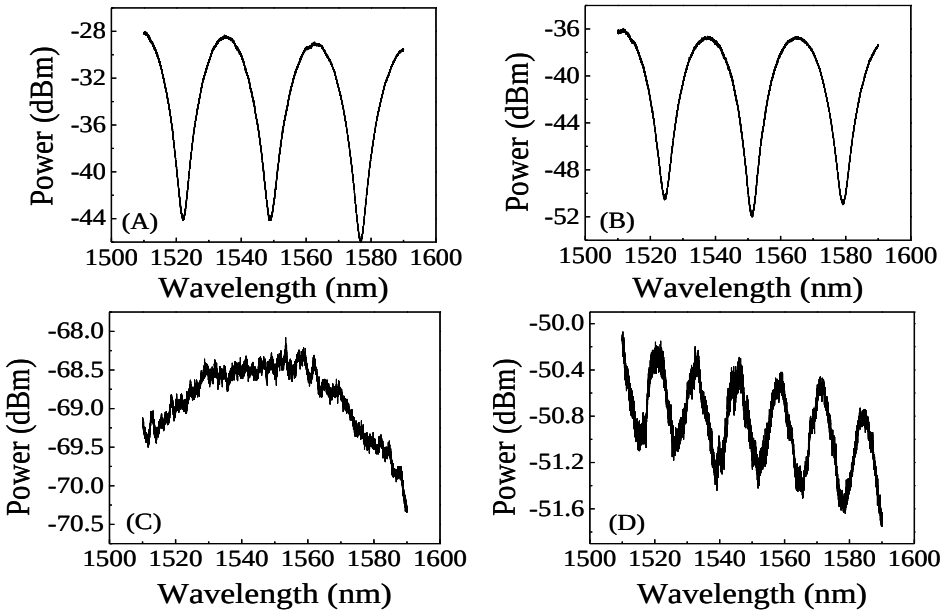

Figure 2.3. Reflection spectrum of the FP sensing probe coated with PEG 400 (A) and Norland Optical Adhesive 81 (B). Reflection spectrum of a bare fiber in absence of the metal layer coated with PEG 400 (C) and Norland Optical Adhesive 81 (D). Reprinted with permission from [13]. Copyright 2009 Optical Society of America.

In the continuous flow mode experiment, air is flowed through the capillary before the introduction of the analyte during which no spectral change in the interference spectrum is observed, indicating that humidity in air does not have any impact on the gas sensor. Two representative sensorgrams of the proposed sensor are shown in Fig. 2.4 by monitoring the interference spectral peak position in real time. Figure 2.4(A) is the sensorgram when PEG 400-coated sensor is exposed to methanol vapor, and Fig. 2.4(B) is when NOA 81-coated sensor interacts with acetone vapor. The interference spectrum shifts to a longer wavelength upon the interaction between analyte vapor and the polymer, and reaches the maximum equilibrium value in approximately 150 and 50 seconds for PEG 400 and NOA 81, respectively. The spectrum then completely returns to the baseline after purge, indicative of complete removal of vapor molecules from the polymer layer.

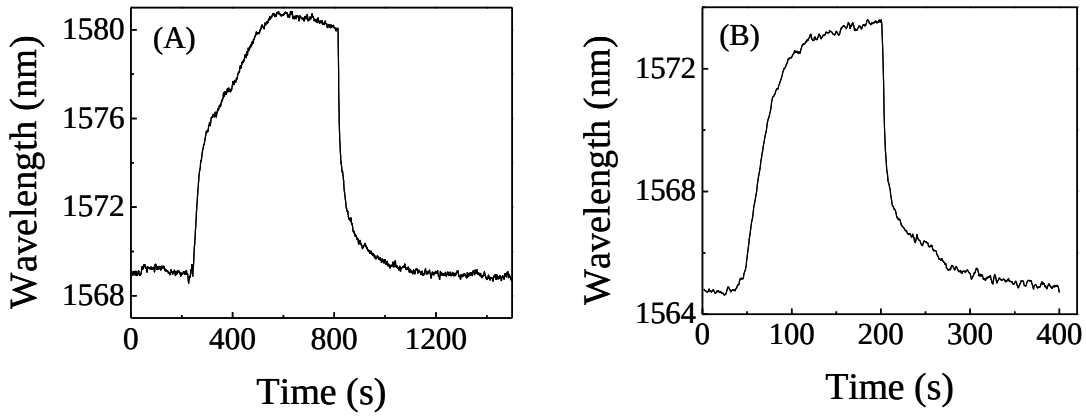

Figure 2.4. Sensorgrams obtained by monitoring the interference spectral shift in real time when sensor probe is exposed to 3410 ppm of methanol (A) and 75500 ppm of acetone (B) vapor. Sensor is coated with PEG 400 (A) and NOA 81 (B). Reprinted with permission from [13]. Copyright 2009 Optical Society of America.

Figure 2.5 depicts the wavelength shift at equilibrium for different concentrations of hexanol, methanol, and acetone vapors for PEG 400 (Fig. 2.5(A)) and NOA 81 (Fig. 2.5(B)) coated sensing probes. The wavelength shift is almost linear to the concentration of analyte

vapor for both PEG 400 and NOA 81. The gas sensor is highly sensitive, because light travels through the whole vapor-sensitive polymer layer, and thus has full interaction with analyte in the polymer. According to Fig. 2.5(A), the sensitivity of the sensing probe to methanol vapor is 3.53 pm/ppm. Using $\Delta(nL)/(nL) = \Delta\lambda/\lambda$, this sensitivity corresponds to a fractional change of 2.3×10^{-6} in the polymer optical path per ppm methanol, which is higher than that for hexanol and acetone (~ 1.1 pm/ppm), because methanol has a higher polarity than hexanol and acetone, and thus, it is more soluble in highly polar PEG 400 polymer. These sensitivities obtained above are similar to what were reported in earlier studies [10, 16-18]. In comparison, NOA 81 is a thiolene-based polymer and has less polarity than PEG 400. As consequence, NOA 81 sensitivity to methanol is only 0.1 pm/ppm, 30 times lower than PEG 400. To estimate the detection limit of the FP sensing probe, we assume that the resolution of wavelength shift is 1 pm. Hence, the detection limit for methanol vapor can potentially be on the order of 1 ppm for PEG 400 and 10 ppm for NOA 81.

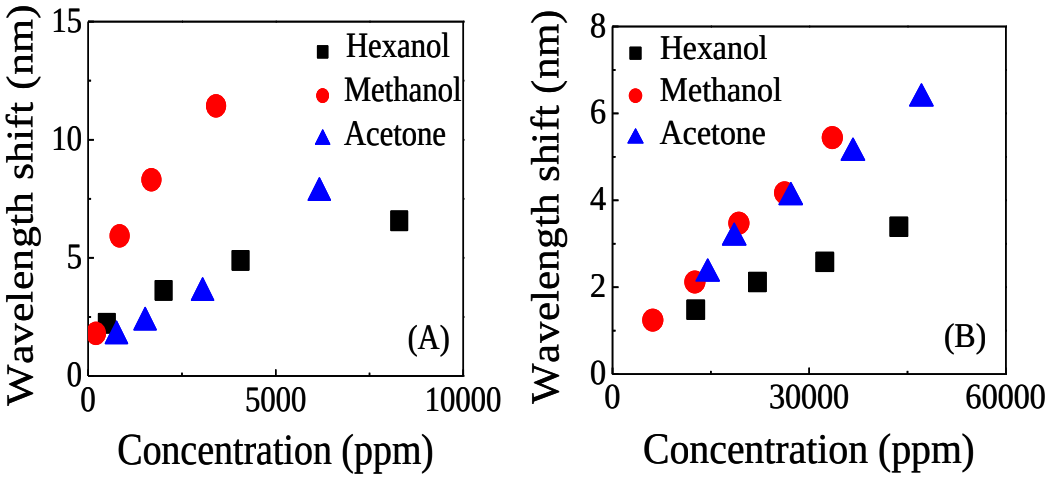

Figure 2.5. Sensor response to various concentrations of hexanol, methanol, and acetone vapor. The sensor is coated with PEG 400 (A) and NOA 81 (B). Reprinted with permission from [13]. Copyright 2009 Optical Society of America.

To test the rapid response of our sensing probe, which is important for many applications where rapid gas detection is critical, we use a SPME fiber to pick up methanol vapor and then release it at a GC injector to introduce methanol vapor pulses. The carrier gas (helium) flow rate is maintained at 19 mL/min. Figure 2.6(A) presents the quick response of PEG 400-coated sensing probe for methanol pulses of different mass loadings. The time response is around 10 seconds, which is much faster than that in the continuous flow mode. The spectrum shift increases with the increased amount of analyte injected. This shows that the FP sensing probe can potentially be used as a GC detector for rapid analysis of the vapor molecules flowing through the GC column.

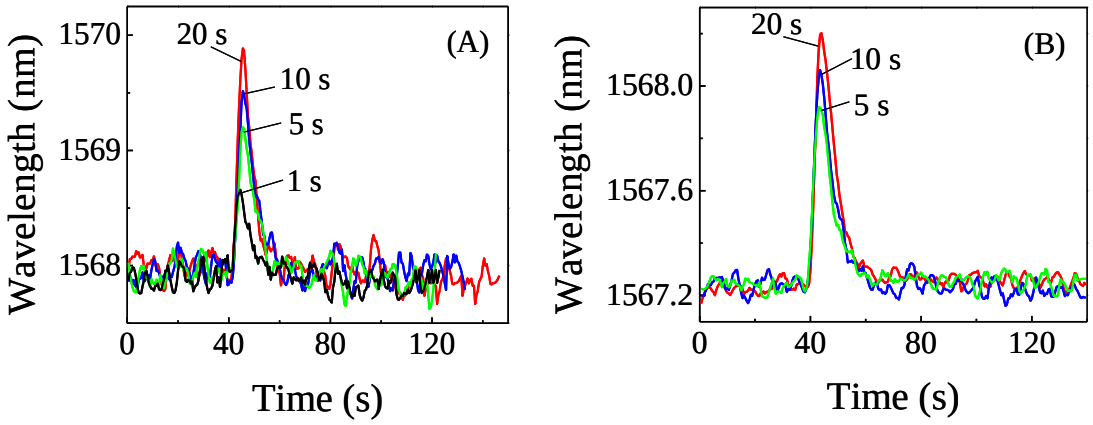

Figure 2.6. Detection of methanol vapor pulses with various SPME sampling times when the analyte is injected in a pulsed mode. Polymer (PEG 400) thickness is 18.6 μm (A) and 31.5 μm (B), respectively. Reprinted with permission from [13]. Copyright 2009 Optical Society of America.

However, our current design is far from its full potential as a rapid sensor. According to our earlier investigation, the pulse width of the methanol less than one second is expected when a pulsed methanol vapor is injected and travels along the PEG 400 coated capillary [19]. The much slower response strongly suggests that the polymer thickness plays an important role in determining the sensor response. To verify this, we carry out a similar

experiment with a much thicker polymer layer. The sensor response is shown in Fig. 2.6(B). Figure 2.7 compares the peak response and the total area, which is proportional to the analyte mass interacting with the polymer, for the two polymer thicknesses, showing that the peak response and the total area for the thicker polymer are consistently lower than those for the thinner polymer. This discrepancy can be accounted for by considering the diffusion of the vapor molecules into the polymer. Within the duration of the molecule pulse, the vapor molecules can diffuse into a certain thickness of polymer. Therefore, only a partial sensitivity of the FP sensor probe can be achieved, in contrast to the continuous flow case where the vapor molecules occupy the whole polymer and the full sensitivity of the FP cavity is realized. For estimation purposes, we assume that pulse width is 1 second and the molecule diffusion constant is 10^{-10} cm^2s^{-1}. In order to achieve the full sensitivity, the vapor molecules should diffuse through the whole polymer within the duration of the vapor pulse, which requires that the polymer thickness be less than 100 nm.

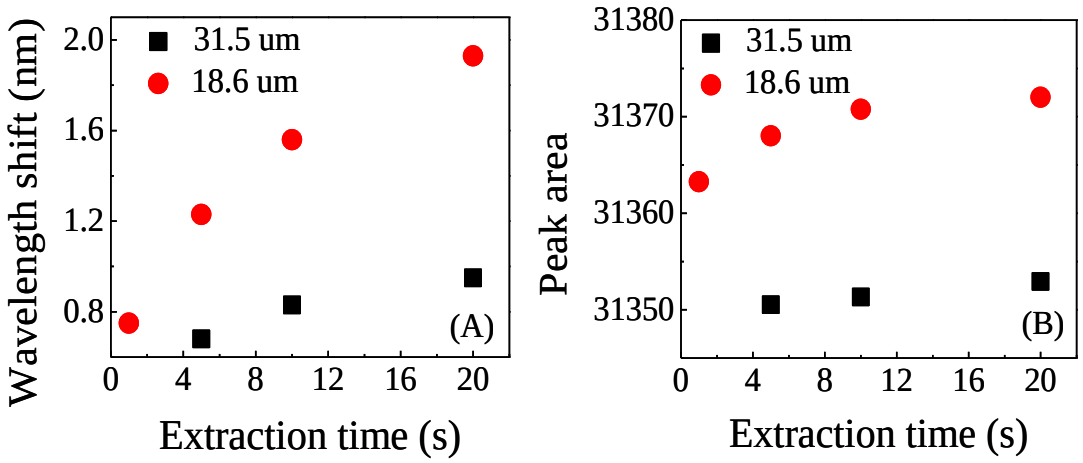

Fig. 2.7. Wavelength shift (A) and peak area (B) vs. SPME extraction time for two different PEG 400 coating thicknesses in Fig. 2.6. Reprinted with permission from [13]. Copyright 2009 Optical Society of America.

2.2.2 Sensing module

2.2.2.1 Assembly process

The FP sensor module (illustrated in Fig. 2.8(A)) is assembled by inserting the FP sensing probe into a hole (approximately 160 μm in diameter, see Fig. 2.8(B)) drilled near the center part of a short (approximately 5 cm) fused-silica capillary from Polymicro by a mechanical drilling machine (Sherline model 2000). The whole assembling process takes place under a microscope to ensure that the end of the FP sensor is flush with the capillary inner wall to avoid any potential disturbance to the gas flow. Finally, the hole is sealed with a UV-curable optical glue.

2.2.2.2 Experimental set-up

The experimental setup is illustrated in Fig. 2.8(C). The FP sensor module is connected to the GC injection port through a 1.6 m long GC guard column, followed by a 1.3 m long Carbowax-coated GC column. Gas analyte extracted from the head space of the bottle containing the analyte by a SPME fiber (PDMS/DVB, 65 μm diameter fiber, Supelco 57310-U) is injected through the GC injector (HP 5890, heated to 250 ^{o}C). The linear installed has an inner diameter (i.d.) of 0.75 mm. Ultrahigh purity (UHP) helium is used as carrier gas. The flow rate is 0.3 mL/min. GC columns and FP sensor modules are all kept at room temperature. For comparison purposes, we also use an FID to detect the analyte. The FID temperature is set at 325 ^{o}C.

A 1550 nm tunable diode laser (JDS Uniphase, CQF935/28 28) is coupled into the FP sensor through an optical circulator (Thorlabs, 6015-3). The laser wavelength is tuned and fixed near the quadrature point around 1550 nm. The reflected light is detected by a photodetector (New Focus, 2033) located at the output port of the circulator. A home-built

LABVIEW program is used to monitor the signal change in real time, and the data is recorded at a rate of 20 Hz.

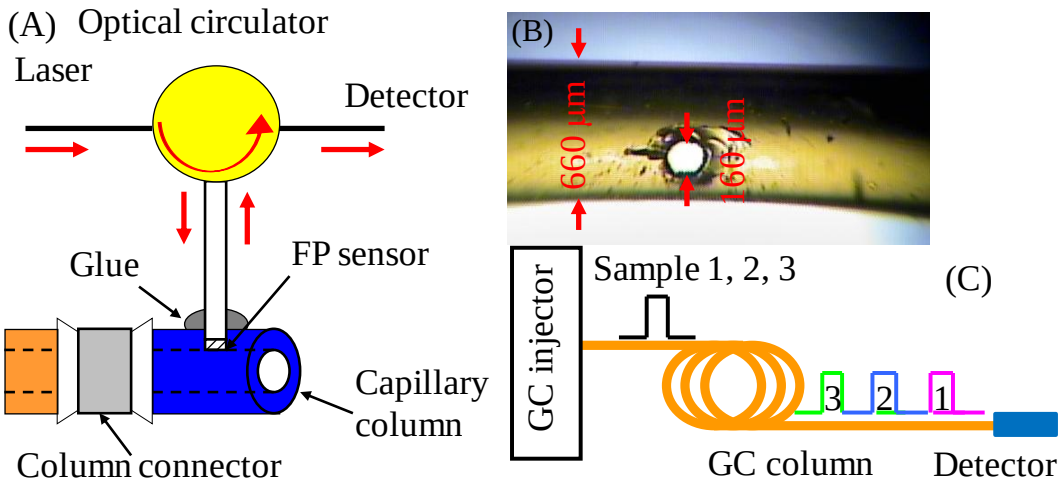

Figure 2.8 (A) Schematic of the sensing module. (B) Photo of the capillary with a hole drilled on it. (C) Schematic of the experimental setup. Reprinted with permission from [7]. Copyright 2010 American Chemical Society.

2.2.2.3 Operation principles

Figure 2.1 shows the details of the FP sensor. Two beams of light reflected from the metal coating layer and from the polymer-air interface form the interference signal, which is governed by

$$I = R_1 + R_2 + 2 \times \sqrt{R_1 R_2} \cos(\phi), \tag{2.1}$$

where $R1$ and $R2$ are the light intensity reflected from the silver layer and the polymer-air interface, respectively.

$$\phi = 4\pi \cdot n \cdot t / \lambda, \tag{2.2}$$

where λ is the laser wavelength and n and t are the polymer refractive index and thickness, respectively. An example of the interference modulation is presented in Fig. 2.9. The

interaction between the polymer and the analyte results in a change in the polymer thickness and/or refractive index and hence in the signal from the photodetector:

$$\Delta I = -2 \times \sqrt{R_1 R_2} \sin(\phi) \Delta\phi \tag{2.3}$$

ΔI becomes the largest when φ is chosen to be at the quadrature point, i.e.:

$$\phi = m \cdot 2\pi + 3\pi / 2, \tag{2.4}$$

where m is an integer, in which case

$$\Delta I / I \propto \Delta\phi, \tag{2.5}$$

assuming $R_1 = R_2$ for simplicity.

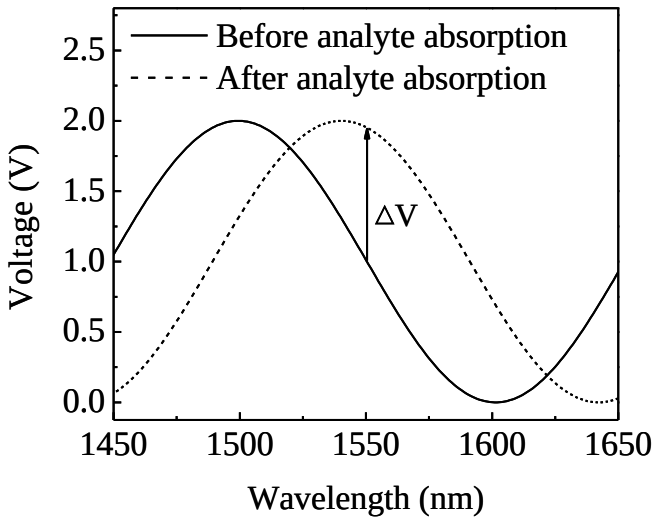

Figure 2.9 An example of the interference spectrum generated by the FP sensor probe based on Eqs. (2.1) and (2.2), where n = 1.47 and t = 4 μm. The signal increases for the fixed laser wavelength centered around 1550 nm, when the interference spectrum shifts to a longer wavelength in response to the polymer-analyte interaction. Reprinted with permission from [7]. Copyright 2010 American Chemical Society.

2.2.2.4 Separation capability

The potential of the FP sensor for rapid, on-column detection is demonstrated in Fig. 2.10, where we show the sensor response to toluene, decane, methanol, and dimethyl methylphosphonate (DMMP), which have various volatilities and polarities. The voltage change resulting from the interaction between the analyte and the polymer layer depends on the amount of the analyte absorbed by the polymer coating layer. Since the FP sensor is coated with polar PEG 1000, different responses for polar and nonpolar analytes are expected. For nonpolar and slightly polar analytes, such as toluene, decane, and methanol, which interact weakly with the polar polymer, a sharp peak is observed with a peak width of several seconds, as shown in Fig. 2.10(A)-(C). In contrast, the signal from highly polar DMMP, which interacts strongly with the polymer layer, returns slowly back to the baseline, as shown in Fig. 3(D). In order to investigate further the temporal response of the FP sensor, we compare the FP results with those obtained from the FID using the same GC columns and flow rate. As shown in Fig. 2.10, the peak widths for nonpolar and slightly polar analytes (i.e., toluene, decane, and methanol) are comparable for the FP sensor and for the FID. The slightly increased retention time in the FID (~10 s) is due to the extra GC column used to link the μGC system to the FID. However, the peak of highly polar DMMP obtained from the FP sensor is much broader than the one obtained from the FID. This phenomenon can be attributed to the inherently different detection principles of the two sensors.

The FID detects the ion current generated by burning analytes. As a result, its temporal response does not vary much for analytes with different polarities. In contrast, the FP sensor detects the interaction between the analyte and the polymer layer. Consequently, its temporal response reflects the polymer change it response to the absorption and desorption processes

of analytes. While for nonpolar or slightly polar analytes, the absorption and desorption are very fast for PEG 1000, leading to at most a very small increase in the peak width, strong interaction between PEG 1000 and DMMP results in an additional broadening of the peak that has already been broadened by the 1.3 m long Carbowax coated GC column. In addition to the polymer polarity, polymer thickness may contribute to the peak broadening, as it takes time for analytes to diffuse into and out of the coating. Usually, for the analytes (such as toluene, decane, and methanol in Fig. 2.10(A)-(C)) that have less interaction with the polymer coating (i.e., lower partition coefficients), a thicker polymer will not introduce significant peak broadening. However, for DMMP, which has strong interaction with PEG 1000, the polymer thickness has a significant impact on the peak width.

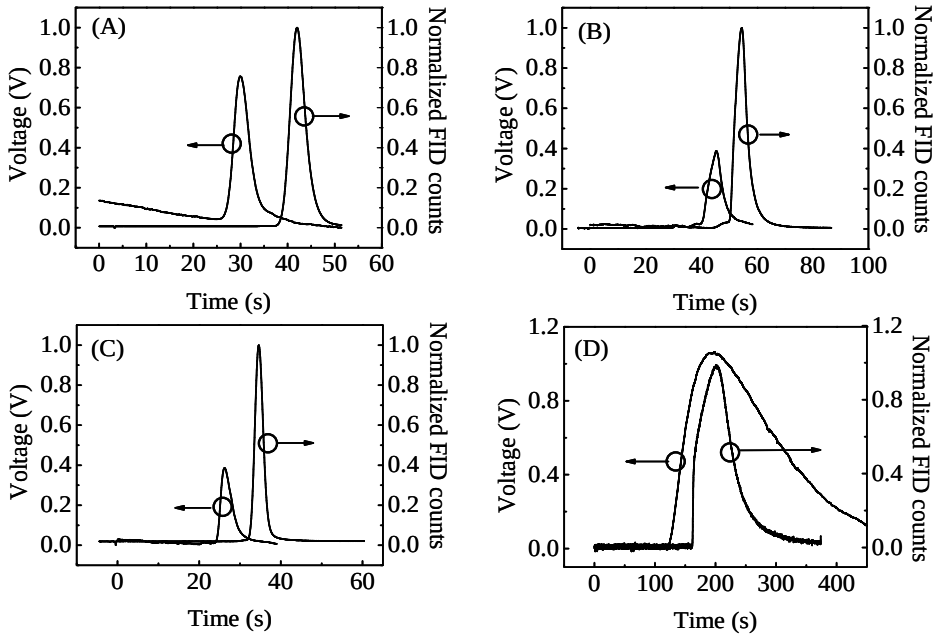

Figure 2.10 Response of the PEG 1000 coated FP sensor and the FID to (A) toluene, (B) decane, (C) methanol, and (D) DMMP. Peak heights from the FID are normalized. The retention time of toluene, decane, methanol and DMMP from the FP sensor (FID) is 30.0 s (42.0 s), 49.8 s (58.8 s), 30.7 s (39.1 s), and 192.3 s (200.3 s), respectively. The corresponding peak width at half maximum is 3.6 s (3.5 s), 5.8 s (5.0 s), 3.2 s (2.4 s), and 164.0 s (66.7 s), respectively. Reprinted with permission from [7]. Copyright 2010 American Chemical Society.

Figure 2.11 compares the DMMP sensing response obtained from the FID and the FP sensors. The two FP sensors are dip-coated in the PEG 1000 in methanol solution with a concentration of 15 mg/mL and 30 mg/mL, respectively. For the purpose of comparison, the FP sensor and the FID are connected directly to the GC injection port through a 1.6 m long GC guard column. The chromatograms obtained from the FP sensors are shifted so that they have the same response onset at the same time as that from the FID. The inset plots the relationship between the polymer layer thickness and the coating solution concentration. Three silicon wafers are used to simulate the coating event taking place on the FP sensor probe. They are dip-coated in the coating solution with the concentration of 30 mg/mL, 10 mg/mL, and 5 mg/mL, respectively. AFM is used to measure the polymer layer thickness on the silicon wafer. The corresponding thicknesses are 2.2 μm, 660 nm, and 330 nm, respectively.

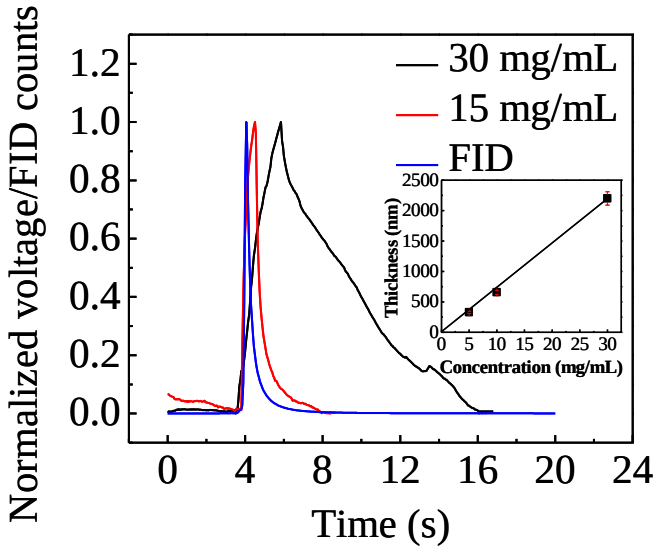

Figure 2.11 Comparison of the DMMP sensing response obtained from the FID and the FP sensors. Reprinted with permission from [7]. Copyright 2010 American Chemical Society.

The FP sensor response to various analyte masses is investigated. Two representative analytes, nonpolar decane and highly polar DMMP are selected. Figure 2.12 plots the peak height as a function of analyte mass. A linear response is observed for both analytes, though DMMP starts to saturate at the mass level larger than 20 ng. The sensitivity of the FP sensor for decane and DMMP is 4.75 and 77 mV/ng, respectively. This huge difference in sensitivity is caused by the different interactions between the analytes and the polymer coated on the FP sensor.

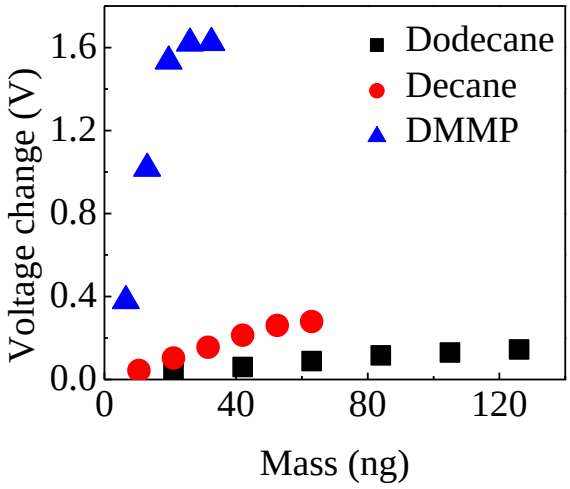

Figure 2.12 PEG 1000 coated FP sensor responses to decane, dodecane, and DMMP with various injected masses. Reprinted with permission from [7]. Copyright 2010 American Chemical Society.

One major contribution to the noise in the FP sensor signal is from thermal fluctuations, as they induce the thickness change (thermal expansion effect) and the refractive index change (thermo-optic effect). The temperature-induced FP sensor signal change can be described by the following equation, based on Eqs 2.2, 4, and 5:

$$\Delta I / I \propto \Delta\phi = \frac{4\pi}{\lambda}\Delta(nt) = (m \cdot 2\pi + 3\pi/2) \times \left(\frac{\partial n}{\partial T} \cdot \frac{1}{n} + \frac{\partial t}{\partial T} \cdot \frac{1}{t} \right) \times \Delta T, \tag{2.6}$$

where ΔT is the temperature variation. For most polymers, the thermal expansion coefficient, $\frac{\partial t}{t \cdot \partial T}$, is usually around 10^{-4} $^{o}C^{-1}$, and the thermo-optic coefficient, $\frac{\partial n}{\partial T}$, is around 10^{-4} $^{o}C^{-1}$. m is usually on the order of 1 for the polymer thickness of 1 μm, $\lambda \approx 1550$ nm, and n is approximately 1.5. Consequently, the corresponding fractional intensity change should be on the order of 10^{-3}-10^{-4} $^{o}C^{-1}$.

On the basis of the above discussion, we experimentally characterize the temperature response of the PEG 1000 coated FP sensor by placing it in a temperature-controlled oven. As expected, the signal change caused by the interference shift is sinusoidal as plotted in Fig. 2.13. The highest temperature change is at the quadrature point with the estimated slope of 0.036 V/^{o}C. Usually, the temperature stability of 0.01 ^{o}C can be achieved, leading to a thermally related noise level on the order of 0.36 mV (which is 4.2×10^{-4} of the baseline signal 0.84 V at 23 or 70 ^{o}C) and hence a detection limit of approximately 75 and 5 pg for decane and DMMP, respectively. However, it should be noted that, in addition to thermally induced noise, electronic noise and laser source noise may contribute to the total system noise. Currently, our system has a noise level of 7 mV, which results in a detection limit of approximately 50 pico-grams for DMMP. Future improvement in data acquisition and in optical design will certainly lower the noise in these aspects.

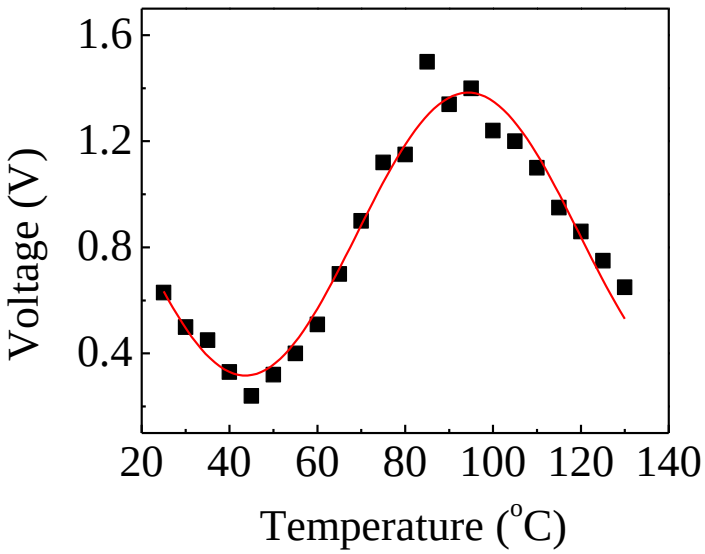

Figure 2.13 Temperature dependent response of the PEG 1000 coated FP sensor. Solid line is the sinusoidal curve fit. Reprinted with permission from [7]. Copyright 2010 American Chemical Society.

Figure 2.14 shows the FP response to various concentrations of DMMP. The FP is connected to a 1.9 meter long Carbowax coated GC column (inner diameter: 0.25 mm). The flow rate is 1.2 mL/min. The chromatograms are obtained isothermally at room temperature. The DMMP retention time is approximately 157 seconds, which is confirmed by our GC-MS system. The FP sensor system has a noise level of 7 mV, which includes thermally-induced noise, electronic noise, and laser source noise. The detection limit for DMMP is approximately 50 pico-grams as shown in Fig. 2.14.

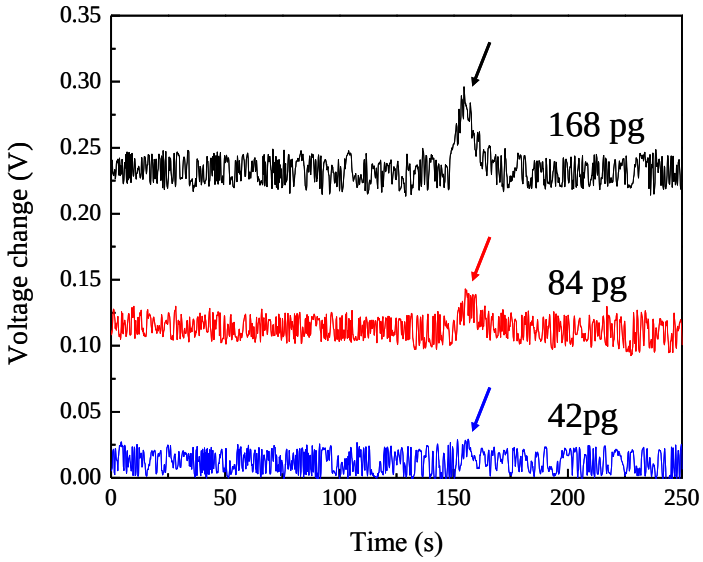

Figure 2.14. The response of the FP sensor to various concentrations of DMMP. The chromatograms are vertically shifted for clarity. Reprinted with permission from [7]. Copyright 2010 American Chemical Society.

Figure 2.15(A) shows the FP response to DMMP and DEMP when the oven temperature is increased at a rate of 10 ^{o}C/min. The DMMP and diethyl methylphosphonate (DEMP) peaks are superimposed on the broad sinusoidal like background induced by the temperature change (see Fig. 2.13). The chromatogram obtained with the FP sensor is confirmed by our GC-MS system (see Fig. 2.15(B)).

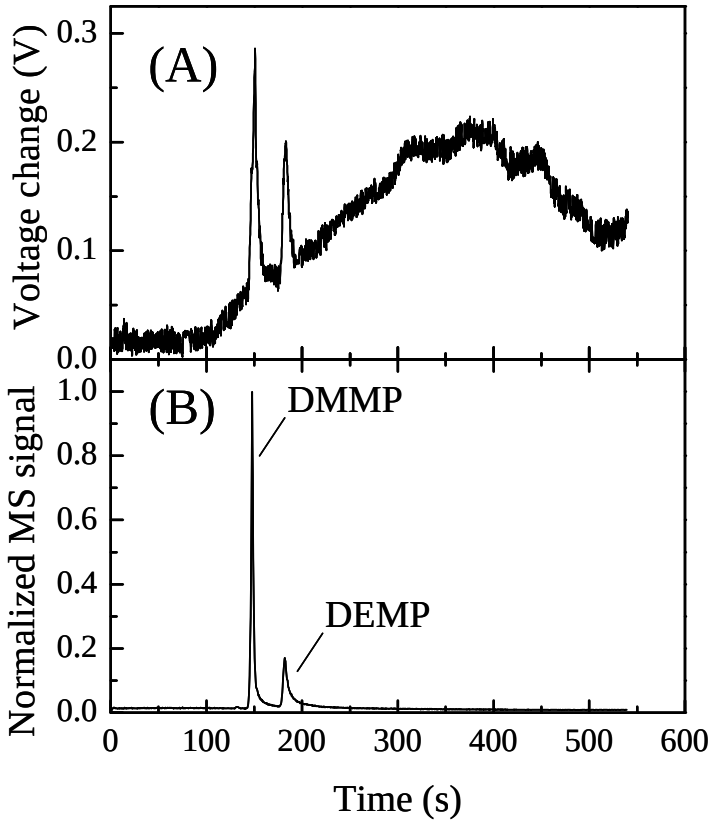

Figure 2.15. Chromatograms with temperature ramping. (A) The response of the FP sensor to DMMP and DEMP. (B) The corresponding results obtained with the GC-MS system. Temperature is started at 30 ^{o}C, held for 1 min, raised to 100 ^{o}C at a rate of 10 ^{o}C/min, and finally held for 1 min. Other parameters are the same as in Fig. 2.14. Reprinted with permission from [7]. Copyright 2010 American Chemical Society.

References

1. P. R. Lewis, R. P. Manginell, D. R. Adkins, R. J. Kottenstette, D. R. Wheeler, S. S. Sokolowski, D. E. Trudell, J. E. Byrnes, M. Okandan, J. M. Bauer, R. G. Manley, and G. C. Frye-Mason, "Recent advancements in the gas-phase MicroChemLab," IEEE Sens. J. **6**, 784-794 (2006).
2. J. Lammertyn, E. A. Veraverbeke, and J. Irudayaraj, "zNose technology for the classification of honey based on rapid aroma profiling," Sens. Actuator. B **98**, 54-62 (2004).
3. S. Sorge, and T. Pechstein, "Fully integrated thermal conductivity sensor for gas chromatography without dead volume," Sens. Actuators A **63**, 191-195 (1997).
4. D. Cruz, J. P. Showalter, F. Gelbard, R. P. Manginell, and M. G. Blain, "Microfabricated thermal conductivity detector for the micro-ChemLab," Sens. Actuators B **121**, 414-422 (2007).
5. J. Sun, D. Cui, X. Chen, L. Zhang, H. Cai, and H. Li, "Design, modeling, microfabrication and characterization of novel micro thermal conductivity detector," Sens. Actuators B **160**, 936-941 (2011).
6. S. K. Kim, H. Chang, and E. T. Zellers, "Microfabricated gas chromatograph for the selective determination of trichloroethylene vapoer at sub-parts-per-billion concentrations in complex mixtures," Anal. Chem. **83**, 7198-7206 (2011).
7. J. Liu, Y. Sun, D. J. Howard, G. Frye-Mason, A. K. Thompson, S.-j. Ja, S.-K. Wang, M. Bai, H. Taub, M. Almasri, and X. Fan, "Fabry-Pérot cavity sensors for multipoint on-column micro gas chromatography detection," Anal. Chem. **82**, 4370-4375 (2010).
8. J. Liu, N. K. Gupta, K. D. Wise, Y. B. Gianchandani, and X. Fan, "Demonstration of motionless Knudsen pump based micro-gas chromatography featuring micro-fabricated columns and on-column detectors," Lab Chip **11**, 3487-3492 (2011).
9. Y. Sun, J. Liu, D. J. Howard, G. Frye-Mason, A. K. Thompson, S.-j. Ja, and X. Fan, "Rapid tandem-column micro-gas chromatography based on optofluidic ring resonators with multi-point on-column detection," Analyst **135**, 165-171 (2010).
10. Y. Sun, S. I. Shopova, G. Frye-Mason, and X. Fan, "Rapid chemical-vapor sensing using optofluidic ring resonators," Opt. Lett. **33**, 788-790 (2008).
11. Y. Sun, and X. Fan, "Analysis of ring resonators for chemical vapor sensor development," Opt. Express **16**, 10254-10268 (2008).
12. Y. Sun, J. Liu, G. Frye-Mason, S.-j. Ja, A. K. Thompson, and X. Fan, "Optofluidic ring resonator sensors for rapid DNT vapor detection," Analyst **134**, 1386-1391 (2009).
13. J. Liu, Y. Sun, and X. Fan, "Highly versatile fiber-based optical Fabry-Pérot gas sensor," Opt. Express **17**, 2731-2738 (2009).
14. Y. S. Cheng, and K. L. Yeung, "Palladium-silver composite membranes by eletroless plating technique," J. Mem. Sci. **158**, 151-156 (1999).
15. S. S. Yun, K. W. Jo, and J. H. Lee, "Inline fiber optic chemical sensor using a self-aligned epoxy microbridge with a metal layer," IEEE J. Sel. Top. Quantum. Elelctron. **13**, 381-385 (2007).
16. R. P. Podgorsek, and H. Franke, "Selective optical detection of aromatic vapors," Appl. Opt. **41**, 601-608 (2002).
17. A. Ksendov, M. L. Homer, and A. M. Manfreda, "Integrated optics ring-resonator chemcial sensor with polymer transduction layer," Electron. Lett. **40**, 63-65 (2004).

18. F. Pang, X. Han, F. Chu, J. Geng, H. Cai, R. Qu, and Z. Fang, "Sensitivity to alchohols of a planar waveguide ring resonator fabricated by a sol-gel method," Sens. Actuators B **120**, 610-614 (2007).
19. S. I. Shopova, I. M. White, Y. Sun, H. Zhu, X. Fan, G. Frye-Mason, A. Thompson, and S. J. Ja, "On-column micro gas chromatography detection with capillary-based optical ring resonators," Anal. Chem. **80**, 2232-2238 (2008).

Chapter III

Other Components in Micro-Gas Chromatography

3.1 Pre-concentrator

The pre-concentrator is widely used in μGC systems to trap gas analytes and re-inject them at a high temperature onto a downstream separation column in a sharp peak, artificially pre-concentrating gas analytes [1-4]. It plays an important role to increase the sensitivity and detection limit of the μGC system.

3.1.1 Fabrication and performance calibration

The pre-concentrator* used in my experiments is a stainless steel tube (0.318 cm i.d.) packed with 2.1 mg of Carboxen 1018 (sieved to ~ 200 μm in diameter(60/80 mesh)) held in place with a wire mesh and salinized glass wool (see Fig. 3.1). It is preconditioned initially at 300 ˚C for 24 hours under N_2. The pre-concentrator is wrapped with an insulated copper heater wire and thermally desorbed at 300 ˚C for 5 min, which served to transfer the vapor mixture to the 1st column by the six-port valve actuation. A thermocouple is installed at the center of the pre-concentrator to monitor its temperature in real-time. The capacity of the pre-concentrator is verified in a separate series of tests, showing that the mass of each analyte trapped and transferred to the downstream GC matched that expected (within 1 %).

*Pre-concentrator is provided by Prof. Kurabayashi at Mechanical Engineering Department, at University of Michigan.

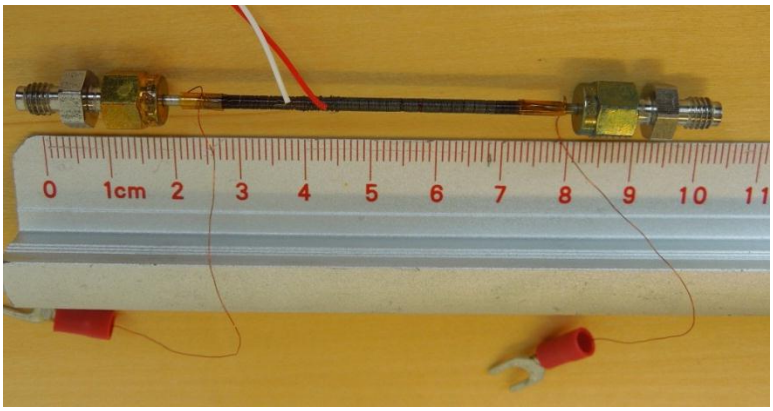

Figure 3.1. Photo of the pre-concentrator.

3.2 Micro-fabricated column

Current μGC systems often use a short capillary column [5, 6] or a micro-fabricated rectangular column [7-16] with attached heating components to satisfy the requirements on system size and detection speed. In our system, micro-fabricated separation column is used.

3.2.1 Fabrication

The micro-fabricated GC column (see Fig. 3.2) is fabricated by deep reactive ion etching of a 25 cm long double spiral channel into a silicon substrate, having a footprint of 1.1 cm by 1.1 cm. A Pyrex 7740 glass cover plate is bonded anodically to the silicon substrate to seal the channel. The rectangular cross section of the channel is 150 μm wide and 240 μm deep. The connection of the micro-fabricated column to other components is made by inserting short conventional GC columns (inner diameter 100 μm, outer diameter 245 μm) to its inlet and outlet ports (245 μm wide and 245 μm deep). Two heaters and one thermal couple are also embedded on the back of the micro-fabricated column for heating and temperature monitoring purposes.

The micro-fabricated columns for this study are coated with non-polar polymer of

OV-1 or polar polymer of OV-215. The coating procedure included four steps. (1) The non-polar coating solution is prepared by dissolving 22.3 mg OV-1 and 0.2 mg dicumyl peroxide in a 6 mL mixture of 1:1 (v:v) pentane and dichloromethane, whereas the polar coating solution is prepared by dissolving 20 mg OV-215 and 0.2 mg dicumyl peroxide in a 5 mL mixture of 1:4 (v:v) ether and ether acetate; (2) The micro-fabricated channel is filled with coating solution and held for 5 min; (3) The solvent is evaporated from one end of the column by a vacuum pump while the other end is sealed with a septum; (4) The polymer coating is cross-linked to the inner wall of the column by ramping the column temperature from 160 ^{o}C to 180 ^{o}C at a rate of 0.2 ^{o}C/min and staying at 180 ^{o}C for one hour. The resultant column coating has a uniform thickness of around 200 nm.

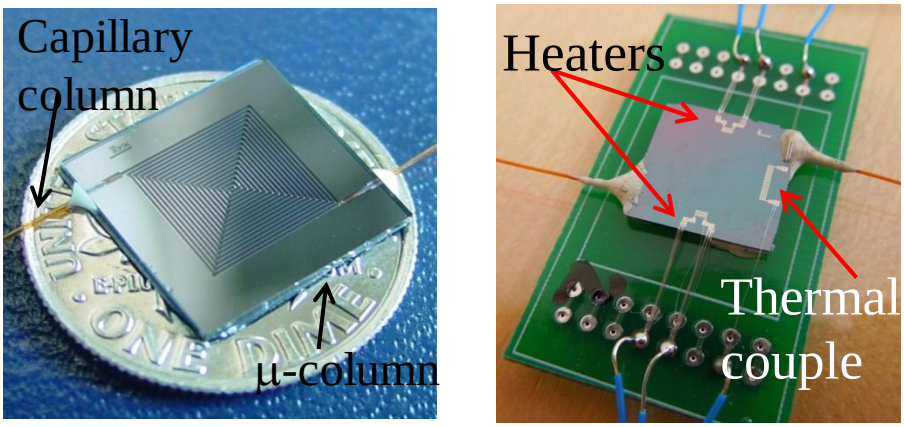

Figure 3.2. Photo of the front (A) and back (B) of the micro-fabricated separation column.

3.2.2 Performance test

In order to test the separation efficiency of the micro-fabricated column, the micro-fabricated column is applied to separate methane and octane. It is 25 cm long and coated with OV-1, which is then connected to GC injection port and FID for detection. The oven temperature is kept at 180 ^{o}C. Various flow rates are used. One of the chromatograms is shown in Fig. 3.3.

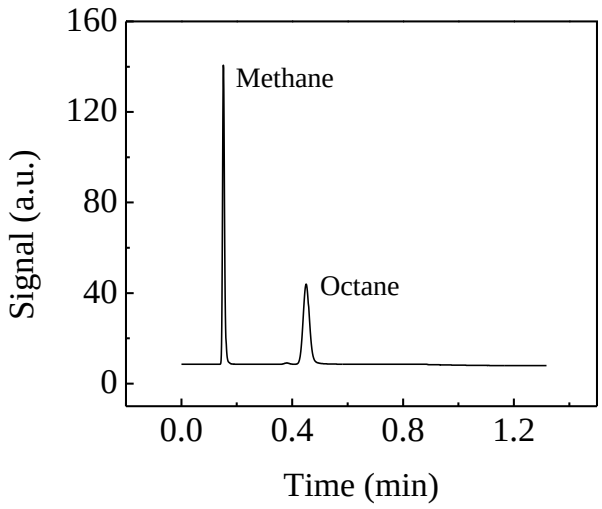

Figure 3.3. Separation chromatogram of methane and octane.

In the following sections, we use two values to evaluate the separation efficiency of the micro-fabricated column.

3.2.2.1 Number of theoretical plates (N)

Number of theoretical plates is also known as column efficiency which is calculated by Equation 3.1[17, 18].

$$N = 5.545 \times \frac{t^2}{w^2} \tag{3.1}$$

where t and w is the retention time and full width at half maximum of an elution peak, respectively.

A column with a high plate number has narrower peak at a given retention time than that with a lower plate number, and thus it is considered to be more efficient. The plate number of the micro-fabricated column is calculated to be 1819.1 by the Eqs. 3.1, which is comparable to that for a commercial capillary based separation column.

3.2.2.2 Height equivalent to a theoretical plate (H)

Another measure of column efficiency is the height equivalent to a theoretical plate denoted as H, which calculates the length of each theoretical plate using Equitation 3.2 [18, 19].

$$H = \frac{L}{N} \tag{3.2}$$

where L is the length of the column, and N is its plate number.

The shorter each theoretical plate, the more plates are contained in a given length of the column. Figure 3.4 plots the height equivalent to a theoretical plate under various flow rates, which is also known as the Golay plot.

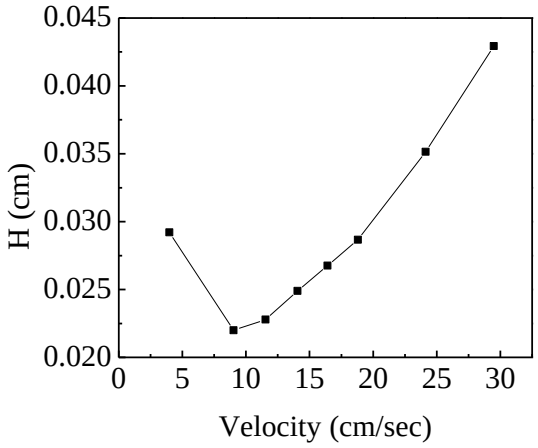

Figure 3.4. Golay plot of the micro-fabricated separation column.

3.2.2.3 Temperature ramping capability

The micro-fabricated column is capable of performing temperature ramp on chip and monitoring its temperature in real time. In order to calibrate the relationship between the resistance of the embedded thermal couple and column temperature, the micro-fabricated column is placed in a temperature controlled oven. The resistance of the thermal couple is recorded at various temperatures, as plotted in Fig. 3.5. The resistance of the thermal

couple is approximately 290 ohms at room temperature and increases almost linearly as the temperature increases. According to this relationship, the column temperature can be predicted by measuring the resistance of the thermal couple.

The temperature ramping speed is tested by applying 6 V to two embedded heaters on the micro-fabricated column. The two heaters are able to achieve a ramping rate of approximately 30 ^{o}C/min.

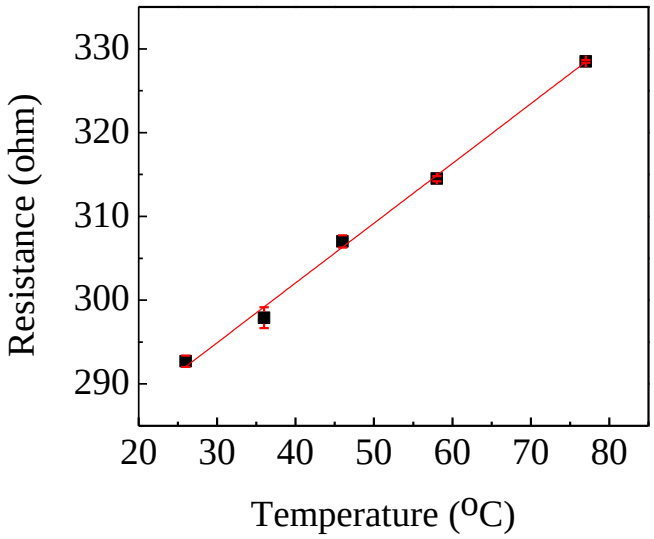

Figure 3.5 Relationship between the resistance of the thermal couple and column temperature.

3.3. Gas pump

3.3.1 Introduction

Compared to the fast development of μGCs, the progress in using new types of miniature pumps, however, has been modest. To date, diaphragm pumps [5, 20, 21] and turbo molecular pumps [22] have been integrated with various μGC systems. Although different in design details and pumping mechanisms, these pumps all rely on mechanical motion to provide the flow needed in μGC systems. The moving parts present challenges with reliability, and typically require lubrication and maintenance, making these

unsuitable for extended deployment in remote locations or harsh environment. Additionally, miniaturization of mechanical pumps compromises performance, as frictional forces assume a dominant role.

3.3.2 Knudsen pump

The Knudsen pump* (KP) is a motionless pump based on thermal transpiration, which drives the flow of gas molecules from the cold end to the hot end within a narrow channel subjected to a temperature gradient [23-29]. In the long term, the KP has a number of potential advantages over the mechanical pump. First, the absence of moving parts results in enhanced reliability and maintenance-free operation exceeding 10^4 hours of continuous operation, making these pumps attractive for operation in remote and inaccessible environments. Second, the absence of any noise or sound from these pumps is appealing for hospital environments or surveillance applications. Third, the KP's performance scales favorably with its size. In order to make the transpiration phenomenon significant in the KP, it is necessary for the channel diameter to be on the order of sub-micron or nanometer.

Although the thermal transpiration phenomenon was first studied back in 1879 and recognized as a promising technology for making motionless pumps, most of the KPs reported before early 2000s were operated at sub-atmospheric pressure due to the lack of appropriate materials or methods to form sufficiently small channels. The introduction of new materials with sub-micron channels and the advance of micro-fabrication technology have recently led to miniaturized KPs capable of operating at the atmospheric pressure and generating reasonably high pumping pressures [24, 29-31]. However, flow rate and

*Knudsen pump is provided by Prof. Gianchandani at Electrical Engineering and Computer Science Department, at University of Michigan.

pressure have remained as challenges, and the practical application of a miniature KP to μGC systems has not been reported prior to this effort.

In our μGC system, a novel KP array consisted of six KPs connected in series is used [24, 29] which can provide a sufficient flow rate (>0.1-1 mL/min) for the μGC system with either helium or dry air as the carrier gas rate.

3.3.2.1 Fabrication process

The KP array consists of six KP elements connected in series. Each KP element is made of a mesoporous polymer membrane (diameter ≈11.5 mm, thickness ≈105 μm, pore diameter ≈25 nm, porosity ≈70%) sandwiched between a heated brass top and a passively cooled brass base. A single KP element is shown in Fig. 3.6(A), whereas series arrangement is illustrated in Fig. 3.6(B). The density of the mesoporous polymer membrane is approximately $10^{11}/cm^2$; this, along with a structure that is relatively free of defects, allow the relatively high flow rate necessary for the μGC operation [24, 29].

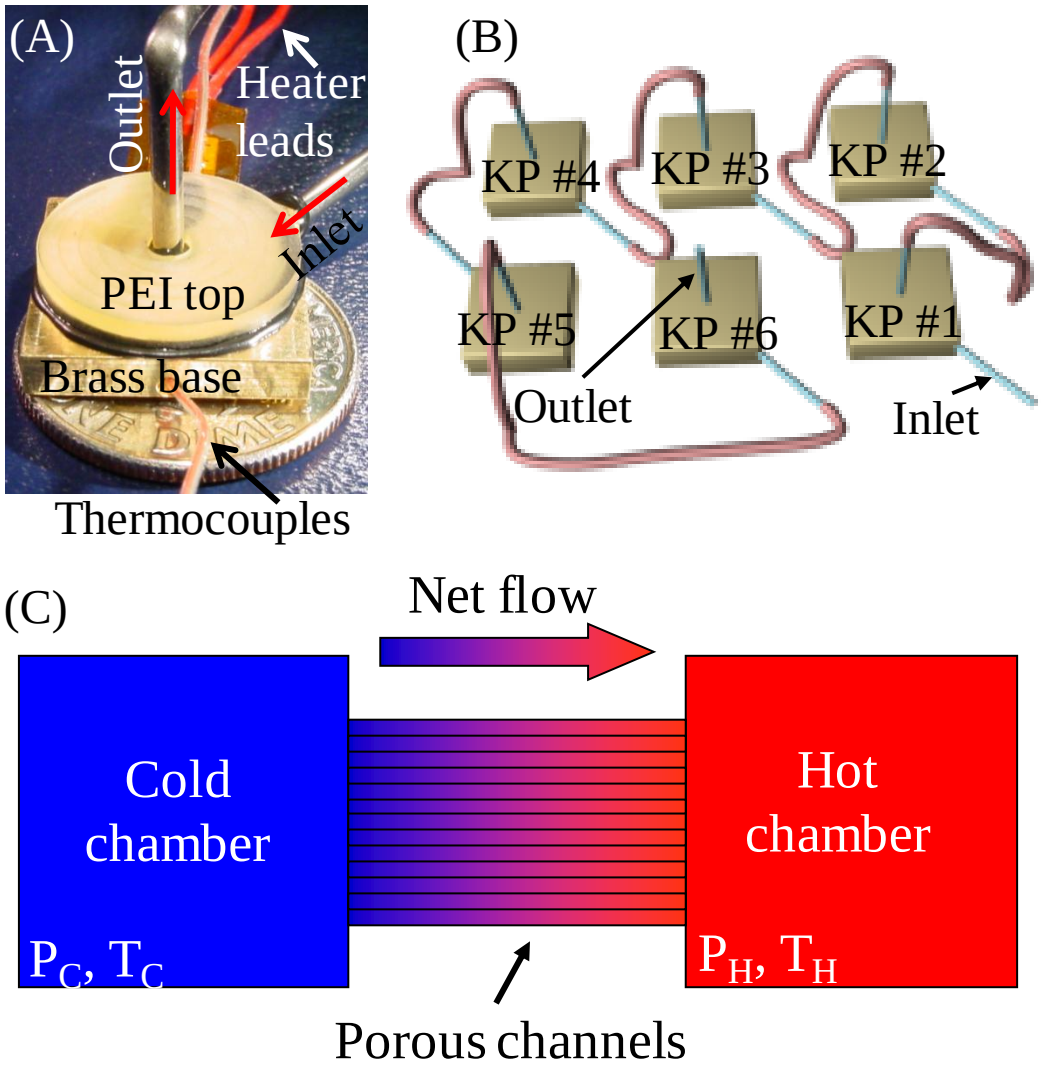

Figure 3.6. (A) Photo of the KP element used as a building block for the KP array; (B) Diagram of the KP array which connects six single KP in series; (C) Schematic of a KP element which uses narrow channels (which can sustain free-molecular or transitional flow) subjected to a longitudinal temperature gradient to pump gas along the temperature gradient.

The temperature bias between the hot and cold brass plates results in the gas movement from the cold end to the hot end, as illustrated in Fig. 3.6(C). At equilibrium, the pressure ratio between the hot end (P_H) and the cold end (P_C) is ideally provided by the ratio of the square roots of the absolute temperature (T_H and T_C): $\frac{P_H}{P_C} = \frac{\sqrt{T_H}}{\sqrt{T_C}}$. In our

experiment, temperature biases ranging from 38 to 96 K are applied across each of the KP elements. The temperature bias across each of the KP elements is controlled and monitored in real-time by a customized LABVIEW^{TM} program through thermocouples (Newport Electronics, 5SRTC-TT-K-40-36) attached to the hot end and the cold end, respectively. Six KP elements connect in series to build a KP array, which can provide a typical flow rate for the proposed μGC system of 0.5mL/min. The hydraulic connections between elements are made by clear Tygon tubes (inner diameter 0.18 mm).

3.3.2.2 Performance calibration

First, the flow rate provided by the KP array is tested when using helium as the carrier gas. As shown in Fig. 3.7, the flow rate delivered by KP array increases almost allometrically as the voltage applied increases. When the total applied voltage is 54 V, corresponding to 9 V applied on each KP element, the flow rate achieves 0.62 mL/min.

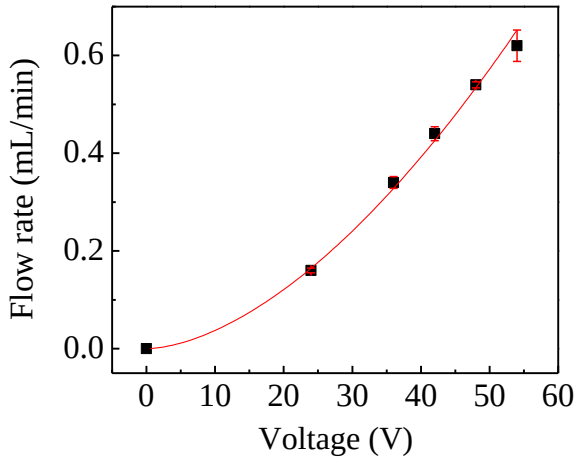

Figure 3.7. Relationship between flow rate and applied voltage when helium is used as the carrier gas.

Next, the flow rate is tested when using dry air as the carrier gas. Figure 3.8 plots the relationship between the flow rate and the applied voltage. The flow rate increases allometrically as the applied voltage increases, which is consistent with the situation

when using helium as the carrier gas. However, the flow rate provided by the KP array when using dry air as the carrier gas is lower than the flow rate when using helium as the carrier gas, which is because the dry air, mainly containing nitrogen, is heavier than helium. The highest flow rate achieved is 0.54 mL/min when dry air is used as the carrier gas.

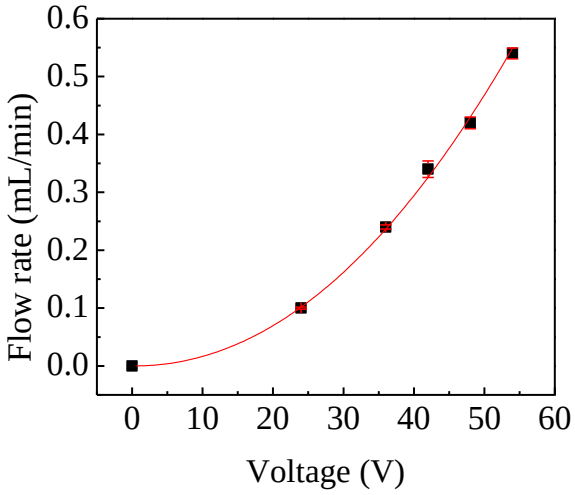

Figure 3.8. Relationship between the flow rate and applied voltage when dry air is used as the carrier gas.

References

1. W.-C. Tian, H. K. L. Chan, C.-J. Lu, S. W. Pang, and E. T. Zellers, "Multiple-stage microfabricated preconcentrator-focuser for micro gas chromatography system," J. Microelectromech. Syst. **14**, 498-507 (2005).
2. P. Ivanov, F. Blanco, I. Gria, N. Sabat, A. Ruiz, X. Vilanova, X. Correig, L. Fonseca, E. Figueras, J. Santander, and C. Can, "Improvement of the gas sensor response via silicon preconcentrator," Sens. Actuator B: Chemical **127**, 288-294 (2007).
3. F. Bender, N. Barié, G. Romoudis, A. Voigt, and M. Rapp, "Development of a preconcentration unit for a SAW sensor micro array and its use for indoor air quality monitoring," Sens. Actuators, B **93**, 135-141 (2003).
4. J. H. Seo, J. Liu, X. Fan, and K. Kurabayashi, "Effect of thermal desorption kinetics on vapor injection peak irregularities by a microscale gas chromatography preconcentrator," Anal. Chem. **84**, 6336-6340 (2012).
5. C.-J. Lu, J. Whiting, R. D. Sacks, and E. T. Zellers, "Portable Gas Chromatograph with Tunable Retention and Sensor Array Detection for Determination of Complex Vapor Mixtures," Anal. Chem. **75**, 1400-1409 (2003).
6. E. J. Staples, and S. Viswanathan, "Ultra-High Speed Chromatography and Virtual Chemical Sensors for Detecting Explosives and Chemical Warfare Agents," IEEE Sens. J. **5**, 622- 631 (2005).
7. H.-S. Noh, P. J. Hesketh, and G. C. Frye-Mason, "Parylene gas chromatographic column for rapid thermal cycling " J. Microelectromech. Syst. **11**, 718-725 (2002).
8. G. Lambertus, A. Elstro, K. Sensening, J. Potkay, M. Agah, S. Scheuering, K. Wise, F. Dorman, and R. Sacks, "Design, Fabrication, and Evaluation of Microfabricated Columns for Gas Chromatography " Anal. Chem. **76**, 2629-2637 (2004).
9. E. B. Overton, K. R. Carney, N. Roques, and H. P. Dharmasena, "Fast GC Instrumentation and Analysis for Field Applications " Field Anal. Chem. Technol. **5**, 97-105 (2001).
10. C. M. Yu, M. Lucas, C. Koo, P. Stratton, T. DeLima, and E. Behymer, "High performance hand-held gas chromatograph," American Society of Mechanical Engineers, Dynamic Systems and Control Division (Publication) **66**, 481-486 (1998).
11. E. S. Kolesar Jr., and R. R. Reston, "Review and summary of a silicon micromachined gas chromatography system " IEEE Trans. Compon., Packag., Manuf. Technol. **21**, 324-328 (1998).
12. L. Lorenzelli, A. Benvenuto, A. Adami, V. Guarnieri, B. Margesin, V. Mulloni, and D. Vincenzi, "Development of a gas chromatography silicon-based microsystem in clinical diagnostics " Biosens. Bioelectron. **20**, 1968-1976 (2005).
13. G. Lambertus, and R. Sacks, "Stop-flow programmable selectivity with a dual-column ensemble of microfabricated etched silicon columns and air as carrier gas," Anal. Chem. **77**, 2078-2084 (2005).
14. M. Stadermann, A. D. McBrady, B. Dick, V. R. Reid, A. Noy, R. E. Synovec, and O. Bakajin, "Ultrafast gas chromatography on single-wall carbon nanotube stationary phases in microfabricated channels " Anal. Chem. **78**, 5639-5644 (2006).
15. S. Reidy, G. Lambertus, J. Geece, and R. Sacks, "High-performance, static-coated silicon microfabricated columns for gas chromatography " Anal. Chem. **78**, 2623-2630 (2006).

16. S. Reidy, D. George, M. Agah, and R. Sacks, "Temperature-programmed GC using silicon microfabricated columns with integrated heaters and temperature sensors " Anal. Chem. **79**, 2911-2917 (2007).
17. G. R. Lambertus, C. S. Fix, S. M. Reidy, R. A. Miller, D. Wheeler, E. Nazarov, and R. Sacks, "Silicon microfabricated column with microfabricated differential mobility spectrometer for GC analysis of volatile organic compounds," Anal. Chem. **77**, 7563-7571 (2005).
18. H. M. McNair, and J. M. Miller, *Basic gas chromatography* (John Wiley&Sons, Inc., Hoboken, 2009).
19. G. E. Spangler, "Height equivalent to a theoretical plate theory for rectangular GC columns," Anal. Chem. **70**, 4805-4816 (1998).
20. J. J. Whiting, C.-J. Lu, E. T. Zellers, and R. D. Sacks, "A Portable, High-Speed, Vacuum-Outlet GC Vapor Analyzer Employing Air as Carrier Gas and Surface Acoustic Wave Detection," Anal. Chem. **73**, 4668-4675 (2001).
21. E. C. Apel, A. J. Hills, R. Lueb, S. Zindel, S. Eisele, and D. D. Riemer, "A fast-GC/MS system to measure C2 to C4 carbonyls and methanol aboard aircraft," J. Geophys. Res. **108**, 8794-8815 (2003).
22. J. A. Syage, B. J. Nies, M. D. Evans, and K. A. Hanold, "Field-portable, high-speed GC/TOFMS," J. Am. Soc. Mass. Spectrom. **12**, 648-655 (2001).
23. O. Reynolds, "On certain dimensional properties of matter in the gaseous state," Phil. Trans. R. Soc. Lond. **170**, 727-845 (1879).
24. N. K. Gupta, and Y. B. Gianchandani, "Thermal transpiration in zeolites: a mechanism for motionless gas pumps," Appl. Phys. Lett. **93**, 193511 (2008).
25. N. K. Gupta, and Y. B. Gianchandani, "Thermal transpiration in mixed cellulose ester membranes: enabling miniature, motionless gas pumps," Micropor. Mesopor. Mater. **142**, 535–541 (2011).
26. J. C. Maxwell, "On stresses in rarified gasses arising from inequalities of temperature," Phil. Trans. R. Soc. Lond. **170**, 231-256 (1879).
27. E. Kennard, *Kinetic Theory of Gases* (McGraw Hill, New York, 1938).
28. L. Loeb, *The Kinetic Theory of Gases* (McGraw Hill, New York, 1934).
29. N. K. Gupta, and Y. B. Gianchandani, "Thermal transpiration in mixed cellulose ester membranes: enabling miniature, motionless gas pumps," Micropor. Mesopor. Mater. (2010).
30. A. A. Alexeenko, S. F. Gimelshein, E. P. Muntz, and A. D. Ketsdever, "Kinetic modeling of temperature driven flows in short microchannels," Int. J. Therm. Sci. **45**, 1045-1051 (2006).
31. S. McNamara, and Y. B. Gianchandani, "On-chip vacuum generated by a micromachined Knudsen pump," J. Microelectromech. Syst. **14**, 741-746 (2005).

Chapter IV

One-Dimensional Micro-Gas Chromatography

In this chapter, one dimensional (1-D) sub-μGC is implemented in two 1-D system configurations: single- and tandem- column configurations. The single-column system has only one stationary phase, polar or non-polar, so that it separates gas analytes either based on their volatilities (non-polar stationary phase) or polarities (polar stationary phase). In contrast, tandem-column system integrates two columns with different stationary phases [1-8] to separate a wide range of samples more efficiently than single-column configuration, compensating for the deficiency of short length usually used in μGCs. Unfortunately, the tandem-column based μGC still inevitably suffers from the same co-elution problem as in a short single-column μGC, *i.e.*, analytes already separated from the first column may co-elute after passing through the second one [9, 10]. Since traditional GC detectors carry out detections only at the terminal end of the tandem-column system, it is difficult to differentiate the co-eluted analytes from each other. Current methods to solve this problem use a pressure valve [2, 6] or a temperature control module [7] to modulate the retention times of the analytes. However, these methods may require samples to be tested several times under different conditions before they can be fully separated [11, 12], which significantly increases the operation complexity and the detection time.

In contrast, the on-column detection provides a very promising approach to addressing the co-elution problem. In this scheme, analytes are detected when they travel along the column, rather than after they elute out from the terminal end of the tandem-column system. The on-column detection scheme has the highly desirable feature of flexibility in selecting the detection location along the column [9, 10]. Moreover, multiple detectors can be installed at pre-determined locations along the column to independently measure the retention time of each analyte and provide complementary chromatograms. As a result, each analyte can be separated on at least one detection location in a single test without having to use any additional components, considerably simplifying the detection operation and system design [9, 10].

4.1 Macro-scale sub-system integration

First, a sub-system integrated with macro-scale components is tested. Conventional GC injection port, capillary separation column and FP on-column detector are used in this section.

4.1.1 Single-column system

4.1.1.1 System description

The experimental setup is illustrated in Fig. 4.1. The FP sensor module is connected to the GC injection port through a 1.6 m long GC guard column, followed by a 1.3 m long Carbowax coated GC column. Gas analyte extracted from the head space of the bottle containing the analyte by a SPME fiber (PDMS/DVB, 65 μm diameter fiber, Supelco 57310-U) is injected through the GC injector (HP 5890, heated to 250 ^{o}C). Ultra high purity (UHP) helium is used as carrier gas. The flow rate is 0.3 mL/min. GC columns and FP sensor modules are all kept at room temperature. For comparison purposes, we also use FID to detect the analyte. The FID temperature is set at 325 ^{o}C.

4.1.1.2 Separation result

A mixture of four different analytes is injected through the GC injection port, which is separated as it travels through the 1.6 m long GC guard column, followed by a 1.3 m long Carbowax coated GC column. The separated analytes are detected by the FP sensor at the terminal end of the single-column system (Fig. 4.1). Nonpolar analytes (*i.e.*, acetone, toluene and decane) interacted weakly with the polar Carbowax coated GC column have sharp peaks and short retention times of within 50 seconds, whereas the heavy dodecane elutes out at around 150 seconds with a relatively broad peak (see Fig. 4.2).

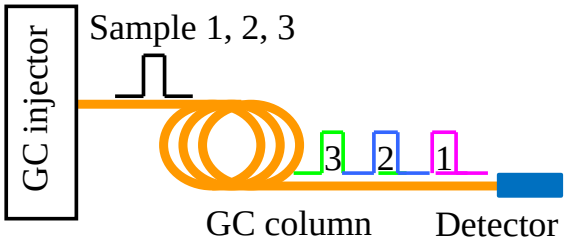

Figure 4.1. Schematic of the experimental setup. Reprinted with permission from [17]. Copyright 2010 American Chemical Society.

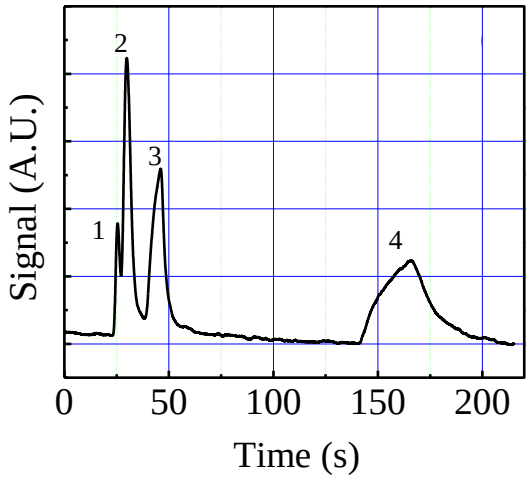

Figure 4.2. Chromatograms of acetone, toluene, decane, and dodecane obtained from the PEG 1000 coated FP sensor module in the single-column system illustrated in Fig. 4.1. The retention time of each analyte is 25.4 s, 29.8 s, 46.0 s, and 165.8 s, respectively. Reprinted with permission from [17]. Copyright 2010 American Chemical Society.

4.1.2 Tandem-column system

4.1.2.1 System description

For the tandem-column system (Fig. 4.3), the first FP sensor module is installed at the end of the first 0.9 m long RTX-1 GC column, and the second one is at the end of the second 0.2 m long Carbowax GC column. Other parameters are the same as the parameters in single column system experiment.

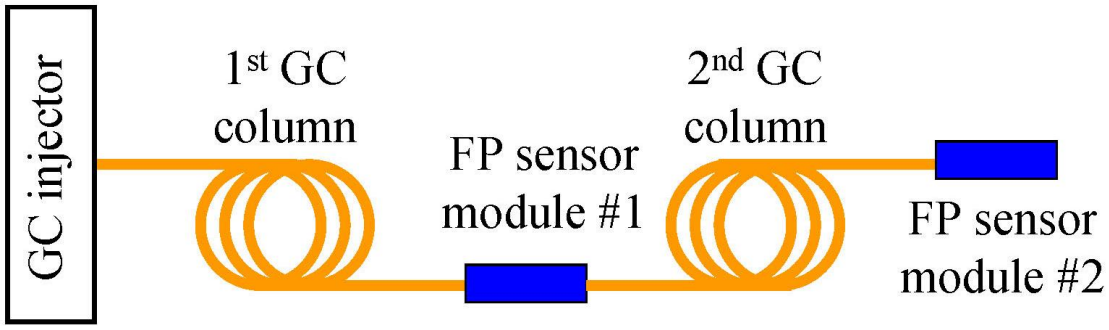

Figure 4.3. Schematic of the experimental setup. Reprinted with permission from [17]. Copyright 2010 American Chemical Society.

4.1.2.2 Separation result

In the tandem-column system plotted in Fig. 4.3, two FP sensors coated with PDMS and PEG 1000 are respectively installed at the end of the first (RTX-1 coated) and second (Carbowax coated) GC column. A mixture comprising both polar and nonpolar analytes is used to investigate the system separation capability and selectivity. Comparison between the two chromatograms from the two FP sensors (Fig. 4.4) shows no significant change in retention time for alkanes (octane, decane and undecane), owing to the weak interaction between nonpolar alkanes and the polar Carbowax coated second column. In contrast, the retention times of the polar DMMP and DEMP are considerably increased by the second column, leading to the co-elution of DMMP and decane. Despite of the co-elution at the

second column, the first FP sensor is able to provide a chromatogram from the first column, in which all the analytes are well resolved. For a comparison, the FID is placed at the terminal end of the tandem-column system (in the absence of the two FP modules) to carry out detection under the same experimental conditions. As expected, the result from the FID is almost consistent with that from the second FP sensor. Note that DMMP and decane from the FID are completely overlapped. Separate experiments using individual analytes confirms that the overlapped peak indeed contained co-eluted DMMP and decane.

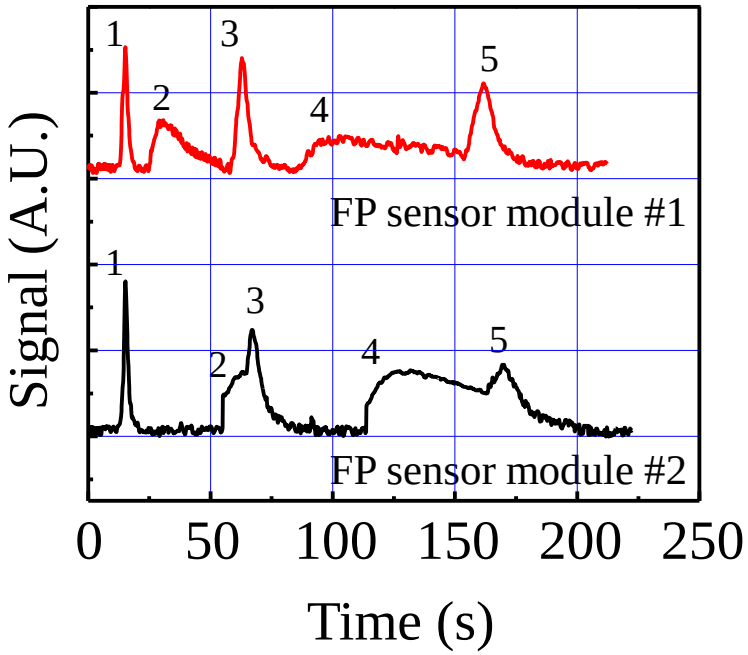

Figure 4.4. Chromatograms obtained from the two FP sensor modules in the tandem-column system illustrated in Fig. 4.3. The first FP sensor is coated with PDMS and the second with PEG 1000. For a comparison, a FID chromatogram obtained at the terminal end of the tandem-column system is also presented. All the peaks are normalized to the first peak. Curves are vertically shifted for clarity. The retention time for each analyte obtained from Module #1 (Module #2 and FID) is: 15.0 s (15.7 s and 15.7 s) for octane, 29.4 s (64.8 s and 66.3 s) for DMMP, 63.1 s (67.3 s and 66.3 s) for decane, 98.5 s (125.0 s and 126.0 s) for DEMP, and 162.1 s (169.5 s and 167.5 s) for undecane. 1, octane; 2, DMMP; 3, decane; 4, DEMP; 5, undecane**.** Reprinted with permission from [17]. Copyright 2010 American Chemical Society.

4.2 Micro-scale system integration

In this section, micro-fabricated separation column, FP on-column detector, and Knudsen pump array are used [13].

4.2.1 Single-column system

4.2.1.1 System description

For the single-column configuration (see Fig. 4.5(A)), an optical on-column detector is connected to the injection port installed on a Varian 3800 GC through a 25 cm long micro-fabricated column coated with OV-1. Columns are kept at room temperature during the experiments in this study. The KP array is installed at the downstream end of both configurations to pull the carrier gas and analytes through the whole system. A pressure sensor (Motorola, Inc. MPX2053DP) is installed to monitor the pressure on-column. Gas samples extracted from the head space of each sample container by a solid phase microextractor (SPME) is injected through the injection port. The temperature of the injection port is kept at 200 ^{o}C and its head pressure is set to zero to prevent inadvertent flow from it. Ultrahigh purity helium is used as the carrier gas. Figure 4.5(B) illustrates the measurement set-up.

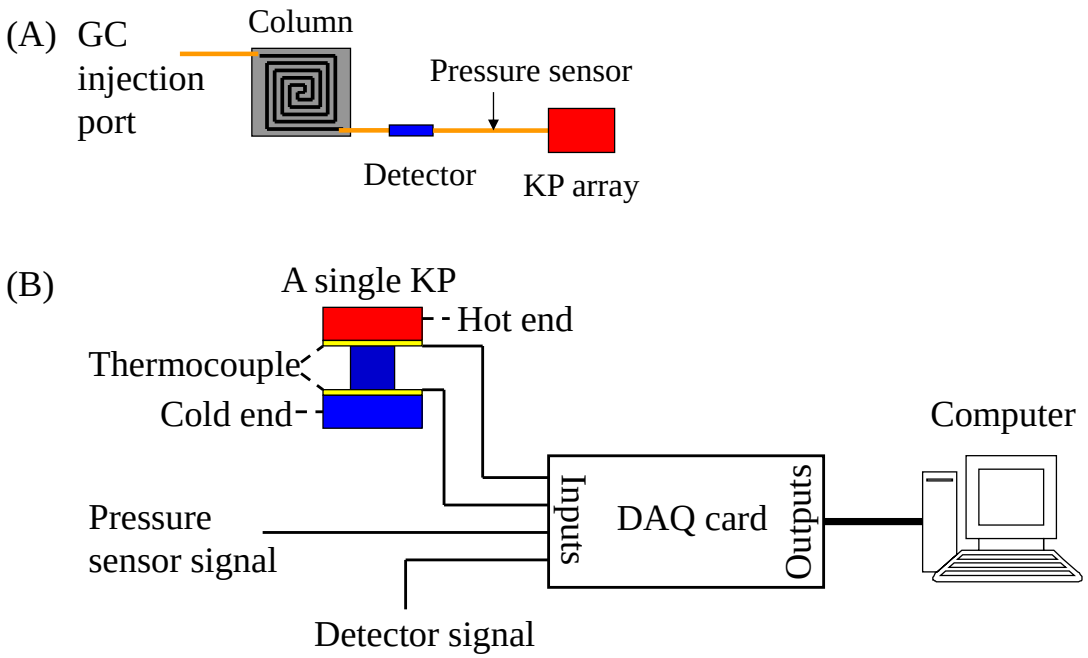

Figure 4.5. Schematic of the single-column system. It consists of a 25 cm long micro-fabricated GC column coated with OV-1 and an on-column optical detector. (B) Schematic of the measurement set-up. Reprinted with permission from [13]. Copyright 2011 Royal Society of Chemistry.

4.2.1.2 Separation result

A gas mixture composing of pentane, heptane, octane, decane, and undecane is used to test the separation and detection capability of the KP-based single-column μGC system. Figure 4.6 shows the separation chromatograms obtained at two different KP pumping pressures. A temperature bias of 84 K applied across each element of the KP array generates a pumping pressure of 20.6 kPa (and a helium flow rate of 1 mL/min), which unambiguously demonstrates the feasibility of using KP in a μGC system. In this effort, a rapid detection is completed within around 4 minutes, with a high resolution between heavy analytes of undecane and decane. However, the three light analytes of pentane, heptane, and octane are eluted out close to each other, making them nearly indiscernible. Another typical

chromatogram is obtained with a lower flow rate (0.55 mL/min) by lowering the temperature bias across each of the KP elements to 38 K. This reduces the pumping pressure to 10.5 kPa, which allows us to easily separate the three light analytes. However, this increased resolution is achieved at the expense of the overall analysis time. As shown in Fig. 4.6, the elution of heavy analytes is significantly slowed down, resulting in an analysis time of around 7 minutes.

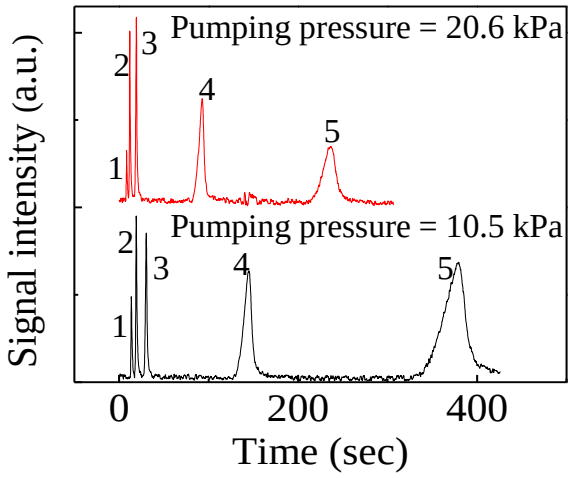

Figure 4.6. Chromatograms obtained from single-column configuration when the pumping pressure is maintained at 20.6 kPa (corresponding flow rate was 1 mL/min) and 10.5 kPa (corresponding flow rate was 0.55 mL/min). Helium is used as the carrier gas. Curves are vertically shifted for clarity. 1. pentane; 2. heptane; 3. octane; 4. decane; 5. undecane. Reprinted with permission from [13]. Copyright 2011 Royal Society of Chemistry.

In order to obtain superior resolution of this set of analytes without sacrificing the detection speed, simple pressure programming is used to modulate the pumping of the KP array during the analysis. A low pumping pressure of 10.5 kPa is applied at the beginning of the test to obtain high resolution for the light analytes. After the elution of the three light analytes, the pumping pressure is increased to 20.6 kPa to accelerate the elution of heavy analytes. In the resultant chromatogram, as illustrated in Fig. 4.7, the light analytes are eluted

at 11.1 seconds, 16.7 seconds, and 27.4 seconds, respectively, and heavy analytes are eluted out within 5 minutes. The inset of Fig. 4.7 shows the temperature measured at the hot end and the cold end of a single KP element. The pressure programming of the KP array is implemented by simply modulating the temperature at the hot end of each KP element while allowing the cold end to remain in equilibrium with the environment. Multi-level pressure programming is certainly possible to analyze more complex gas mixtures and to optimize both system chromatographic resolution and detection speed.

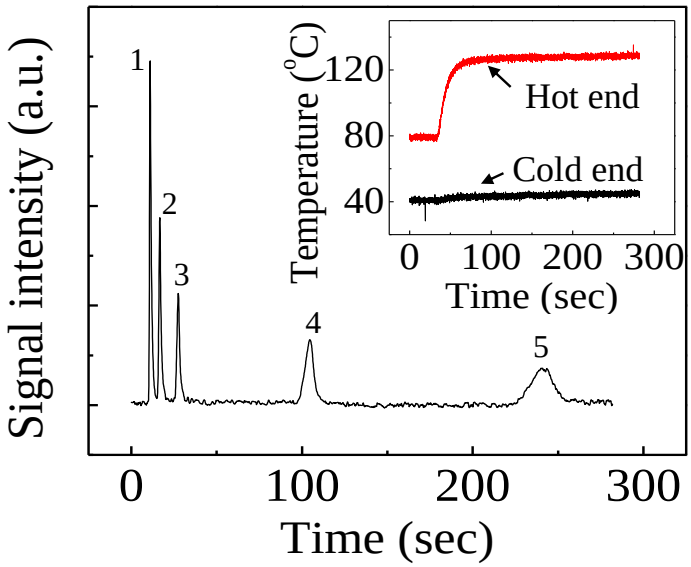

Figure 4.7. Chromatogram obtained from single-column configuration with pressure programming of the KP array. The pumping pressure is set at 10.5 kPa at the beginning. After the elution of the third analyte, the pressure is increased to 20.6 kPa. Inset: Temperature recorded at the hot and cold end of a single KP element. 1. pentane; 2. heptane; 3. octane; 4. decane; 5. undecane. Reprinted with permission from [13]. Copyright 2011 Royal Society of Chemistry.

We further tests the performance of the KP-based μGC system using dry air as the carrier gas. Employment of dry air for gas analysis is particularly appealing for μGC systems intended for use in environmental VOC monitoring. The use of inert carrier gas (such as

helium and nitrogen) would require storage and replenishment adding to operation costs, and eliminating the possibility of use in remote and in accessible environments. In our experiment, the dry air is obtained by passing ambient air through a desiccant. Figure 4.8 shows the separation chromatogram of five gas analytes: pentane, octane, decane, DMMP and undecane using the single-column μGC configuration when a temperature bias of 96 K is applied across each of the KP elements in the KP array. Note that because the average molecular diameter of air is larger than helium, the thermal transpiration driven flow rate decreases to 0.26 mL/min, compromising the chromatographic resolution and broadened peak width. Consequently, as shown in Fig. 4.8, pentane/octane and DMMP/undecane are co-eluted. This type of co-elution problem can be addressed, as described in the next section, using a tandem-column μGC configuration with two on-column detectors for better chromatographic resolution.

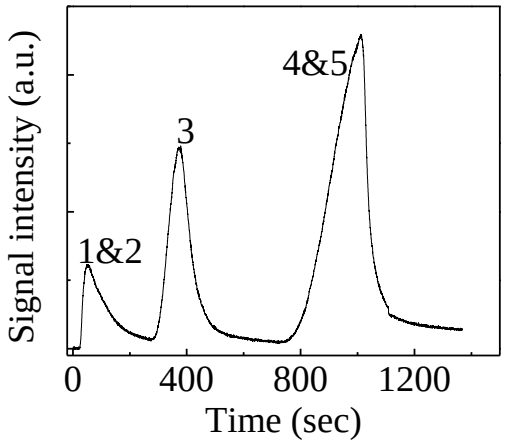

Figure 4.8. Chromatogram obtained from single-column configuration. Dry air is used as the carrier gas with a flow rate of 0.26 mL/min. 1. pentane; 2. octane; 3. decane; 4. DMMP; 5. undecane. Reprinted with permission from [13]. Copyright 2011 Royal Society of Chemistry.

4.2.2 Tandem-column system

4.2.2.1 System description

For the tandem-column configuration (see Fig. 4.9), the first FP on-column detector is installed at the end of a 50 cm long micro-fabricated column coated with OV-1, and the second detector is installed at the end of a 25 cm long micro-fabricated column coated with OV-215. Other parameters are kept the same as the parameters set in the single-column system experiment.

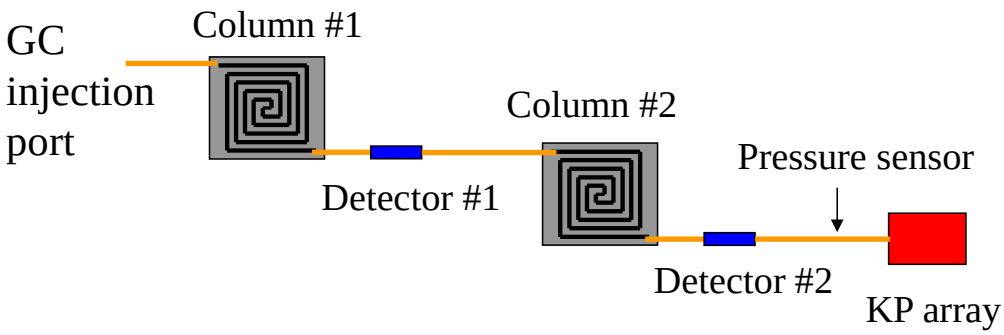

Figure 4.9. Schematic of the tandem-column system. It has two micro-fabricated GC columns. The first column is 50 cm long and is coated with OV-1, whereas the second column is 25 cm long and is coated with OV-215. Two on-column FP detectors are installed at the end of the first and the second column, respectively. Reprinted with permission from [13]. Copyright 2011 Royal Society of Chemistry.

4.2.2.2 Separation result

The tandem-column configuration has been used in μGC systems aimed to improve the μGC separation capability. It employs two columns with different coatings to first separate analytes by vapor pressure, followed by another separation by polarity [14-16]. In this study, two micro-fabricated GC columns with coatings of different polarities are used; two on-column detectors are installed at the end of the first and the second column, respectively (see Fig. 4.9), to provide complementary chromatograms for enhanced chromatographic

resolution [17, 18]. Dry air is once again used as the carrier gas in this configuration. The temperature bias across each element of the KP array is maintained at 96 K, which results in a pumping pressure of 10 kPa and a flow rate of 0.14 mL/min. As shown in Fig. 4.10(A), although octane and trans-2-hexenal co-elutes after the first column because of the limited separation capability of the single-column, all analytes are separated at the end of the tandem-column system. Note that the benefit of the tandem-column configuration may not be fully realized with the traditional end-column detector placed at the terminal end of the second column, as the analytes already separated after the first column may still co-elute after the second column [17, 18], which creates the same co-elution problem as in the single-column configuration. In contrast, installation of an additional on-column detector at the end of the first column allows us to monitor the separation from the first and the second column simultaneously, thus providing complementary chromatograms that significantly improve the analyte separation and identification capability of the μGC system. This point is well illustrated in Fig. 4.10(B), where the two complementary chromatograms are obtained from the first and the second on-column optical detectors, respectively. Although a co-elution of DMMP and undecane occurs after the second column, the complementary chromatogram obtained from the first detector is able to adequately separate the gas mixture.

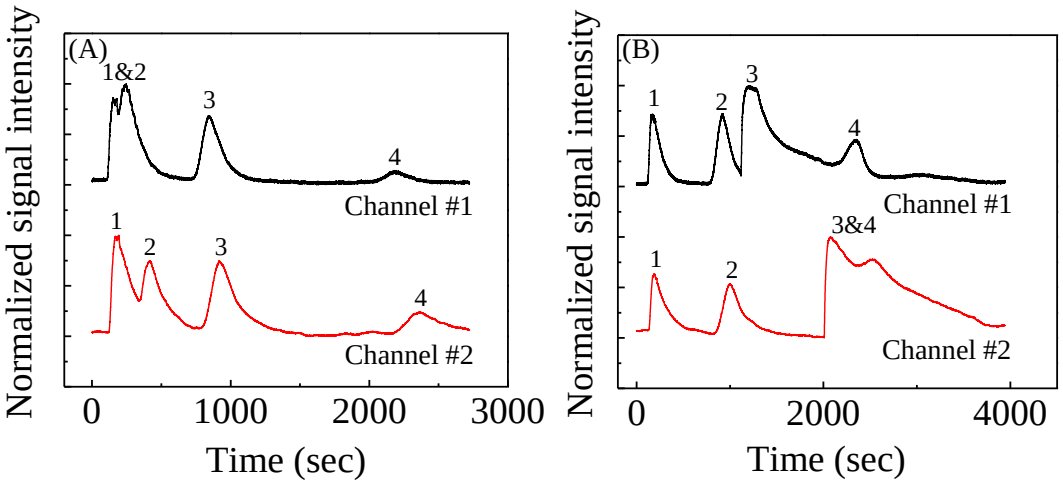

Figure 4.10. Chromatograms obtained from the two optical detectors installed in the tandem-column configuration. Dry air is used as the carrier gas with a flow rate of 0.14 mL/min. All peaks are normalized to the highest peak in each chromatogram. Curves are vertically shifted for clarity. (A) At Channel #1 (placed after the first column), analyte #1 and #2 co-elute, while at Channel #2 (placed after the second column) all analytes are resolved. Analytes: 1. octane; 2. trans-2-hexenal; 3. decane; 4. undecane. (B) At Channel #1, all analytes are resolved, while at Channel #2 analyte #3 and #4 co-elute. 1. octane; 2. decane; 3. DMMP; 4. undecane. Reprinted with permission from [13]. Copyright 2011 Royal Society of Chemistry.

References

1. M. P. Rowe, W. H. Steinecker, and E. T. Zellers, "Chamber evaluation of a portable GC with tunable retention and microsensor-array detection for indoor air quality monitoring," J. Environ. Monit. **8**, 270-278 (2007).
2. C.-J. Lu, J. Whiting, R. D. Sacks, and E. T. Zellers, "Portable Gas Chromatograph with Tunable Retention and Sensor Array Detection for Determination of Complex Vapor Mixtures," Anal. Chem. **75**, 1400-1409 (2003).
3. J. R. Jones, and J. H. Purnell, "Prediction of retention times in serially linked open-tubular gas chromatographic columns and optimization of column lengths," Anal. Chem. **62**, 2300-2306 (2002).
4. D. R. Deans, and I. Scott, "Gas chromatographic columns with adjustable separation characteristics," Anal. Chem. **45**, 1137-1141 (2002).
5. J. H. Purnell, and M. H. Wattan, "Separation of aliphatic hydrocarbon mixtures by gas chromatography using serial liquid-phase and solid-phase columns," Anal. Chem. **63**, 1261-1264 (2002).
6. T. Veriotti, and R. Sacks, "A Tandem Column Ensemble with an Atmospheric Pressure Junction-Point Vent for High-Speed GC with Selective Control of Peak-Pair Separation," Anal. Chem. **73**, 813-819 (2001).
7. M. Libardoni, M. McGuigan, Y. J. Yoo, and R. Sacks, "Band acceleration device for enhanced selectivity with tandem-column gas chromatography," J. Chromatogr. A **1086**, 151-159 (2005).
8. R. Sacks, C. Coutant, T. Veriotti, and A. Grail, "Pressure-tunable dual-column ensembles for high-speed GC and GC/MS," J. Sep. Sci. **23**, 225-234 (2000).
9. Y. Sun, J. Liu, D. J. Howard, G. Frye-Mason, A. K. Thompson, S.-j. Ja, and X. Fan, "Rapid tandem-column micro-gas chromatography based on optofluidic ring resonators with multi-point on-column detection," Analyst, DOI: 10.1039/b917154a.
10. J. Liu, Y. Sun, D. J. howard, G. Frye-Mason, A. K. Thompson, S.-J. Ja, S.-K. Wang, M. Bai, H. Taub, M. Almasri, and X. Fan, "Fabry-Perot cavity sensors for multipoint on-column micro gas chromatography detection," Anal. Chem. **82**, 4370-4375 (2010).
11. J. Whiting, and R. Sacks, "Selectivity Enhancement for High-Speed GC Analysis of Volatile Organic Compounds with Portable Instruments Designed for Vacuum-Outlet and Atmospheric-Pressure Inlet Operation Using Air as the Carrier Gas," Anal. Chem. **74**, 246-252 (2001).
12. M. Akard, and R. Sacks, "Pressure-Tunable Selectivity for High-Speed Gas Chromatography," Anal. Chem. **66**, 3036-3041 (2002).
13. J. Liu, N. K. Gupta, K. D. Wise, Y. B. Gianchandani, and X. Fan, "Demonstration of motionless Knudsen pump based micro-gas chromatography featuring micro-fabricated columns and on-column detectors," Lab Chip **11**, 3487-3492 (2011).
14. D. R. Deans, and I. M. Scott, "Gas chromatographic columns with adjustable separation characteristics," Anal. Chem. **45**, 1137-1141 (1973).

15. J. H. Purnell, and M. H. Wattan, "Theoretical and experimental comparison of serially llinked and mixed-packing gas-liquid chromatography columns," J. Chromatogr. **555**, 173-182 (1991).
16. J. R. Jones, and J. H. Purnell, "Prediction of retention times in serially linked open-tubular gas chromatographic columns and optimization of column lengths," Anal. Chem. **62**, 2300-2306 (1990).
17. J. Liu, Y. Sun, D. J. Howard, G. Frye-Mason, A. K. Thompson, S.-j. Ja, S.-K. Wang, M. Bai, H. Taub, M. Almasri, and X. Fan, "Fabry-Pérot cavity sensors for multipoint on-column micro gas chromatography detection," Anal. Chem. **82**, 4370-4375 (2010).
18. Y. Sun, J. Liu, D. J. Howard, X. Fan, G. Frye-Mason, S.-j. Ja, and A. K. Thompson, "Rapid tandem-column micro-gas chromatography based on optofluidic ring resonators with multi-point on-column detection," Analyst **135**, 165-171 (2010).

Chapter V

Smart Multi-Channel Two-Dimensional Micro-Gas Chromatography

5.1 Introduction

Micro-gas chromatography (μGC) has attracted tremendous research interest due to its wide applications in areas such as environmental protection [1, 2], biomedical diagnostics [3, 4], industrial monitoring and occupational safety [5], homeland security, and the battlefield [6-8]. As compared to the conventional bench-top GC, μGC offers a compact size and a light weight, and the ability to conduct rapid, on-site vapor analysis. However, μGC achieves these advantages at the expense of separation capability, which is one of the most important features of a GC system in analyzing complex gas mixtures. This loss of separation capability is due primarily to the shortened length of the separation columns used. To date, a number of methods have been developed to address this challenge [2, 9-19], among which comprehensive two-dimensional GC (or 2-D GC) technology is the best and most widely used solution.

Comprehensive two-dimensional GC system integrates two different GC columns in series with a modulator in between [20-22]. The modulator collects effluent from the first column (1^{st} column) for a fraction of the time equal to peak width, dividing the peak from the 1^{st} column into several cuts. Each cut is focused into a very narrow band in the modulator

and then sequentially introduced onto the second column (2^{nd} column), resulting in additional separation. Since the modulator makes the separation at two columns independently, analytes can be differentiated from each other by the retention times at the 1^{st} and the 2^{nd} column, thus providing the 2-D separation information. Current modulator devices are mainly categorized into two types: thermal based modulators [22-26] and valve based modulators [27-31]. Thermal based modulators create a cold zone to trap analytes eluting out from the 1^{st} column and re-inject them onto the 2^{nd} column in a narrow band by rapidly raising its temperature [26], whereas the valve based modulators generate pressure difference to immobilize analytes in the 1^{st} column and in the meanwhile mobilize analytes in the 2^{nd} column.

Despite the significantly improved separation capability, existing 2-D GC technology faces several challenges. (1) Since the modulator has to continuously cut and send the effluent from the 1^{st} column to the 2^{nd} column at a high frequency, the separation at the 2^{nd} column needs to be finished within only a few seconds before the modulator injects the next effluent to the 2^{nd} column, which greatly limits the separation capability of the 2^{nd} column. (2) High frequency operation of the modulator consumes considerably large amount of power, which is not suitable for portable instruments such as those used for on-site gas analysis or in remote distributed gas surveillance/monitoring. (3) Very precise synchronization is required between the modulator and vapor detector at the terminal end of the 2^{nd} column. Failure in synchronization may cause a serious problem in data reconstruction. (4) 2-D GC generates a much larger amount of data than 1-D GC, making the data analysis extremely complicated and challenging [32].

5.2 Macro-scale smart multi-channel two-dimensional gas chromatography

We propose and investigate a concept of smart multi-channel 2-D μGC that provides better, more flexible, and more adaptable separation, and simplified 2-D chromatogram reconstruction. As illustrated in Fig. 5.1, this system consists of one 1st column, multiple parallel 2nd columns, and a decision-making module installed between the 1st and 2nd columns. The decision-making module normally comprises an on-column non-destructive vapor detector (Detector #1 in Fig. 5.1), a flow routing system (such as multi-port valves and thermal modulators) and a computer that monitors the detection signal from the detector and sends out the trigger signal to the flow routing system. Since all columns are independent of each other, this system can be called 1xN 2-D GC, where N is the number of the 2nd columns.

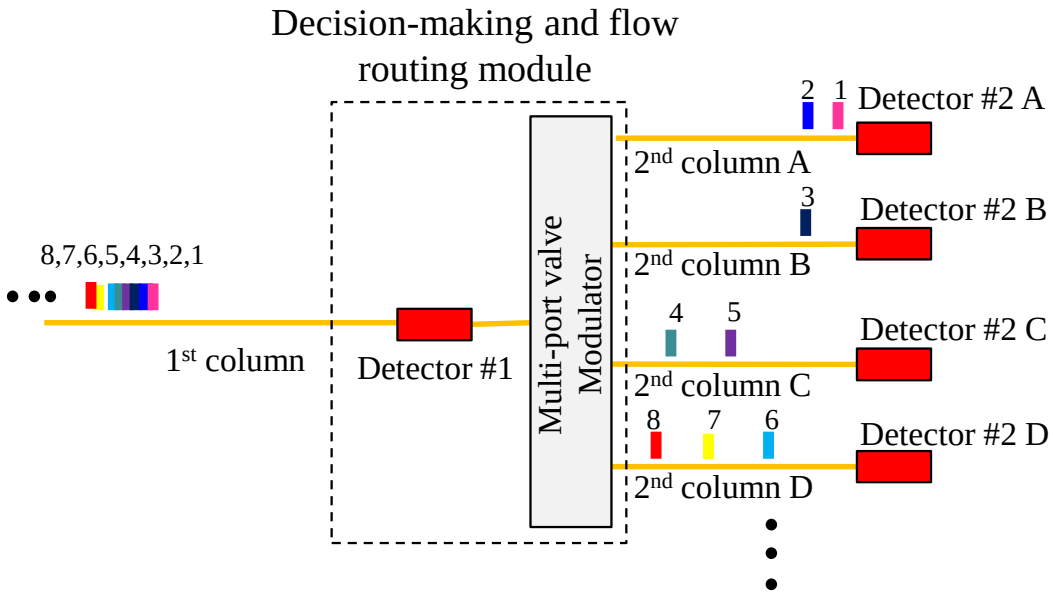

Figure 5.1 Conceptual illustration of the smart adaptive multi-channel 2-D GC system. It consists of one 1st column, multiple parallel 2nd columns, and a decision-making module installed between the 1st and 2nd columns. The decision-making module normally comprises an on-column non-destructive vapor detector (such as Detector #1), a flow routing system (such as multi-port valves and thermal modulators), and a computer that monitors the detection signal from the detector and sends out the trigger signal to the flow routing system.

During operation, Detector #1 monitors the effluents from the 1st column, providing the 1st dimensional retention time and the information for the decision-making module to decide which 2nd column the effluent should be routed to and when the thermal modulator should be turned on. After the entire effluent peak coming out of the 1st column is trapped by the thermal modulator, the thermal modulator is turned on and the entire trapped effluent is then sent to the 2nd column for further separation, which can be detected by Detector #2. The decision-making module may also contain a timing system or receive feedback from Detector #2 in order to determine whether a 2nd column is busy (*i.e.*, separation is still on-going) or available (*i.e.*, separation is complete). If all 2nd columns are busy, the flow in the 1st column is halted. To increase the versatility and to optimize the separation capability of the proposed adaptive μGC system, the 2nd columns can use different lengths, stationary phase coatings, flow rates, and temperatures.

The proposed smart multi-channel 2-D μGC proposed has a number of unique and advantageous features. (1) The on-column detector (Detector #1 in Fig. 5.1) detects the analytes eluted from the 1st column, which not only records the analytes' retention time at the 1st column, but also triggers the flow routing system to focus and re-inject an entire effluent peak containing one or several analytes into the 2nd column. Therefore, the time interval between the two adjacent injections becomes very flexible and can be adjusted for each injection. Consequently, a longer 2nd column can be used to increase its separation capability, resulting in improved resolution in the 2nd column. (2) Multiple 2nd columns allow effluents from the 1st column to be distributed to different 2nd columns. It is possible to use different 2nd columns with various lengths, coatings, flow rates, and temperatures for best separation and maximal versatility. (3) The flow routing system works only when it is triggered by the

on-column detector at the end of the 1st column, instead of working at a high frequency during the whole analysis process, which can significantly reduce the power consumption. This feature is particularly attractive when the μGC is used in remote distributed gas surveillance/monitoring. (4) The adaptive 2-D μGC lowers the requirements for timing and synchronization. (5) Injection of the entire eluted peak coming out of the 1st column into the 2nd column avoids cutting it into several fractions as in conventional 2-D GC so that the recorded retention time of each peak can be directly used to reconstruct the 2-D chromatogram, thus eliminating complex post-data processing. It should be noted that multiple parallel 2nd columns described here are also used in 2-D liquid chromatography (LC) systems [33-40]. However, all the 2nd columns in the LC system need to be exactly the same (stationary phase, length, temperature, and flow rate, *etc*.) in order to reconstruct the 2-D chromatogram.[41] A 2-D GC system with two different 2nd columns has also been reported, where the effluent from the 1st column is equally split into the two 2nd columns [42, 43]. Although this 2-D GC system produces a pair of 2-D chromatograms for each run, and thus enhances the GC separation efficiency and sample identification capability, it suffers from the potential loss of samples for each 2nd column, and more complicated 2-D chromatogram reconstruction processes and data analysis. Furthermore, the maximal time available for separation on the 2nd column is still limited by the thermal modulator modulation frequency (approximately 0.2-1 Hz) [42]. Recently, another 2-D GC design was demonstrated by diverting part of effluents from the 1st column to an off-column detector for direct measurement of the 1st dimensional retention time [44]. Again, it encounters the same or similar drawbacks aforementioned (such as loss of samples).

5.2.1 System description

To implement the smart multi-channel 2-D GC concept, we employ an experimental setup illustrated in Fig. 5.2(A) and (B) [45]. In the single 2nd column system (Fig. 5.2 (A)), the 1st column is coated with RTX-1 or HP-5 (coating thickness is 200 nm), whereas the 2nd column is coated with Carbowax (coating thickness is 200 nm). The two columns are connected through a decision-making module, which consists of an on-column non-destructive detector (Detector #1), a three-port valve (Parker, part no. 009-0269-900), a thermal modulator, and a computer. Detector #1 is an optical fiber based FP vapor sensor discussed in Chapter Two [16, 46, 47]. It could be installed inside a GC column in a manner that does not interfere with the gas flow while non-destructively detecting the vapor eluted out from the 1st (2nd) column. A chromatographic peak recorded by Detector #1 indicates the passage of an effluent, which is later trapped by a customized thermal modulator installed after Detector #1. The modulator is made of a quartz tube (i.d. = 2 mm, length = 2 cm) packed with 6 mm long sorbent bed (Carbopack B and Tenax TA). An electrical coil is wrapped into a cylindrical shape (i.d. = 1.5 cm, length = 1 cm) to cover the outer surface of the modulator for heating. Another detector (Detector #2, which is the same as Detector #1) is installed at the end of the 2nd column. A mini-diaphragm pump (Parker, part no. D713-22-01) is placed at the end of the system to provide the flow. All connections between two components are through a press-tight column connector.

Gas analyte is extracted from the head space of the bottle containing the analyte by a SPME fiber (PDMS/DVB, 65 μm diameter fiber, Supelco 57310-U) and is injected through the GC injector (Varian 3800, heated to 250 °C), which connects to the 1st column. The head pressure of the GC injector is set to zero. Gas analytes and ultrahigh purity (UHP) helium

(used as carrier gas) are drawn into the system by the mini-diaphragm pump. To maintain a constant flow rate of 1 mL/min at both 1st and 2nd columns, an additional column with the same dimensions (i.d. and length) as the 1st column is attached to the upstream of each 2nd column via the three-port valve (see Fig. 5.2(A) and (B)). All the components are kept at room temperature, unless otherwise noted. A customized LABVIEW program is used to monitor signals from detectors in real-time, and the data is recorded at a rate of 20 Hz.

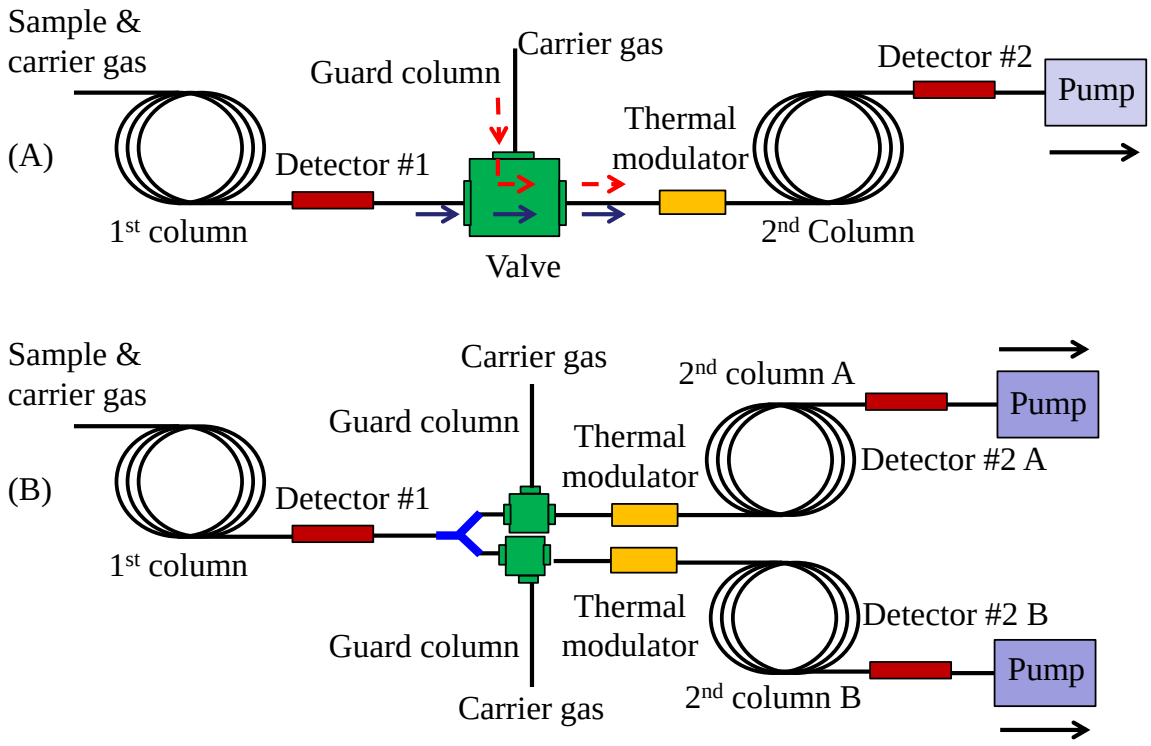

Figure 5.2. Schematic of embodiments of the proposed adaptive 2-D GC. (A) shows the adaptive 2-D GC with a single 2nd column. Solid arrows represent the flow direction when system works in Step 1, whereas, dashed arrows represent the flow direction when the system works in Step 2 and 3. (B) Schematic of 2-D GC with dual 2nd columns. A Y-connector connects both 2nd columns to the 1st column. A valve is installed for each of the 2nd columns. In this manner, the effluents from the 1st column are sent to the two 2nd columns alternately, significantly shortening the overall analysis time. Note that only when both 2nd columns are busy would the flow in the 1st column be suspended until at least one of the 2nd columns becomes available. Reprinted with permission from [50]. Copyright 2012 American Chemical Society.

5.2.2 Working principle

The operation procedures can be divided into the following three steps:

Step 1: The valve connects the 1st and 2nd column. The effluent eluted from the 1st column is detected by Detector #1. Then it passes through the valve and is trapped by the thermal modulator. When a chromatographic peak detected by Detector #1 returns back to the baseline, indicative of complete passage of the effluent, a signal is generated from the computer to trigger the flow routing system (the three-port valve and the thermal modulator in this particular case).

Step 2: After being triggered, the valve connects the 2nd column to the carrier gas directly. The 1st and 2nd columns are disconnected and the flow of analytes in the 1st column is stopped. Meanwhile, the modulator is heated from room temperature to 300 ^{o}C within 3 seconds, re-injecting the trapped effluent into the 2nd column. As soon as its temperature reaches 300 ^{o}C, the modulator is naturally cooled down to room temperature (in about 30 seconds) to trap the next effluent from the 1st column.

Step 3: Further separation takes place in the 2nd column. Detector #2 detects the separated peak(s) at the 2nd column and records their elution time. Upon the completion of separation (or after pre-set time lapse), the valve reconnects the 1st and the 2nd columns and Step 1 is resumed.

The dual 2nd column system (Fig. 5.2(B)) adds another independent 2nd column to the 1st column via a "Y" connector. Each column (1st column, 2nd column A and B) has a detector installed at its end. A mini diaphragm pump is attached to each of the 2nd columns. The overall operation procedures are similar to those for the single 2nd column system described above. Initially, the 2nd column A is connected to the 1st column whereas the 2nd column B is

disconnected from the 1st column. When an effluent passes from the 1st column, it is routed to the 2nd column A, which is subsequently disconnected from the 1st column. Meanwhile, the 2nd column B is connected to the 1st column to accommodate the following effluent. In this manner, the effluents from the 1st column are sent to the two 2nd columns alternately, significantly shortening the overall analysis time. Note that only when both 2nd columns are busy will the flow in the 1st column be suspended until at least one of the 2nd columns become available.

5.2.3 Separation test

5.2.3.1 Stop flow test

Before conducting real 2-D separation, the system is demonstrated to be able to suspend the separation at the 1st column without interrupting the separation in the 2nd column. The experimental setup is the same as the single 2nd column system illustrated in Fig. 5.2(A), except that the thermal modulator is not in use. The chromatograms shown in Fig. 5.3(A) are obtained from Detector #1 and #2 with no stop-flow manipulation, which serves as the reference. In the stop-flow test shown in Fig. 5.3(B), the valve is switched to disconnect the 1st and 2nd column twice. The first time starts at t=20 s after the elution of Analyte #1 and the second starts at t=180 s after the elution of Analyte #2. The stop-flow (*i.e.*, the disconnection) duration in both cases is 120 seconds. Comparison of the elution times with and without the stop-flow shows that Analyte #2 and #3 in the 1st column are delayed once (120 seconds) and twice (240 seconds), respectively, whereas the retention time of all analytes in the 2nd column (elution time at Detector #2 – elution time at Detector #1) remains the same. In addition, no significant peak broadening caused by the stop-flow manipulation is observed. These results suggest that, when the 1st and 2nd columns are disconnected, the separation at the 1st column

can be successfully suspended without any interference to the subsequent separation at the 2nd column.

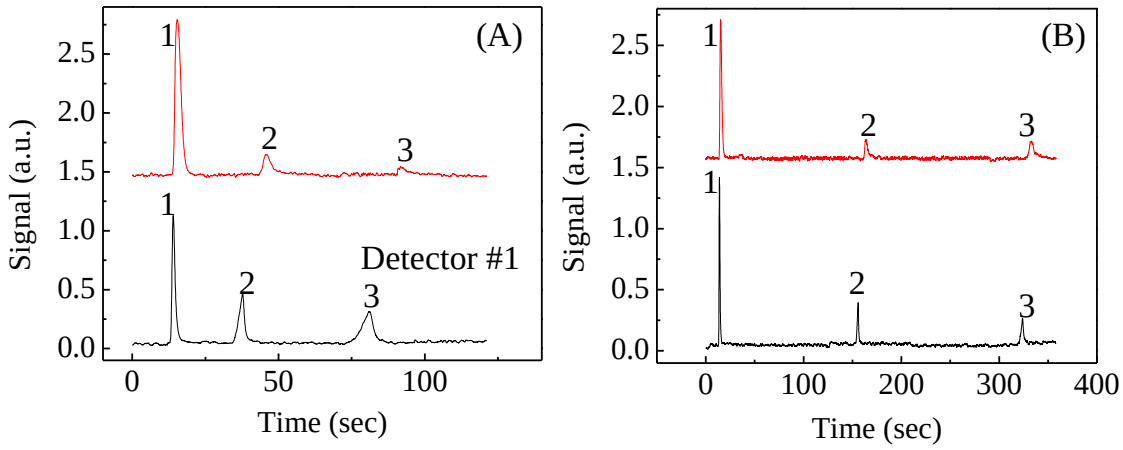

Figure 5.3. Chromatograms of three alkanes obtained from the adaptive system shown in Fig. 5.2(A) without a thermal modulator. (A) Chromatograms corresponding to the configuration in which the 1st and 2nd column are connected all the time. (B) The valve is disconnected twice. The first disconnection is from 20 s to 140 s (disconnection time=120 s), and the second from 180 s to 300 s (disconnection time=120 s). The retention delay of Analyte #2 and #3 at 1st (2nd) column is 117.8 (118) s and 239.3 (238) s, respectively. The delay time agrees well with the total disconnection time that Analyte # 2 and #3 experience, suggestion that the flow of analytes in the 1st column can be completely stopped. Analytes: 1. pentane; 2. octane; 3. nonane. The 1st column is 1.5 m long and coated with RTX-1. The 2nd column is 0.8 m long and coated with Carbowax. Curves are vertically shifted for clarity. Reprinted with permission from [50]. Copyright 2012 American Chemical Society.

5.2.3.2 Single-2nd-column system

The feasibility and working principle of the proposed adaptive 2-D μGC system are well illustrated by separating a mixture of five analytes in Fig. 5.4. The mixture sample is gradually separated as it travels in the 1st column until Detector #1 detected the first eluted peak. When the signal of Detector #1 returns back to the baseline, indicating that the eluted analyte(s) has passed through the 1st column and is trapped by the thermal modulator, the valve is switched to disconnect the 1st column from the 2nd column so that the separation in the 1st column is suspended. Meanwhile, the thermal modulator is heated up to 300 °C to

release the trapped analyte(s) in a sharp peak for further separation in the 2nd column. In order to ensure the completion of the separation at the 2nd column, a 60-second operation time is applied to the 2nd column before switching the valve back to reconnect the 1st and 2nd column. After reconnection, the separation at the 1st column resumes until Detector #1 detects the second eluted peak, and then the separation and detection cycle continues as described above.

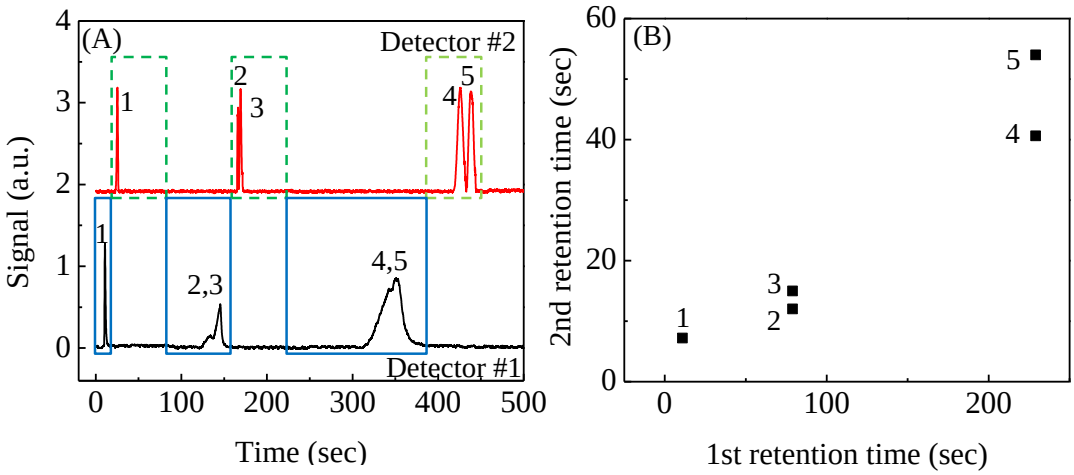

Figure 5.4. 2-D separation results obtained from the adaptive μGC system illustrated in Fig. 5.2(A). (A) Chromatograms from Detector #1 and #2. Solid and dashed boxes represent the separation at the 1st and 2nd column, respectively. Spaces outside the solid and dashed boxes represent the durations when separation is suspended at the 1st and 2nd column, respectively. The duration of the dashed boxes is 60 seconds to ensure that all the analytes in the 2nd column are eluted. (B) The corresponding 2-D chromatogram. Analytes: 1. pentane; 2. nonane; 3. 1-hexanol; 4. decane; 5. cis-3-hexenyl acetate. The first column is 1.5 m long and is coated with RTX-1. The 2nd column is 0.8 m long and is coated with Carbowax. The retention time of a peak is measured at its apex. Curves in (A) are vertically shifted for clarity. Reprinted with permission from [50]. Copyright 2012 American Chemical Society.

The corresponding chromatograms obtained from Detector #1 and #2 are shown in Fig. 5.4(A). The total analysis time is approximately 450 seconds, which is mainly determined by the retention time of the last analyte at the 1st column (approximately 230 seconds for the case in Fig. 5.4. Note: extra 40 seconds are needed for the last analyte to *completely* elute out

of the 1st column.) and the sum of all operation time at the 2nd column (approximately 180 seconds for the case in Fig. 5.4). During the above procedures, whenever the 2nd column is in operation the flow in the 1st column is suspended, thus adding the overall analysis time. The analysis time can certainly be shortened significantly by implementing multiple 2nd columns, which will be discussed in detail later. The 2-D chromatogram of the mixture is presented in Fig. 5.4(B). The detailed calculation of the retention time at each column is discussed later.

The strong separation capability and simple data processing merit of the proposed system are further demonstrated by an analysis of a mixture of 20 analytes with various volatilities and polarities. As shown in the chromatograms from Detector #1 and #2 (Fig. 5.5(A)), although there are eight co-elution peaks occurring in the 1st column, all 20 analytes are well separated by the 2nd column. The 2-D chromatogram is presented in Fig. 5.5(B), having the longest retention time at the 1st and 2nd column of approximately 500 seconds and 80 seconds, respectively. Note that although the retention time of the last co-elution peak in the 2nd column exceeds the 60-second operation time, the system is able to adapt itself to extend the operation time until Detector #2 detected the analyte(s). This capability is not obtainable with conventional 2-D GC systems, whose separation time at the 2nd column is fixed and is determined by the operation frequency of the modulator (usually about several seconds). The total analysis time is approximately 1200 seconds, longer than 580 seconds (~500 seconds in the 1st column and ~80 seconds in the 2nd column) if a conventional 2-D GC system has been used to separate the same mixture under the same experimental conditions. Once again, this long analysis process is limited mainly by the use of a single 2nd column, because the separation at the 1st column has to be suspended until the separation at the 2nd column is

completed. By implementing multiple parallel 2nd columns, the analysis time is expected to be significantly shorter.

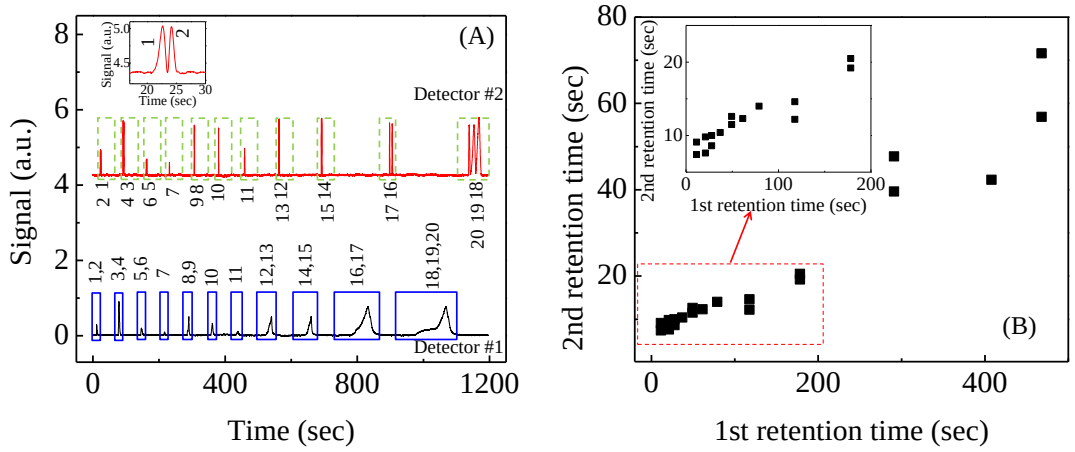

Figure 5.5. 2-D separation results of 20 analytes obtained from the adaptive 2-D μGC system shown in Fig. 5.2(A). (A) Chromatograms from Detector #1 and #2. Solid and dashed boxes represent the separation at the 1st and 2nd column, respectively. Spaces outside the solid and dashed boxes represent the durations when separation is suspended at the 1st and 2nd column, respectively. All analytes are resolved by Detector #2. Inset is the enlarged peaks of Analyte #1 and #2 detected by Detector #2. (B) The corresponding 2-D chromatogram extracted from (A). Analytes: 1. pentane; 2. acetic acid; 3. chlorotrimethysilane; 4. heptane; 5. pyridine; 6. 1-propanol; 7. 1-butanol; 8. tetramethyl orthosilicate; 9. octane; 10. cis-3-hexen-1-ol; 11. trans-2 hexenal; 12. nonane; 13. 1-hexanol; 14. tetraethyl orthosilicate; 15. limonene; 16. decane; 17. cis-3-hexenyl acetate; 18. undecane; 19. 1-octanol; 20. diethyl methyl-phosphonate. The 1st column is 2 m long and is coated with RTX-1. The 2nd column is 0.8 m long and is coated with Carbowax. The retention time of a peak is measured at its apex. Curves in (A) are vertically shifted for clarity. Reprinted with permission from [50]. Copyright 2012 American Chemical Society.

5.2.3.3 Dual-2nd-column system

A 2-D GC system with dual 2nd columns is demonstrated as the simplest illustration of the multiple parallel 2nd column system. The system is capable to deliver the eluted peaks from the 1st column to one of the parallel 2nd columns whichever is available (or at the stand-by mode). Only when both 2nd columns are busy (*i.e.*, in operation), will the separation at the 1st column be suspended until at least one of the 2nd columns becomes available. In this

analysis, the same mixture of 20 analytes is tested and the analysis results are shown in Fig. 5.6(A) and (B). The operation time for each 2nd column is set to be 30 seconds, but could certainly be shortened or extended if needed, as discussed previously.

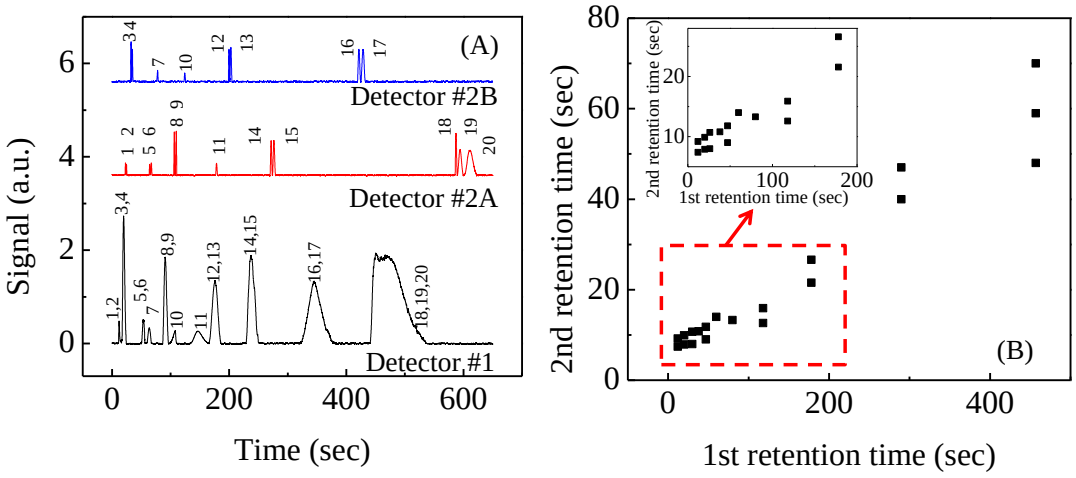

Figure 5.6. 2-D separation results of 20 analytes obtained from the adaptive 2-D μGC system shown in Fig. 5.2(B). (A) Chromatograms from Detector #1 and #2A and #2B. Solid and dashed boxes represent the separation at the 1st and 2nd column, respectively. Spaces outside the solid and dashed boxes represent the durations when separation is suspended at the 1st and 2nd column, respectively. All analytes are resolved by Detector #2A and #2B. (B) The corresponding 2-D chromatogram extracted from (A). Analytes are the same as in Fig. 5.4. The 1st column is 2 m long and coated with RTX-1. The two 2nd columns are 0.8 m long and are coated with Carbowax. The retention time of a peak is measured at its apex. Curves in (A) are vertically shifted for clarity. Reprinted with permission from [50]. Copyright 2012 American Chemical Society.

Compared to the single 2nd column system, the dual 2nd column system has the same high chromatographic resolution, but significantly shortened analysis time of approximately 650 seconds (the calculation of the retention time at the 1st and 2nd column can be found in the next section). Since the minimum analysis time is determined by the retention time of the last analyte eluted out from the 1st column (~500 seconds), the added analysis time by the 2nd column is only around 150 seconds, which is close to the added analysis time in a conventional 2-D GC system (~80 seconds) and about 4.6 times shorter than in the single 2nd

column system (~700 seconds). Note that the above ~150 seconds are mainly caused by the very short suspension time on the 1st column when both 2nd columns are busy. If enough parallel 2nd columns are installed so that the separation at the 1st column does not have to be suspended, the added analysis time caused by the 2nd separation is expected to be the same as in a conventional 2-D GC system.

We further employ the adaptive 2-D GC system in one practical application to analyze plant emitted volatile organic compounds (VOCs) mixed with alkanes and toluene. Plants release VOCs in response to many environmental stimuli and volatile emission "signatures" can provide highly specific information with broad applications for use in agriculture and defense [48, 49]. For demonstration purposes, we use commercially available standards to mimic the actual emission of plants. The analysis results are shown in Fig. 5.7(A) and (B). During the operation, the entire 1st column is placed into a GC oven for temperature ramping to accelerate the elution of heavy analytes. During the ramping, the oven is kept at room temperature for 3 minutes and then heated up to 150 ^{o}C at a rate of 20 ^{o}C/min. All other components remain at room temperature. The operation time for each 2nd column is initially set to be 20 seconds for separation of fast effluents. It is extended up to nearly 200 seconds during the later stage of separation to accommodate slow effluents (see, for example, Analyte #14-#18). The total analysis time is 1270 seconds, of which the 1st column analysis time is 1100 seconds and the added analysis time resulting from the 2nd column is only 170 seconds. The retention times of each analyte at 1st and 2nd separation are presented in Appendix A. Fig. 5.7 clearly showcases the advantages of the adaptive 2-D GC in comparison with the conventional 2-D GC that usually encounters increasing challenges when dealing with analytes that have long 2nd-dimensioal retention times (*e.g.*, ~180 s for Analyte #14). In

addition, the thermal modulator is turned on/off only 13 times, which leads to nearly 100-fold reduction in modulator power consumption in the conventional 2-D GC with a modulation frequency of 1 Hz.

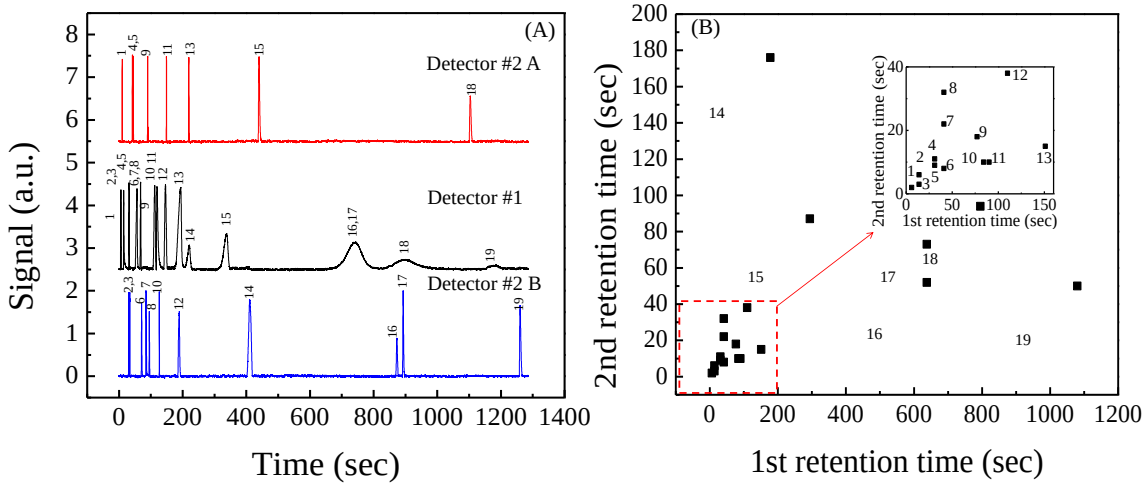

Figure 5.7 2-D separation results of plant emitted VOCs mixed with alkanes and toluene using the adaptive 2-D μGC system shown in Fig. 5.2(B). (A) Chromatograms from Detector #1 and #2A and #2B. All analytes are resolved by Detector #2A and #2B. (B) The corresponding 2-D chromatogram extracted from (A). Analytes: 1. pentane; 2. heptane; 3. dimethyl disulfide; 4. octane; 5. toluene; 6. pinene; 7. cis-3-hexen-1-ol; 8. trans-2 hexenal; 9. decane; 10. limonene; 11. ocimene; 12.undecane; 13. cis-3-hexenyl acetate; 14. methyl salicylate; 15. dodecane; 16. trans-β-farnesene; 17. jasmone; 18. methyl jasmonate; 19. caryophyllene. The 1st column is 2.7 m long and is coated with HP-5. The two 2nd columns are 0.7 m long and are coated with Carbowax. The 1st column is kept at room temperature for 3 minutes and then heated up to 150 ^{o}C at a rate of 20 ^{o}C/min. All other components are kept at room temperature. The retention time of a peak is measured at its apex. Curves in (A) are vertically shifted for clarity. Reprinted with permission from [50]. Copyright 2012 American Chemical Society.

5.2.4 Two-dimensional chromatogram construction

The retention time at the 1st and 2nd column can be calculated by the following equations:

1st retention time=Elution time recorded by Detector #1–total prior suspension time in the 1st column.

2^{nd} retention time=Elution time recorded by Detector #2–the corresponding thermal modulator turn-on time.

The parameters described in above equations can be found in the real-time chromatogram obtained from Detector #1 and #2. The total prior suspension time in the 1^{st} column is represented by the sum of the durations outside the solid boxes that precede the peak recorded by Detector #1. The corresponding thermal modulator turn-on time is represented by the beginning of the dashed box that contains the peak(s) recorded by Detector #2. Below we show some examples.

Single-2^{nd}-column system. In Fig. 5.5(A), the 1^{st} retention time of Analyte #2 = 139 s (elution time recorded by Detector #1) – 60 s (total prior suspension time in the 1^{st} column) = 79 s. The 2^{nd} retention time of Analyte #2 = 166 s (elution time recorded by Detector #2) – 154 s (the corresponding thermal modulator turn-on time) = 12 s.

Dual-2^{nd}-column system. In Fig. 5.6(A), the 1^{st} retention time of Analyte #5 = 52 s (elution time recorded by Detector #1) – 22 s (total prior suspension time in the 1^{st} column) = 30 s. The 2^{nd} retention time of Analyte #5 = 64 s (elution time recorded by Detector #2A) – 56 s (the corresponding thermal modulator turn-on time) = 8 s.

Once the 1^{st} and 2^{nd} retention times are known, construction of a 2-D chromatogram becomes very straightforward. The overall 2-D construction process is much simpler than that in a conventional 2-D GC system where tremendous and complex information needs to be extracted and re-assembled.

5.3 Micro-scale smart two-dimensional gas chromatography

Previously, we have demonstrated the smart multi-channel 2-D GC concept using conventional macro-scale components [50]. In this section, a complete and automated smart

multi-channel 2-D μGC system is built (see Fig. 5.8), which integrates a pre-concentrator, micro-fabricated columns, on-column gas detectors, a flow routing system, thermal injectors and gas pumps, as well as an algorithm for control/operation of the system. We subsequently characterize and optimize this μGC system, and finally employ it in two important applications that highlight its uniqueness and advantages: (1) analysis of 31 workplace hazardous VOCs reported by California Standard Section 01350 Specification (Feb 2010 version 1.1) [51] and (2) rapid detection and identification of particular analytes out of interference background.

5.3.1 System description

The schematic of the smart 2-D μGC is illustrated in Fig. 5.8. It includes a pre-concentrator, a six-port valve, a 1st Column, 1st Detector installed at the end of 1st Column, and two parallel 2nd columns: 2nd Column A and B, each of which is attached with a three-port valve, a thermal injector, 2nd Detector A or B and a gas pump. Note that to highlight the flexibility of the smart μGC two different lengths of the 2nd columns are used. The major components of the system are described in Chapter Three.

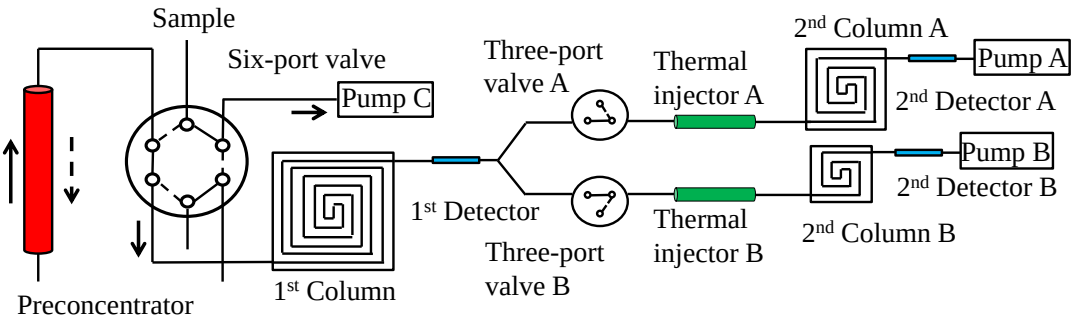

Figure 5.8. Schematic of the proposed smart 2-D μGC with dual 2nd columns. A pre-concentrator is connected to the 1st column through a six-port valve. During sampling (as shown by the dashed lines), sample is drawn into the pre-concentrator by Pump C. During analysis (as shown by the solid lines), the trapped sample in the pre-concentrator is released at high temperature and delivered onto the 1st column by a back-flush flow. The 1st column is connected to both 2nd columns by a Y-connector. Each of the 2nd columns has a three-port valve to control its connection with the 1st column. In this manner, the eluent from the 1st column is sent to the two 2nd columns alternately.

5.3.2 Control/operation algorism

A home-made LabView program is developed for automated control and operation of the system. It is based on our previous studies and characterization of the smart GC architecture using macro-scale components [50]. The operation procedures can be divided into three steps.

Step 1: 1st Column is connected to 2nd Column A and disconnected from 2nd Column B. The gas mixture is initially separated at 1st Column until 1st Detector detected a peak elutes out from 1st Column. When the entire eluted peak passes 1st Detector and trapped by Thermal injector A at 2nd Column A, a signal is generated to trigger Three-port valve A to disconnect 2nd Column A from 1st Column and turn on Thermal injector A to inject the trapped analytes into 2nd Column A for further separation. The system then registers the status of 2nd Column A as “busy”. The “busy” status could be changed to “available” by a signal generated by 2nd

Detector A when 2nd Column A completed separation or after certain pre-determined time lapse.

Step 2: When Three-port valve A disconnects 2nd Column A from 1st Column during operation of Step 1, 2nd Column B is connected to 1st Column. The remaining procedures are the same as in Step 1.

Step 3: When Three-port valve B disconnects 2nd Column B from 1st Column during operation of Step 2, the system inquires the status of 2nd Column A. If it is "available", 2nd Column A is reconnected to 1st Column and the procedures in Step 1 are repeated. If it is "busy" (note that 2nd Column B is "busy" at this moment), both 2nd columns are disconnected from 1st Column and the separation at 1st Column is suspended, until one of the two 2nd columns becomes "available", at which time the separation at 1st Column resumes and the eluent is sent to this "available" 2nd column.

The control/operation algorithm includes two major modules: peak identification module and system control module.

The peak identification module is implemented by using a Schmitt trigger coded in LabView to analyze the signal from the detector. Each detector in the smart 2-D μGC (1st Detector, 2nd Detector A and B) has one Schmitt trigger attached. Two thresholds are set to the Schmitt trigger (see Fig. 5.9): a high threshold to identify the elution peak from noise and a low threshold to judge whether the peak has passed through the detector. When the vapor sensing signal from the detector exceeds the high threshold, the operation algorithm registers one elution peak to its respective detector and waits for the vapor sensing signal to fall below the low threshold. Once a pair of such vapor sensing signals is received, a "peak passed" signal is sent to the system control module.

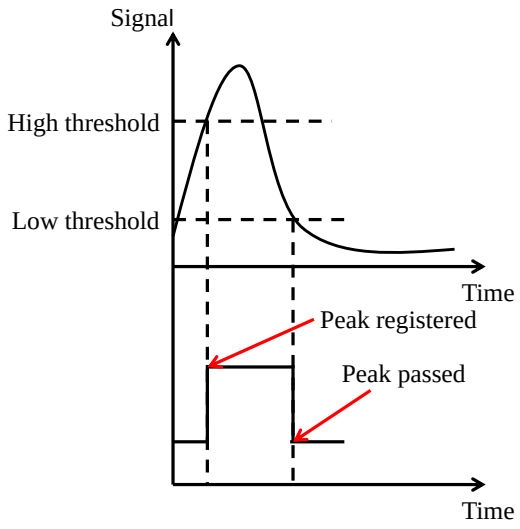

Figure 5.9. Illustration of a Schmitt trigger.

The system control module controls the operation of Three-port valve A and B, Thermal injector A and B, and temperature ramping of 1st Column. It is implemented by both software and hardware (see Fig. 5.10). The software control receives the "peak passed" signals from all detectors to decide which and when the trigger signal(s) to be sent out. Each component listed above has one specific trigger signal to activate its corresponding hardware control. The activation of hardware by the trigger signal is controlled through a relay, which toggles the connection between this component and its power supply. When the trigger signal stays at a low voltage (0 V), the relay disconnects the component from the power supply. When the trigger signal sends a high voltage (5 V), the relay connects the component to the power supply.

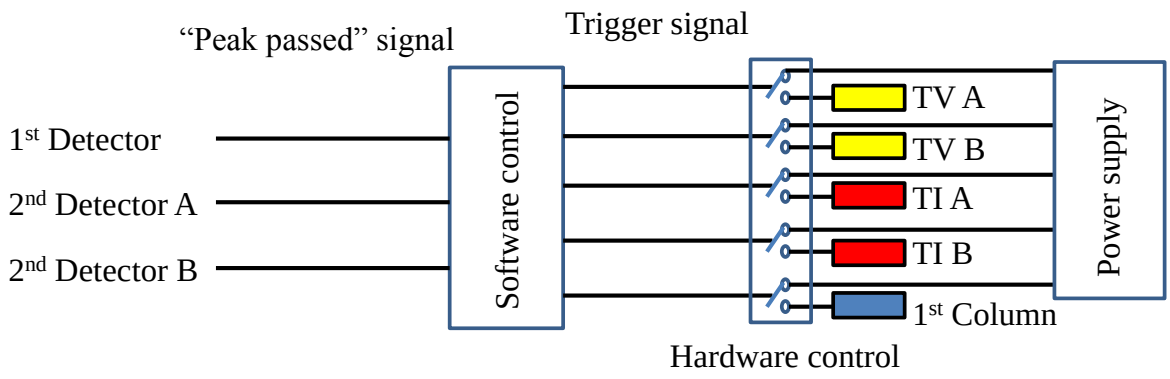

Figure 5.10. Schematic of the control/operation algorithm. TV: three-port valve; TI: thermal injector.

5.3.3 System calibration

The separation capability of a μGC system is affected by the factors such as stationary phase, column length, and temperature ramping, *etc*. Optimization is needed before actual analysis to ensure that the system is well tuned to separate all components in the sample within a reasonably short amount of time. For the 2-D μGC, the system separation capability is determined by the separation capability of both the 1st and the 2nd column. The optimal separation is achieved when analytes are sufficiently separated at both columns. In a conventional 2-D μGC system, optimization is usually accomplished through a trial-and-error process. In contrast, in our smart 2-D μGC system, the on-column detectors provide critical assessment of the separation capability of the 1st and the 2nd column.

To demonstrate this unique capability, a gas mixture containing six analytes (Analytes #15 - #20 listed in Table 1) is used as the model system. We first implement a system with one 1st column of 25 cm long and two 2nd columns of 50 cm and 25 cm long, respectively. Figure 5.11(A) shows the real-time chromatograms obtained from this configuration. Apparently, significant co-elution occurs at 1st Column. Since the trigger signal is designed

to be generated near the baseline, the entire co-eluted analytes (all six analytes in this particular case) are sent to 2nd Column A, resulting in insufficient separation of those analytes. The chromatograms provided by 1st Detector and 2nd Detector A allow us to conclude that the above failure is due primarily to the insufficient separation of the analytes in the 1st column.

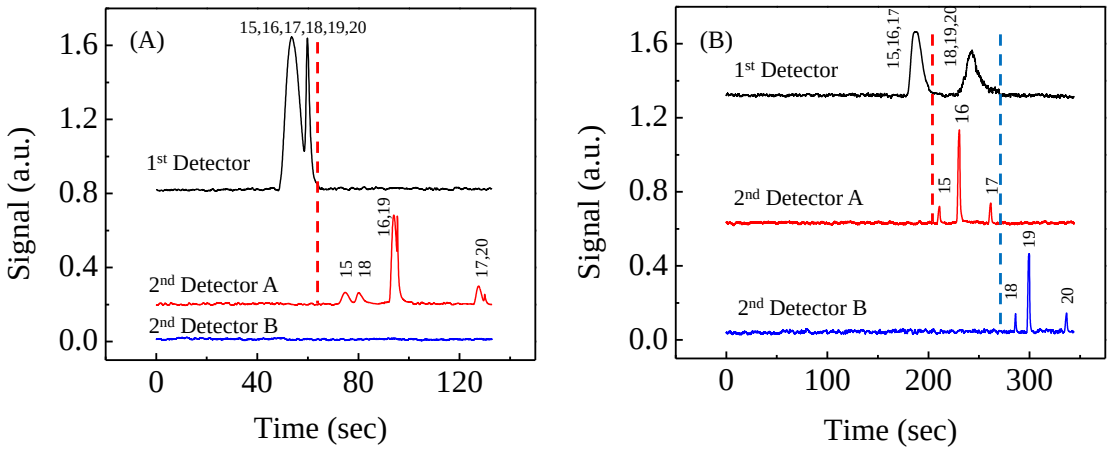

Figure 5.11. 2-D separation chromatograms obtained from the smart 2-D μGC illustrated in Fig. 5.8 under isothermal condition at room temperature. The length of the 1st column is 0.25 m for (A) and 1 m for (B), respectively. The length of the 2nd column A and B are 0.5 m and 0.25 m, respectively, for both (A) and (B). (A) shows an insufficient 2-D separation before optimization, where co-elution occurs for Analyte #16 and #19, and for Analyte #17 and #20. Dashed line represents the time when separation starts at 2nd column A. (B) shows a sufficient 2-D separation after optimization. Dashed lines represent the time when separation starts at 2nd column A and B, respectively.

Once the cause of failure is identified, a number of methods are readily available to address this problem, such as changing the 1st column length, the 2nd column length, the flow rate, or the temperature ramping profile. As a quick remedy, in our experiment we simply increase the length of the 1st column to 1 m, while keeping all other settings unchanged. As shown in Fig 5.11(B), the gas mixture is separated into two (yet still co-eluted) peaks in the 1st column and all six analytes could be completely separated after the 2nd columns. It should

be emphasized that such optimization is difficult to implement with the conventional 2-D μGC, as it is difficult to determine whether the insufficient 2-D separation is caused by the insufficient separation at the 1st column, the 2nd column, or both.

5.3.4 Separation test

5.3.4.1 Separation of 31 workplace hazardous VOCs

After optimization of our smart 2-D μGC system in the same manner as described previously, we employ it in analyzing 31 workplace hazardous VOCs reported by California Standard Section 01350 Specification (Feb 2010 version 1.1), which is the most popular US standard for evaluating and restricting indoor VOC emissions [51]. The name and the maximally allowable concentration of each analyte are listed in Table 1.

The first analysis is conducted under isothermal condition at room temperature. As shown in Fig. 5.12(A), three real-time chromatograms are obtained from 1st Detector, 2nd Detector A and B, respectively. At 1st Column, 31 analytes are separated into 12 baseline-separated peaks, which are then sent to 2nd Column A and B alternately for further separation. Total analysis is completed within 38 minutes. Figure 5.12(B) is the extracted 2-D chromatogram, from which we can observe a wide range of the retention time at the 2nd column up to approximately 4 minutes. Such long 2nd dimensional retention time would pose a significant challenge for a conventional 2-D μGC system due to the wrap-around issue [52], whose maximal 2nd column separation time is limited by the modulation period (ranging from sub-second to a few seconds). The retention times of each analyte at 1st and 2nd columns are presented in Appendix B.

Table 1. List of 31 workplace hazardous VOCs and their maximally allowable concentrations

No.	Analytes Name	Maximally Allowable Concentration (ng/L)
1	Carbon disulfide	400
2	Dichloroethylene	35
3	Methyl t-butyl ether	4000
4	Acetaldehyde	70
5	Methylene chloride	200
6	Chloroform	150
7	Hexane	3500
8	Dimethylformamide	40
9	Benzene	30
10	Carbon tetrachloride	20
11	Trichloroethylene	300
12	Dioxane	1500
13	Toluene	150
14	Vinyl acetate	100
15	Tetrachloroethylene	17.5
16	Ethylbenzene	1000
17	Ethylene glycol	200
18	Ethylene glycol monomethyl ether	30
19	Chlorobenzene	500
20	Ethylene glycol monoethyl ether	35
21	Isopropanol	3500
22	Methyl chloroform	500
23	Styrene	450
24	m-Xylene	350
25	Ethylene glycol monomethyl ether acetate	45
26	Propylene glycol monomethyl ether	3500
27	Formaldehyde	16.5
28	Ethylene glycol monoethyl ether acetate	150
29	Phenol	100
30	Dichlorobenzene	400
31	Isophorone	1000

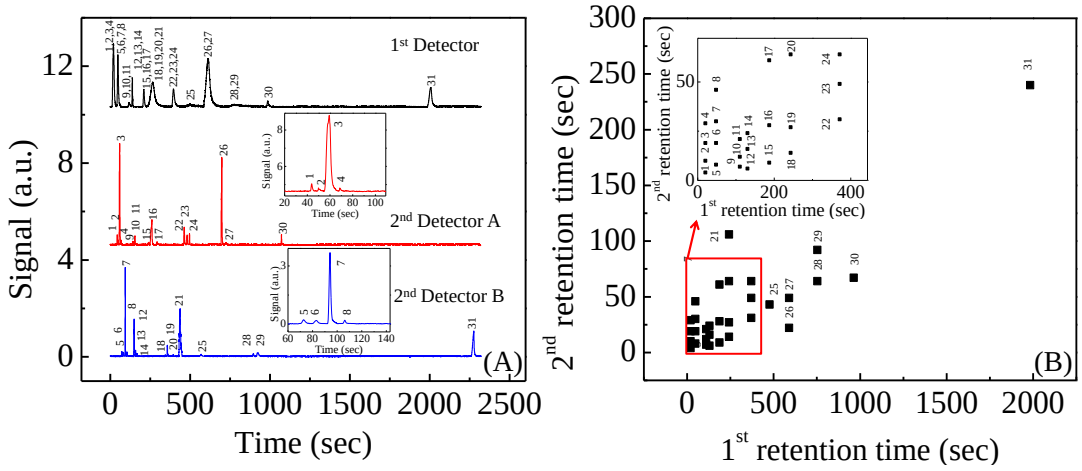

Figure 5.12. 2-D separation results of 31 workplace hazardous VOCs obtained from the 2-D μGC system shown in Fig. 5.8 under isothermal condition at room temperature. (A) Real-time chromatograms from 1st Detector, 2nd Detector A and B. Curves are vertically shifted for clarity. Insets are enlarged parts from chromatograms at 2nd Column A and B, respectively. (B) The corresponding 2-D chromatogram extracted from (A). The 1st Column is 1 m long and is coated with OV-1. The 2nd Column A and B is 0.5 m and 0.25 m long, respectively. Both are coated with OV-215.

To accelerate the analysis, temperature ramping is applied in this test. The 1st column is initially kept at 35 ^{o}C until the elution of the 11th peak at the 1st column, which is then heated up to 100 ^{o}C in 3 minutes. Both 2nd columns are kept at 45 ^{o}C during the whole analysis. Figure 5.13(A) plots the three chromatograms from the 1st and two 2nd columns. Total analysis time is shortened to 20 min. Figure 5.13(B) shows the extracted 2-D chromatogram. The longest 2nd dimensional retention time is approximately 110 seconds, which is still difficult to handle with the conventional 2-D μGC system.). The retention times of each analyte at 1st and 2nd columns are presented in Appendix B.

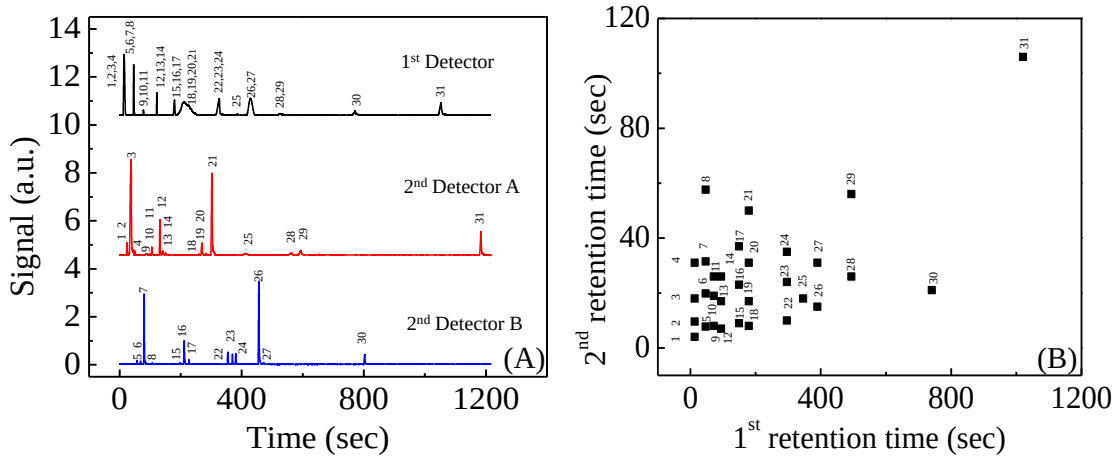

Figure 5.13. 2-D separation results of 31 workplace hazardous VOCs obtained from the smart 2-D μGC system shown in Fig. 5.8 with temperature ramping (other conditions are the same as in Fig. 5.12). (A) Real-time chromatograms from 1st Detector, 2nd Detector A and B. Curves are vertically shifted for clarity. (B) The corresponding 2-D chromatogram extracted from (A).

5.3.4.2 Identification of target analytes from background

In many applications, we are more interested in detection and identification of a particular target gas analyte or a set of analytes from interference background in a short time. In this scenario, a complete separation of all components in a gas mixture may not be necessary. Rather, only the target analytes need to be separated out, which can greatly simplify the analysis procedures and shorten the analysis time.

To demonstrate such versatility of our μGC system, we use the same 31 VOCs, among which toluene and phenol are used as the target analytes and the remaining 29 VOCs serve as interference background. The system configuration is the same as used in Fig. 5.12(B). According to Fig. 5.12(B), the 1st and 2nd dimensional retention time of toluene (phenol) is 130 (753) seconds and 16 (92) seconds, respectively. Therefore, modifications are made in the LabView codes to define two time windows from 126 seconds to 136 seconds and from

720 seconds to 820 seconds, respectively, at the 1st dimension. If an eluent peak is detected within these two windows, the peak will be then sent to the 2nd Column B for further separation/analysis. Any eluents outside these two windows are simply vented through 2nd Column A without conducting any further analysis. Note that the window at the 1st dimension can be very narrow (narrower than the elution peak) to ensure that most part of the target analyte is sent to the 2nd column while significantly rejecting interference background (even though they may co-elute with the target analyte). Therefore, the 2nd column separation becomes even easier, as fewer interferents are mixed in. At the 2nd dimension, the 2nd Detector B identifies the peaks that have the same 2nd retention times as the target analytes.

As shown in Fig. 5.14, the 1st Detector detects an eluent peak within the 1st time window, which is sent to 2nd Column B for further separation. The 2nd Detector B then identifies a peak that has the same 2nd retention time as toluene, indicating that toluene is contained in the gas mixture. Meanwhile, when the eluent in the 1st time window is analyzed at 2nd Column B, the separation at the 1st Column continues without interruption. The 1st Detector then detects another eluent peak within the 2nd time window, which is again sent to 2nd Column B for detection of phenol. Since no separation and analysis are conducted at 2nd Column A, the signal of 2nd Detector A is not present.

This detection and identification scenario is especially attractive for power hungry applications, such as remote autonomous monitoring, because it reduces the number of modulations for each analysis (no more than the number of the target analytes). When applied in the remote autonomous monitoring application, the system can be placed in the stand-by mode, only awakened by a suspicious peak(s) detected within the pre-determined window(s) at the 1st column.

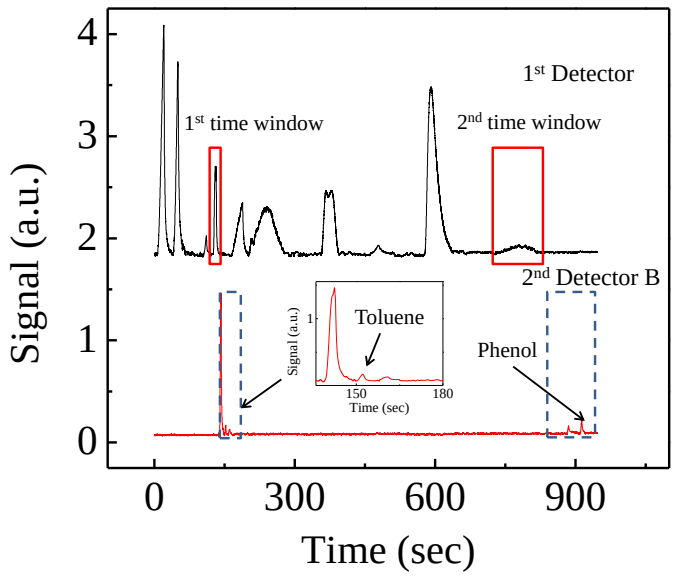

Figure 5.14. 2-D separation chromatograms obtained from the smart 2-D μGC shown in Fig. 5.8, when it is employed to detect toluene and phenol (as the target analyte) from interference background. Two time windows at the 1st dimensional separation are set to be from 126 s to 136 s and from 720 s to 820 s, respectively, as shown by the solid boxes. Dashed boxes show the 2nd dimensional separation of the eluents within the time windows defined by the solid boxes at the 1st dimension. Inset shows the enlarged first dashed box.

5.4 Conclusion

We have proposed and demonstrated a novel adaptive 2-D GC system that consists of a 1st column, multiple parallel 2nd columns, a decision-making module installed between the 1st and 2nd columns, and a control/operation algorism. The major advantage of the proposed 2-D GC over the conventional 2-D GC is that it is smarter and more adaptive in analyzing the effluents from the 1st column and in selecting the following 2nd columns, which can be of various lengths, coatings, flow rates, and temperatures. This unique feature renders the proposed adaptive 2-D GC much higher versatility and significantly enhanced separation capability. It has been applied in analyzing plant emitted VOCs, workplace hazardous VOCs, as well as specific detection of target analytes. The results demonstrate that 1) it can be used

as a general-purpose gas analysis instrument having significantly enhanced second dimensional separation capability unattained with the conventional 2-D μGC, and 2) it can be adapted for particular applications where only a set of target analytes need to be detected.

References

1. F. J. Santos, and M. T. Galceran, "The application of gas chromatography to environmental analysis," TrAC Trend Anal. Chem. **21**, 672-685 (2002).
2. J. L. Chia, C. Jin, and E. T. Zellers, "Chamber evaluation of a portable GC with tunable retention and microsensor-array detection for indoor air quality monitoring," J. Environ. Monitor. **8**, 270-278 (2006).
3. M. Philips, K. Gleeson, J. M. B. Hughes, J. Greenberg, R. N. Cataneo, L. Baker, and W. P. McVay, "Volatile organic compounds in breath as markers of lung cancer: a cross-sectional study," Lancet **353**, 1930-1933 (1999).
4. T. H. Risby, and S. F. Solga, "Current status of clinical breath analysis," Appl. Phys. B **85**, 421-426 (2006).
5. B. Veyrand, A. Brosseaud, L. Sarcher, V. Varlet, F. Monteau, P. Marchand, F. Andre, and B. Lebizec, "Innovative method for determination of 19 polycyclic aromatic hydrocarbons in food and oil samples using gas chromatography coupled to tandem mass spectrometry based on an isotope dilution approach," J. Chromatogr. A **1149**, 333-344 (2007).
6. Y. Sun, J. Liu, G. Frye-Mason, S.-j. Ja, A. K. Thompson, and X. Fan, "Optofluidic ring resonator sensors for rapid DNT vapor detection," Analyst **134**, 1386-1391 (2009).
7. G. W. Cook, P. T. LaPuma, G. L. Hook, and B. A. Eckenrode, "Using gas chromatography with ion mobility spectrometry to resolve explosive compounds in the presence of interferents," J. Forensic. Sci. **55**, 1582-1591 (2010).
8. S. Popiel, and M. Sankowska, "Determination of chemical warfare agents and related compounds in environmental samples by solid-phase microextraction with gas chromatography," J. Chromatogr. A **1218**, 8457-8479 (2011).
9. D. R. Deans, and I. Scott, "Gas chromatographic columns with adjustable separation characteristics," Anal. Chem. **45**, 1137-1141 (1973).
10. J. R. Jones, and J. H. Purnell, "Prediction of retention times in serially linked open-tubular gas chromatographic columns and optimization of column lengths," Anal. Chem. **62**, 2300-2306 (1990).
11. J. H. Purnell, and M. H. Wattan, "Separation of aliphatic hydrocarbon mixtures by gas chromatography using serial liquid-phase and solid-phase columns," Anal. Chem. **63**, 1261-1264 (1991).
12. J. Blomberg, P. J. Schoenmakers, J. Beens, and R. Tijssen, "Compehensive two-dimensional gas chromatography (GC×GC) and its applicability to the characterization of complex (petrochemical) mixtures," J. High. Resolut. Chromatogr. **20**, 539-544 (1997).
13. J. Beens, H. Boelens, R. Tijssen, and J. Blomberg, "Quantitative Aspects of Comprehensive Two-Dimensional Gas Chromatography (GC×GC)," J. High. Resolut. Chromatogr. **21**, 47-54 (1998).
14. R. Sacks, C. Coutant, T. Veriotti, and A. Grall, "Pressure-Tunable Dual-Column Ensembles for High-Speed GC and GC/MS," J. High. Resolut. Chromatogr. **23**, 225-234 (2000).

15. M. Adahchour, J. Beens, R. J. J. Vreuls, and U. A. T. Brinkman, "Recent developments in comprehensive two-dimensional gas chromatography: I. Introduction and instrumental set-up," TrAC Trend Anal. Chem. **25**, 438-454 (2006).
16. J. Liu, Y. Sun, D. J. Howard, G. Frye-Mason, A. K. Thompson, S.-j. Ja, S.-K. Wang, M. Bai, H. Taub, M. Almasri, and X. Fan, "Fabry-Perot Cavity Sensors for Multipoint On-Column Micro Gas Chromatography Detection," Anal. Chem. **82**, 4370-4375 (2010).
17. S.-J. Kim, S. M. Reidy, B. P. Block, K. D. Wise, E. T. Zellers, and K. Kurabayashi, "Microfabricated thermal modulator for comprehensive two-dimensional micro gas chromatography: design, thermal modeling, and preliminary testing," Lab Chip **10**, 1647-1654 (2010).
18. Y. Sun, J. Liu, D. J. Howard, G. Frye-Mason, A. K. Thompson, S.-j. Ja, and X. Fan, "Rapid tandem-column micro-gas chromatography based on optofluidic ring resonators with multi-point on-column detection," Analyst **135**, 165-171 (2010).
19. J. J. Whiting, C. S. Fix, J. M. Anderson, A. W. Staton, R. P. Manginell, D. R. Wheeler, E. B. Myers, M. L. Roukes, and R. J. Simonson, "High-speed two-dimensional gas chromatography using microfabricated GC columns combined with nanoelectromechanical mass sensors," in *Transducers*(Denver, CO, 2009).
20. J. Blomberg, P. J. Schoenmakers, J. Beens, and R. Tijssen, "Compehensive two-dimensional gas chromatography (GC×GC) and its applicability to the characterization of complex (petrochemical) mixtures," J. High. Resolut. Chromatogr. **20**, 539-544 (1997).
21. M. Adahchour, J. Beens, R. J. J. Vreuls, and U. A. T. Brinkman, "Recent developments in comprehensive two-dimensional gas chromatography (GC X GC): I. Introduction and instrumental set-up," TrAC Trend. Anal. Chem. **25**, 438-454 (2006).
22. J. Beens, H. Boelens, R. Tijssen, and J. Blomberg, "Quantitative Aspects of Comprehensive Two-Dimensional Gas Chromatography (GC×GC)," J. High. Resolut. Chromatogr. **21**, 47-54 (1998).
23. Z. Liu, S. R. Sirimanne, D. G. Patterson, L. L. Needham, and J. B. Phillips, "Comprehensive Two-Dimensional Gas Chromatography for the Fast Separation and Determination of Pesticides Extracted from Human Serum," Anal. Chem. **66**, 3086-3092 (1994).
24. J. B. Phillips, and E. B. Ledford, "Thermal modulation: A chemical instrumentation component of potential value in improving portability," Field Anal. Chem. Technol. **1**, 23-29 (1996).
25. P. J. Marriott, and R. M. Kinghorn, "Longitudinally Modulated Cryogenic System. A Generally Applicable Approach to Solute Trapping and Mobilization in Gas Chromatography," Anal. Chem. **69**, 2582-2588 (1997).
26. S.-J. Kim, S. M. Reidy, B. P. Block, K. D. Wise, E. T. Zellers, and K. Kurabayashi, "Microfabricated thermal modulator for comprehensive two-dimensional micro gas chromatography: design, thermal modeling, and preliminary testing," Lab Chip **10**, 1647-1654 (2010).
27. C. A. Bruckner, B. J. Prazen, and R. E. Synovec, "Comprehensive Two-Dimensional High-Speed Gas Chromatography with Chemometric Analysis," Anal. Chem. **70**, 2796-2804 (1998).
28. C. G. Fraga, B. J. Prazen, and R. E. Synovec, "Comprehensive Two-Dimensional Gas Chromatography and Chemometrics for the High-Speed Quantitative Analysis of Aromatic

Isomers in a Jet Fuel Using the Standard Addition Method and an Objective Retention Time Alignment Algorithm," Anal. Chem. **72**, 4154-4162 (2000).
29. B. J. Prazen, K. J. Johnson, A. Weber, and R. E. Synovec, "Two-Dimensional Gas Chromatography and Trilinear Partial Least Squares for the Quantitative Analysis of Aromatic and Naphthene Content in Naphtha," Anal. Chem. **73**, 5677-5682 (2001).
30. J. V. Seeley, F. J. Kramp, and K. S. Sharpe, "A dual-secondary column comprehensive two-dimensional gas chromatograph for the analysis of volatile organic compound mixtures," J. Sep. Sci. **24**, 444-450 (2001).
31. C.-J. Lu, J. Whiting, R. D. Sacks, and E. T. Zellers, "Portable Gas Chromatograph with Tunable Retention and Sensor Array Detection for Determination of Complex Vapor Mixtures," Anal. Chem. **75**, 1400-1409 (2003).
32. S. E. Reichenbach, M. Ni, V. Kottapalli, and A. Visvanathan, "Information technologies for comprehensive two-dimensional gas chromatography," Chemometr. Intell. Lab. **71**, 107-120 (2004).
33. G. J. Opiteck, S. M. Ramirez, J. W. Jorgenson, and M. A. Moseley, "Comprehensive Two-Dimensional High-Performance Liquid Chromatography for the Isolation of Overexpressed Proteins and Proteome Mapping," Anal. Biochem. **258**, 349-361 (1998).
34. T. Murahashi, "Comprehensive two-dimensional high-performance liquid chromatography for the separation of polycyclic aromatic hydrocarbons," Analyst **128**, 611-615 (2003).
35. **K. Wagner, T. Miliotis, G. Marko-Varga, R. Bischoff,** and **K. K. Unger,** "An Automated On-Line Multidimensional HPLC System for Protein and Peptide Mapping with Integrated Sample Preparation," Anal. Chem. **74**, 809-820 (2002).
36. O. P. Haefliger, "Universal two-dimensional HPLC technique for the chemical analysis of complex surfactant mixtures," Anal. Chem. **75**, 371-378 (2003).
37. N. Tanaka, H. Kimura, D. Tokuda, K. Hosoya, T. Ikegami, N. Ishizuka, H. Minakuchi, K. Nakanishi, Y. Shintani, M. Furuno, and K. Cabrera, "Simple and comprehensive two-dimensional reversed-phase HPLC using monolithic silica columns," Anal. Chem. **76**, 1273-1281 (2004).
38. E. J. C. v. d. Klift, G. Viv´o-Truyols, F. W. Claassen, F. L. v. Holthoon, and T. A. v. Beek, "Comprehensive two-dimensional liquid chromatography with ultraviolet, evaporative light scattering and mass spectrometric detection of triacylglycerols in corn oil," J. Chromatogr. A **1178**, 43-55 (2008).
39. A. J. Alexander, and L. Ma, "Comprehensive two-dimensional liquid chromatography separations of pharmaceutical samples using dual fused-core columns in the 2nd dimension," J. Chromatogr. A **1216**, 1338-1345 (2009).
40. S. R. Groskreutz, M. M. Swenson, L. B. Secor, and D. R. Stoll, "Selective comprehensive multi-dimensional separation for resolution enhancement in high performance liquid chromatography, part 1- principles and instrumentation," J. Chromatogr. A (2011).
41. J. N. Fairchild, K. Horváth, and G. Guiochon, "Theoretical advantages and drawbacks of on-line, multidimensional liquid chromatography using multiple columns operated in parallel," J. Chromatogr. A **1216**, 6210-6217 (2009).
42. J. V. Seeley, F. J. Kramp, and K. S. Sharpe, "A dual-secondary column comprehensive two-dimensional gas chromatograph for the analysis of volatile organic compound mixtures," J. Sep. Sci. **24**, 444-450 (2001).

43. S. Bieri, and P. J. Marriott, "Generating multiple independent retention index data in dual-secondary column comprehensive two-dimensional gas chromatography," Anal. Chem. **78**, 8089-8097 (2006).
44. S. Bieri, and P. J. Marriott, "Dual-Injection System with Multiple Injections for Determining Bidimensional Retention Indexes in Comprehensive Two-Dimensional Gas Chromatography," Anal. Chem. **80**, 760-768 (2008).
45. J. Liu, M. K. K. Oo, K. Reddy, Y. B. Gianchandani, J. C. Schultz, h. M. Appel, and X. Fan, "Adaptive two-dimensional microgas chromatography," Anal. Chem. **84**, 4214-4220 (2012).
46. J. Liu, N. K. Gupta, K. D. Wise, Y. B. Gianchandani, and X. Fan, "Demonstration of motionless Knudsen pump based micro-gas chromatography featuring micro-fabricated columns and on-column detectors," Lab Chip **11**, 3487-3492 (2011).
47. J. Liu, Y. Sun, and X. Fan, "Highly versatile fiber-based optical Fabry-Perot gas sensor," Opt. Express **17**, 2731-2738 (2009).
48. M. Dicke, J. J. A. van Loon, and R. Soler, "Chemical complexity of volatiles from plants induced by multiple attack," Nature Chem. Biol. **5**, 317 - 324 (2009).
49. C. M. D. Moraes, J. C. Schultz, M. C. Mescher, and J. H. Tumlinson, "Induced Plant Signaling and its Implications for Environmental Sensing," J. Toxicol. Environ. Health A **67**, 819-834 (2004).
50. J. Liu, M. K. Khaing Oo, K. Reddy, Y. B. Gianchandani, J. C. Schultz, H. M. Appel, and X. Fan, "Adaptive two-dimensional microgas chromatography," Anal. Chem. **84**, 4214−4220 (2012).
51. M. Horton, K. Belshe, and A. Schwarzenegger, "Standard method for the testing and evaluation of volatile organic chemical emissions from indoor sources using environmental chambers," California Department of Public Health, ed. (2010).
52. G. Serrano, D. Paul, S.-J. Kim, K. Kurabayashi, and E. T. Zellers, "Comprehensive two-dimensional gas chromatographic separations with a microfabricated thermal modulator," Anal. Chem. **84**, 6973–6980 (2012).

Chapter VI

Contributions, Conclusions, and Future Work

In this Chapter, I will summarize the work in this dissertation and look into the experiments and research directions for the future.

6.1 Contributions and conclusions

6.1.1 Detector

We have developed a versatile fiber-based FP gas sensing probe that is easy to fabricate and highly sensitive. This FP gas sensing probe can employ vapor-sensitive polymer with any refractive indexes, and hence significantly broadening its applications in various areas. Its detection limit is demonstrated to be 50 pico-grams. The FP sensing probe is further assembled into a sensor module which is easily adaptable to traditional GC columns, enabling multiple on-column detection points along the column. Each sensor module can be tailored for a certain class of analytes, thus improving the detection sensitivity. We then thoroughly characterize the FP sensor module and successfully integrate it with a conventional GC to demonstrate its capability of rapid detection.

6.1.2 Sub-system integration

We report the integration of a KP array based sub-μGC system featuring on-column FP

detectors and the micro-fabricated GC column. Using helium and dry air as the carrier gas the system demonstrate both strong separation and detection of gas mixtures with various polarities and volatilities. Pressure programming of the KP array allows chromatographic resolution while shortening the analysis time. We also evaluate a tandem-column configuration utilizing two on-column FP detectors, which provides complementary chromatograms following each of the two micro-fabricated columns.

6.1.3 Smart multi-channel two-dimensional gas chromatography

We have proposed and demonstrated a novel smart multi-channel adaptive 2-D GC system that consists of a 1st column, multiple parallel 2nd columns, and a decision-making module installed between the 1st and 2nd columns. A mixture of 20 analytes with various volatilities and polarities and plant emitted VOCs are used as model systems, and are separated in ~650 seconds and ~1270 seconds, respectively. The major advantage of the proposed 2-D GC over the conventional 2-D GC is that it is smarter and more adaptive in analyzing the effluents from the 1st column and in selecting the following 2nd columns, which can be of various lengths, coatings, flow rates, and temperatures. This unique feature renders the proposed adaptive 2-D GC much higher versatility and significantly enhanced separation capability.

We further optimize and develop a complete smart multi-channel 2-D μGC system, and apply it in analyzing workplace hazardous VOCs, as well as specific detection of target analytes. Our results have shown that (1) the smart μGC can be used as a general-purpose gas analysis instrument having significantly enhanced second dimensional separation capability unattained with the conventional 2-D μGC, and (2) it can be adapted for particular applications where only a set of target analytes need to be detected..

6.2 Future work

6.2.1 Detector improvement

Previously, we demonstrated the feasibility of an FP optical gas sensor and its potential for on-column detection. In the future, we will further optimize the sensor structure to achieve a lower detection limit, faster response time, and higher fluidic compatibility.

The polymer layer coated on the sensor is very important to its performance. As discussed above, the interaction between gas analytes and the polymer layer changes the sensing signal. The stronger the interaction is, the larger the signal becomes. Therefore, it is desirable to use polymer that interacts strongly with target gas analytes. Porous materials have been reported as sensing layers for various gas sensors, because they can trap gas molecules more efficiently than normal polymers by their micro-channels, and thus provide a larger sensing signal. Two of the commonly used porous materials are zeolite [1] and sol-gel polymers [2, 3]. We will also explore the feasibility of using those materials as the sensing layer in our FP sensor.

The thickness of the polymer layer is another important factor affecting the response time of the FP sensor. As the polymer layer becomes thicker, it takes longer time for gas analytes to diffuse into and be purged out of the layer, resulting in a broadened response peak. If one analyte diffuses into the polymer layer before the previous one is purged out, it may cause two peaks to become indistinguishable, which dramatically degrades the system resolution. On the other hand, if the polymer layer is too thin, it may not be able to generate detectable signal. Hence, we will optimize the thickness of the polymer layer to achieve fast response without compromising its sensitivity.

In order to make the sensing probe more compatible to GC columns, we will further decrease the diameter of the sensing probe. Typically, the inner diameter (ID) of a GC column is 250 μm or 100 μm, while the diameter of an optical fiber is 125 μm, which makes it difficult to be directly inserted into the column. We will use a well-controlled fiber tapering system installed in our lab to taper down the fiber diameter to around 100 μm to make it more compatible to GC columns.

We will improve the fabrication processes to increase the fabrication yield and device reliability. For the sensing probe fabrication, the sputtering method will be used to coat a gold layer, and spin coating method to deposit the polymer layer, which has accurate control over the coating thickness and high re-productively. Through this method, we will be able to obtain the same reflectivity at the gold layer for each probe. Meanwhile, the spin coating method provides accurate thickness control and high re-productivity to deposit the polymer layer. For the sensor assembling, an accurate three-dimensional stage will be used to assemble the sensing probe with a GC column. Besides, the whole assembling process will take place under the microscope to ensure that the sensing probe will not be damaged during the assembling and the end of the probe flushes with the inner surface of the GC column.

We will introduce various characterization mechanisms to evaluate the sensor. A broadband laser will be used to inspect the interference of the sensor to calculate the polymer layer thickness and the quality factor of the FP cavity. The temporal response of the sensor will be tested by a conventional GC system, by connecting the FP sensor to the injection port of the GC system through a conventional GC column, whose length and coating will be kept the same as the micro-column to be used in the μGC system in order to best mimic the micro-column. Since the FP sensor enables on-column detection, we will be able to connect the

outlet of the sensor to a standard GC detector, for example, flame ionization detector (FID) and mass spectrometry (MS), which will give us highly reliable comparison results. To determine the limit of detection (LOD), a solid phase micro-extractor (SPME) will be used to sample target analytes. By varying the SPME sampling time and the split ratio in the GC injector, the amount of analyte injected into the GC column can be varied over a wide range so that both the LOD, and response dynamic range and linearity can be characterized.

6.2.2 System improvement

We will further miniaturize the system by using micro-fabricated valves, thermal modulators and on-chip on-column detectors, as well as optimize the performance of each component. Improvement will be made to the operation algorithm to make the system smarter and more adaptive in control/operation, peak identification and trigger mechanism.

6.2.3 Breast cancer screening based on exhaled breath biomarkers

Breast cancer is one of the most commonly diagnosed cancers among women in the United States, having an incident rate of about 13%. Early diagnosis of breast cancer is important to cure the disease. Current screening tests for early signs of the cancer include magnetic resonance imaging (MRI) [4], mammogram [5], ultrasound [6], physical exam, and ductal lavage [7], *etc.*. However, these tests have limited sensitivity and specificity so that some of them are only recommended in combination of other tests. They also expose subjects to potentially harmful radiation and perceivable discomfort. Additionally, most of the clinically available screening tests are expensive, and require highly specialized equipment and highly trained experts, which significantly restricts their accessibility for on-site

diagnosis and daily monitoring purposes. Therefore, it is desirable to develop a new screening test that is more sensitive, more specific, safer, and less invasive.

One of the most promising technologies is breath analysis, which diagnoses the cancer by identifying its distinctive biomarkers in the breath. Oxidative stress has been implicated as an important indicator of breast cancer [8-10], which occurs when increased reactive oxygen species (ROS) are produced in mitochondria and leak into cytoplasm. In the cytoplasm, ROS oxidize important biomolecules, such as DNA and protein, and peroxidize polyunsaturated fatty acids in cell membranes, generating alkanes and methylalkanes, which are subsequently excreted in the breath. The abundance of alkanes and methylalkanes varies as the intensity of oxidative stress [11, 12]. For example, it has been reported that the amount of pentane in breath of women who have breast cancer is much higher than that of healthy women [13], which demonstrates the potential value of breath testing. However, pentane alone is a nonspecific marker of breast cancer, as it can be also found in breath of patients who have rheumatoid arthritis [14], acute myocardial infarction [15], schizophrenia [16], and bronchial asthma [15]. Phillips et al. recently reported an extensive set of breath markers for breast cancer, including eight volatile organic compounds (VOCs) of nonane, 5-methyl tridecane, 3-methyl undecane, 6-methyl pentadecane, 2-methyl propane, 3-methyl nonadecane, 4-methyl dodecane, and 2-methyl octane [17]. The screening test based on these markers can accurately indentify women having breast cancer, with a negative predictive value superior to a screening mammogram. Micro–GC, a powerful method for VOC analysis, will be an ideal technique to analyze biomarkers in the breath.

References

1. H. Xiao, J. Zhang, J. Dong, M. Luo, R. Lee, and V. Romero, "Synthesis of MFI zeolite films on optical fibers for detection of chemical vapors," Opt. Lett. **30**, 1270-1272 (2005).
2. N. R. Walker, M. J. Linman, M. M. Timmers, S. L. Dean, C. M. Burkett, J. A. Lloyd, J. D. Keelor, B. M. Baughamn, and P. L. Edmiston, "Selective detection of gas-phase TNT by integrated optical waveguide spectrometry using molecularly imprinted sol-gel sensing films," Anal. Chim. Acta. **593**, 82-91 (2007).
3. G. Bunte, J. Hurttlen, H. Pontinus, K. hartlieb, and H. Krause, "Gas phase detection of explosive such as 2,4,6-trinitrotoluene by molecularly imprinted polymers," Anal. Chim. Acta. **591**, 49-56 (2007).
4. D. Saslow, C. Boetes, W. Burke, S. Harms, M. O. Leach, C. D. Lehman, E. Morris, E. Pisano, M. Schnall, S. Sener, R. A. Smith, E. Warner, M. Yaffe, K. S. Andrews, and C. A. Russell, "American cancer society guidelines for breast screening with MRI as an adjunct to mammography," CA Cancer J. Clin. **57**, 75-89 (2007).
5. O. Olsen, and P. C. Gozsche, "Cochrane review on screening for breast cancer with mammography," Lancet **358**, 1340-1342 (2001).
6. P. B. Gordon, and S. L. Goldenberg, "Malignant breast masses detected only by ultrasound. A retrospective review," Cancer **76**, 626-630 (1995).
7. S. Badve, E. Wiley, and N. Rodriguez, "Assessment of Utility of Ductal Lavage and Ductoscopy in Breast Cancer - A Retrospective Analysis of Mastectomy Specimens," Mod. Pathol. **16**, 206-209 (2003).
8. C. M. F. Kneepkens, G. Lepage, and C. C. Roy, "The hydrocarbon breath test in the study of lipid peroxidation: princile and practice," Clin. Invest. Med. **15**, 163-186 (1992).
9. C. B. Ambrosone, "Oxidants and antioxidants in breast cancer," Anti. Redox. Sign. **2**, 903-917 (2000).
10. D. Li, W. Zhang, A. A. Sahin, and W. N. Hittelman, "DNA adducts in normal tissue adjacent to breast cancer: a review," Cancer Detect. Prev. **23**, 454-462 (1999).
11. C. M. F. Kneepkens, G. Lepage, and C. C. Roy, "The potential of the hydrocarbon breath test as a measure of lipid peroxidation," Free Radic. Biol. Med. **17** (1994).
12. M. Phillips, Renee N Cataneo, Joel Greenberg, Ratnasiri Gunawardena, Aijit Naidu, and F. Rahbari-Oskoui, "Effect of age on the breath methylated alkane contour, a display of apparent new markers of oxidative stress," J. Lab Clin. Med. **136**, 243-249 (2000).
13. E. Hietanen, H. Bartsch, J. C. Bereziat, A. M. Camus, S. McClinton, O. Eremin, L. Davidson, and P. Boyle, "Diet and oxidative stress in breast, colon and prostate cancer patients: a case-control study," Eur. J. Clin. Nutr. **48**, 575-586 (1994).
14. Satyendra Humad, Edwin Zarling, M. Clapper, and J. L. Skosey, "Breath Pentane Excretion as a Marker of Disease Activity in Rheumatoid Arthritis," Free Radic. Biol. Med. **5**, 101-106 (1988).
15. Z. W. Weitz, A. J. Birnbaum, J. L. Skosey, P. A. Sobotka, and E. J. Zarling, "High breath pentane concentrations during acute myocardial infarction," Lancet **337**, 933-935 (1991).

16. M. Phillips, M. Sabas, and J. Greenberg, "Increased pentane and carbon disulfide in the breath of patients with schizophrenia," J. Clin. Pathol. **46**, 861-864 (1993).
17. M. Phillips, R. N. Cataneo, B. A. Ditkoff, P. Fisher, J. Greenberg, R. Gunawardena, C. S. Kwon, F. Rahbari-Oskoui, and C. Wong, "Volatile Markers of Breast Cancer in the Breath," Breast J. **9**, 184-191 (2003).

Appendices

Appendix A

Retention times of 19 volatile organic compounds emitted by plants

Name	1st Retention time (sec)	2nd Retention time (sec)
Pentane	6	2
Heptane	14	3
Dimethyl disulfide	14	6
Octane	31	11
Toluene	31	9
Pinene	41	8
Cis-3-hexen-1-ol	41	32
Trans-2-hexenal	41	22
Decane	77	18
Limonene	84	10
Ocimene	90	10
undecane	110	38
Cis-3-hexenyl acetate	151	15
Methyl salicylate	178	176
Dodecane	294	87
Trans-β-farnesene	638	73
Jasmone	638	52
Methyl jasmonate	795	94
Caryophyllene	1080	50

Appendix B

Retention times of 31 workplace hazardous volatile organic compounds

B.1 Separation under isothermal condition at room temperature

Name	1st Retention time (sec)	2nd Retention time (sec)
Carbon disulfide	20	4
Dichloroethylene	20	10
Methyl t-butyl ether	20	19
Acetaldehyde	20	29
Methylene chloride	48	8
Chloroform	48	19
Hexane	48	30
Dimethylformamide	48	46
Benzene	110	7
Carbon tetrachloride	110	12
Trichloroethylene	110	21
Dioxane	130	6
Toluene	130	16
Vinyl acetate	130	24
Tetrachloroethylene	187	9
Ethylbenzene	187	28
Ethylene glycol	187	61
Ethylene glycol monomethyl ether	243	14
Chlorobenzene	243	27
Ethylene glycol monoethyl ether	243	64
Isopropanol	243	106

Methyl chloroform	371	31
Styrene	371	49
m-Xylene	371	64
Ethylene glycol monomethyl ether acetate	477	43
Propylene glycol monomethyl ether	590	22
Formaldehyde	590	49
Ethylene glycol monoethyl ether acetate	753	64
Phenol	753	92
Dichlorobenzene	963	67
Isophorone	1983	240

B.2 Separation under temperature ramping condition

Name	1st Retention time (sec)	2nd Retention time (sec)
Carbon disulfide	13	4
Dichloroethylene	13	9.6
Methyl t-butyl ether	13	18
Acetaldehyde	13	31
Methylene chloride	47	7.8
Chloroform	47	19.8
Hexane	47	31.5
Dimethylformamide	47	57.6
Benzene	72	8
Carbon tetrachloride	72	19
Trichloroethylene	72	26
Dioxane	94	7
Toluene	94	17
Vinyl acetate	94	26
Tetrachloroethylene	149	9
Ethylbenzene	149	23
Ethylene glycol	149	37
Ethylene glycol monomethyl ether	179	8
Chlorobenzene	179	17
Ethylene glycol monoethyl ether	179	31
Isopropanol	179	50
Methyl chloroform	296	10
Styrene	296	24

m-Xylene	296	35
Ethylene glycol monomethyl ether acetate	346	18
Propylene glycol monomethyl ether	390	15
Formaldehyde	390	31
Ethylene glycol monoethyl ether acetate	494	26
Phenol	494	56
Dichlorobenzene	741	21
Isophorone	1021	106